(12) INTERNATIONAL APPLICATION PUBLISHED UNDER THE PATENT COOPERATION TREATY (PCT)

(19) World Intellectual Property Organization
International Bureau

(43) International Publication Date
21 January 2010 (21.01.2010)

PCT

(10) International Publication Number
WO 2010/008625 A2

(51) **International Patent Classification:**
G21B 1/21 (2006.01)

(21) **International Application Number:**
PCT/US2009/038616

(22) **International Filing Date:**
27 March 2009 (27.03.2009)

(25) **Filing Language:** English

(26) **Publication Language:** English

(30) **Priority Data:**
61/040,040 27 March 2008 (27.03.2008) US

(71) **Applicant** *(for all designated States except US):* **UNIFIED GRAVITY CORPORATION** [US/US]; P.o.box 60940, Palo Alto, CA 94306 (US).

(72) **Inventors; and**
(75) **Inventors/Applicants** *(for US only):* **LIPINSKI, Stephen,** A. [US/US]; 761 Encina Grande Drive, Palo Alto, CA 94306 (US). LIPINSKI, Hubert, M.; 761 Encina Grande Drive, Palo Alto, CA 94306 (US).

(74) **Agent:** BEFFEL, Ernest, J., Jr.; HAYNES BEFFEL & WOLFELD LLP, P.O. Box 366, Half Moon Bay, CA 94019 (US).

(81) **Designated States** *(unless otherwise indicated, for every kind of national protection available):* AE, AG, AL, AM, **AO, AT,** AU, **AZ, BA, BB, BG, BH, BR, BW, BY, BZ, CA, CH, CN, CO, CR, CU, CZ, DE, DK, DM, DO, DZ, EC,** EE, **EG,** ES, **FI, GB, GD, GE, GH, GM, GT, HN, HR, HU, ID, IL, IN, IS, JP, KE, KG, KM, KN, KP, KR, KZ, LA, LC, LK, LR, LS, LT, LU, LY, MA, MD, ME, MG, MK, MN, MW, MX, MY, MZ,** NA, **NG, NI, NO, NZ, OM, PG, PH, PL, PT, RO, RS, RU, SC, SD,** SE, **SG, SK, SL, SM, ST, SV, SY, TJ, TM, TN, TR, TT, TZ,** UA, **UG,** US, **UZ, VC, VN, ZA, ZM, ZW.**

(84) **Designated States** *(unless otherwise indicated, for every kind of regional protection available):* ARIPO (BW, GH, GM, KE, LS, MW, MZ, NA, SD, SL, SZ, TZ, UG, ZM, ZW), Eurasian (AM, AZ, BY, KG, KZ, MD, RU, TJ, TM), European (AT, BE, BG, CH, CY, CZ, DE, DK, EE, ES, FI, FR, GB, GR, HR, HU, IE, IS, **IT,** LT, LU, LV, MC, MK, MT, NL, NO, PL, PT, RO, SE, SI, SK, TR), OAPI (BF, BJ, CF, CG, CI, CM, GA, GN, GQ, GW, ML, MR, NE, SN, TD, TG).

Published:

— *without international search report and to be republished upon receipt of that report (Rule 48.2(g))*

WO 2010/008625 A2

(54) Title: FUSION HEAT ENGINE AND ELECTROGRAVITY GENERATOR METHODS AND APPLICATIONS

(57) Abstract: The Hydrogen-Lithium Fusion Device is a revolutionary new device that consists of a proton accelerator, lithium foil target, and a target holder of specified geometry. The invention enables a proton-lithium fusion efficiency that may be close to 100% and the fusion byproducts to exit the lithium target without transferring significant fusion energy to the target as heat. Energy from the fusion reaction may be collected as heat or gravity waves from the fusion reaction may be converted directly to electricity.

FUSION HEAT ENGINE AND ELECTROGRAVITY GENERATOR METHODS AND APPLICATIONS

RELATED APPLICATIONS

[0001] This application claims the benefit of US provisional application 61/040,040, filed March 27, 2008, entitled "Fusion Heat Engine and Electrogravity Generator". This related application is incorporated by reference.

BACKGROUND OF THE INVENTION

[0002] The invention enables a proton-lithium fusion efficiency that may be close to 100% and the fusion byproducts to exit the lithium target without transferring significant fusion energy to the target as heat. Energy from the fusion reaction may be collected as heat or gravity waves from the fusion reaction may be converted directly to electricity.

[0003] The most comprehensive summary of prior research in hydrogen-lithium fusion is offered by Herb et al. (Herb, R.G., Parkinson, D.B., Kerst, D.W. 1935. Yield of Alpha-Particles from Lithium Films Bombarded by Protons. Physical Review 48: 118-124) who cite 3 previous experiments involving hydrogen/lithium fusion as well as their own experimental results. Herb's paper concludes that at proton energies comparable to those used by these inventors during recent experiments in Huntsville, Alabama, very little fusion takes place. Herb's data show a fusion efficiency of 0.334×10^{-7} compared to 1.0 for perfect fusion - that is, for every 30,000,000 protons in the beam, only one will fuse with lithium to produce a detectable alpha particle.

[0004] In this section, the inventors introduce hydrogen-lithium fusion and contrast it with traditional hot and cold fusion efforts. In relation to the current fusion research programs that are in process today, a Hydrogen-Lithium Fusion Device made according to the present invention has a very different implementation for achieving nuclear fusion. The Hydrogen-Lithium Fusion Device is believed to enable a rate of fusion efficiency that is close to 100% and the energy of the fusion byproducts to be harnessed without heat effects.

[0005] Applicants wish to emphasize that in this application various theories will be discussed and positions will be taken with regard to various aspects of the invention. These statements and positions will be based upon the novel theories discussed below, such as in paragraphs [0039] through [0047]; [0130] through [0149] and [0180] through [0232], and also

on the experiments conducted by the inventors and discussed in paragraphs [0049] through [0069] and [0077] through [0129]. Statements that do not find support in the experiments are necessarily theoretical and not based upon specific experimental findings. For example, applicants' belief that the rate of fusion efficiency will be close to 100% is based upon the novel theories associated with the invention and upon the belief that the experimental results tend to support this position. Also, the experiments discussed at paragraphs [0180] through [0177] have not been conducted and the inventors' projected results describe what is expected to occur.

[0006] Research institutes and laboratories that work on conventional (hot) fusion have been taking a very different approach. This approach has been to mimic the fusion reaction inside a star by using deuterium and tritium ions. The goal of these reactions is to harness the heat energy from extra neutrons that are expelled at high velocity from this reaction type. To date, no experiment has been able to harness energy or sustain a fusion reaction past the break even point of energy consumption.

[0007] To the inventors' knowledge, no research institute has ever been able to utilize the two-step method for hot hydrogen fusion in a practical and economical way. The second step, which involves the heating of water from the fusion reaction, has not been attempted because the first step for conventional fusion containment has not been adequate.

[0008] So-called cold fusion does not require the extremely high temperatures and plasma containment necessary for hot fusion. Rather, cold fusion relies on electrolytic techniques to promote fusion using heavy water (D_2O). Cold fusion approaches are still being investigated. To the inventors' knowledge, there have been no definitive positive results from cold fusion.

[0009] A Hydrogen-Lithium Fusion Device, hot fusion, and cold fusion approaches are summarized and compared below.

[0010] COMPARISON OF FUSION APPROACHES

Hydrogen-Lithium Fusion Device	Hot Fusion	Cold Fusion
Fuel: Hydrogen gas and lithium	Fuel: Deuterium and tritium	Fuel: Heavy water (D_2O)
Fusion Creation: Accelerated hydrogen ion beam striking a lithium target	Fusion Creation: Magnetic pulsing and laser heating	Fusion Creation: D_2O electrolysis
Temperature: Room temperature	Temperature: 100 million °C	Temperature: Room temperature
Containment: Vacuum chamber	Containment: Magnetic bottle	Containment: None
Protective Shielding: Helium ions	Protective Shielding: Neutrons	Protective Shielding: Neutrons

[0011] The opportunities presented by a new approach to fusion are virtually limitless. They include propulsion and power generation. They may extend to warping space with gravity effects of the new fusion.

SUMMARY

[0012] The Hydrogen-Lithium Fusion Device ("HLFD") is a revolutionary new device that includes a proton accelerator, lithium target, and a target support or holder, preferably of specified geometry. The HLFD enables a proton-lithium fusion efficiency that is expected to be close to 100% with the fusion byproducts exiting the lithium target without transferring significant fusion energy to the target as heat.

[0013] The Hydrogen-Lithium Fusion Device is expected to produce proton-lithium fusion at very high efficiencies. Hydrogen gas is supplied to an ion accelerator which creates a proton beam with the desired beam energy and current. The proton beam is aimed at a lithium target, typically a lithium foil target, supported by a target holder, the target holder preferably having specific physical characteristics. The incoming protons enter the lithium target and undergo continual small random direction changes until nuclear fusion occurs. The helium ion fusion byproducts undergo similar continual small random direction changes until they exit the target without transferring significant energy to the target as heat.

[0014] An example of a target assembly for use with a proton generator of the type capable of generating a proton beam along an axis, the proton beam having a transverse dimension at a target position, comprises a target support and a lithium target. The target support is locatable at the target position. The lithium target has front and back surfaces

supported by the target support. The target has a maximum target thickness, measured generally parallel to the axis, less than the first zero of the J_0 Bessel function times the gravity wavelength of the proton. The target support is configured so that the target has exposed front and back target surfaces free of target support material. A projection of the exposed front surface onto the exposed back target surface defines the target area as an intersection between areas of the exposed front and back target area. In some examples the target support has a minimum thickness of at least 2.4 mm measured generally parallel to the axis, and more preferably has a minimum thickness of at least 3.14 mm measured generally parallel to the axis. In some examples the target has a minimum transverse dimension of at least 19.2 mm plus the transverse dimension of the proton beam.

[0015] An example of a method for making a target assembly for use with a proton generator of the type capable of generating a proton beam along an axis, the proton beam having a transverse dimension at a target position, is carried out as follows. A lithium target material having front and back surfaces is selected. The target material at the target area has a maximum target thickness, measured generally parallel to the axis, less than a the value of the first zero of the J_0 Bessel function times the gravity wavelength of the proton. A target support is chosen. The target material is mounted to the target support to create a target assembly locatable at the target position. The selecting, choosing and mounting steps are carried out so that the target assembly comprises a lithium target having exposed front and back target surfaces free of target support material. A projection of the exposed front surface onto the exposed back target surface defines the target area as an intersection between areas of the exposed front and back target area. In some examples the target support choosing step is carried out so that the target support has a minimum thickness of at least 2.4 mm, and more preferably at least 3.14 mm, measured generally parallel to the axis.

[0016] Particular aspects of the present invention are described in the claims, description and drawings.

BRIEF DESCRIPTION OF THE DRAWINGS

[0017] FIG. 1 is a simplified view of an ion accelerator directing a proton beam at an exploded orthographic view of a target assembly;

[0018] FIG. 2 is an isometric view of the ion accelerator and target assembly of FIG. 1;

[0019] FIG. 3 is a simplified view of a six-way vacuum chamber;

[0020] FIGS. 4 and 5 are front and back views of the lithium target of FIG. 2 after a test procedure;

[0021] FIG. 6 is a simplified view of a target assembly showing the location of a proton beam and an exit ring on the target area;

[0022] FIG. 7 is a simplified cross-sectional view of the structure of FIG. 6;

[0023] FIG. 8 as a view similar to that of FIG. 7 in which the target support is in the form of a ring having a circular cross-sectional shape;

[0024] FIG. 9 shows a target support similar to that of FIG. 7 but in which the target material is secured to one side of the target support;

[0025] FIG. 10 is a simplified view of a further example of a target assembly in which the target material is supported by and spooled on and off of pickup and supply spindles;

[0026] FIGS. 11, 12, 13, 14, 15, and 16 are simplified schematic illustrations of the Fusion Heat Engine and are provided to help explain the orientation and geometric parameters for the Fusion Heat Engine. Like elements may be referred to with like reference numerals.

[0027] FIG. 11 presents examples of the geometric configurations derived from the gravity theory for conduits and other components of a heat collection device to preserve the high fusion efficiency that prevents the destruction of the HLFD's lithium target by heat.

[0028] FIG. 12 is a simplified view of an ion accelerator directing a proton beam at an exploded orthographic view of a target assembly next to a heat collection device.

[0029] FIG. 13 is an isometric view of the ion accelerator, target assembly, and heat collection device of FIG. 5.

[0030] FIG. 14 is a simplified view of a six-way cross vacuum chamber with HLFD and heat collection device.

[0031] FIG. 15 is a cross section view of a spherical vacuum chamber containing conduits of a heat collection device.

[0032] FIG. 16 is an example of a configuration for the Fusion Heat Engine. In this example, conduits are used to heat a liquid or condensate which then is expelled from a nozzle which turns a turbine and generator.

[0033] FIGS. 17, 18, and 19 are simplified schematic illustrations of the Electrogravity Generator. Like elements may be referred to with like reference numerals.

[0034] FIG. 17 is a simplified view of an ion accelerator directing protons at an exploded orthographic view of the HLFD with a lithium target and a pair of conducting elements.

[0035] FIG. 18 is a simplified view of a conducting element with ohmic contacts used in an Electrogravity Generator.

[0036] FIG. 19 is an array of conducting elements of FIGS. 17 and 18 surrounding a HLFD.

DETAILED DESCRIPTION

[0037] The following detailed description is made with reference to the figures. Preferred embodiments are described to illustrate the present invention, not to limit its scope, which is defined by the claims. Those of ordinary skill in the art will recognize a variety of equivalent variations on the description that follows.

[0038] This work stems from a fundamental unanswered question in physics. The question is where kinetic energy is stored. The classical and relativistic formulas for kinetic energy are well known. However, after searching the physics literature, the inventors could find no definitive answer as to where kinetic energy is actually stored; nor could the inventors answer a follow-up question: how does the storage of kinetic energy affect gravity? In addition to the literature search, the inventors talked to numerous physicists including a Nobel Prize winner. None could provide an answer to the kinetic energy storage question; the Nobel laureate said that this was a profound question to which he did not know the answer.

[0039] It is the inventors' belief that kinetic energy is stored in a field and that the storage of kinetic energy satisfies Einstein's mass-energy equivalence. As a result, the inventors looked for a mass density function that when integrated over the entire fabric of space would result in mass-energy equivalence. This process led to the development of the technical paper, "Gravity Theory Based on Mass-Energy Equivalence" and the disclosures herein. Subsequent to filing of the priority applications, the inventors' gravity theory published as, "Gravity Theory Based on Mass-Energy Equivalence" Acta Physica Polonica B 39, 2823 (2008) The inventors' gravity theory is reproduced at the end of this Detailed Description, starting at paragraph **[0256]** before the claims.

[0040] The Hydrogen-Lithium Fusion Device does not require additional containment beyond the vacuum chamber, nor does it initiate fusion through heat. Thus the problems of current hot fusion research programs are not present in the Hydrogen-Lithium Fusion Device.

[0041] In relation to the current fusion research programs, the Electrogravity Generator application described later has a very different implementation for achieving energy production. It is believed that the energy harnessed by the Electrogravity Generator is a one step process that transfers the kinetic energy released by proton-lithium fusion directly into DC electric power via electron vibration by gravity waves. The Gravity Portal and Gravity Propulsion Engine sections of this disclosure also described later are completely novel. To the inventors' knowledge, there are currently no other research projects or inventions which try to create and utilize gravity as a means for communication, transport, or propulsion.

CONCEPT OF HYDROGEN-LITHIUM FUSION DEVICE

[0042] The reader should understand the sense in which "fabric of space" is used in this disclosure. Space is sometimes defined as a three-dimensional expanse in which all matter is located and all events take place, extending in all directions and variously described as extending indefinitely or as finite but immeasurably large. Many people think of space or outer space as emptiness between stars. Astrophysicists and others do not fully understand the composition of the space between stars. Some believe that particles and anti-particles are continuously created and annihilated in this space, which requires that there be more to space than emptiness. Reference in this disclosure to the fabric of space includes the energy or essence of space, beyond the nothingness that people think of as outer space.

[0043] The Hydrogen-Lithium Fusion Device presents a practical application of these inventors' gravity theory. In this theory, the rest mass and kinetic energy of an object separately distort the fabric of space according to mass-energy equivalence. Gravitational attraction between two objects results from the interaction of their mass density fields integrated over the entire fabric of space. The gravity experienced by each object is dependent on its own gravity wavelength.

[0044] The gravity theory predicts two types of gravity. Type I gravity reduces to classical gravity in the appropriate limits. It also includes a set of eight logarithmic singularities in the gravity force when the masses are equal or under special circumstances. Type II gravity is a new form of gravity. It includes an extremely strong wave gravity arising from a first-order singularity in the gravity potential that enables, for example, a moving helium ion to vibrate electrons or the units of the fabric of space. Type II gravity also enables a highly relativistic small object or units of the fabric of space to exert a very strong classical-type force on a large object.

[0045] The Hydrogen-Lithium Fusion Device creates the well-known hydrogen-lithium fusion reactions that release the indicated kinetic energies.

$$p + {}^{6}Li \rightarrow {}^{3}He\ (2.3\ MeV) + {}^{4}He\ (1.7\ MeV)$$

$$p + {}^{7}Li \rightarrow {}^{4}He\ (8.6\ MeV) + {}^{4}He\ (8.6\ MeV)$$

[0046] The HLFD uses well-known ion accelerator technology to create a beam of protons. The beam of protons then strikes a lithium target which is held by a target holder. The geometry of the lithium target and the target holder as derived from the gravity theory enables a

high fusion efficiency that can be close to 100%, while enabling the fusion byproducts to exit the lithium target without transferring significant fusion energy to the target as heat.

[0047] In the sections that follow, this disclosure will present three further applications of the Hydrogen-Lithium Fusion Device: the Electrogravity Generator, the Gravity Portal, and the Gravity Propulsion Engine.

EXPERIMENTAL PROOF

[0048] The inventors conducted a set of experiments to provide experimental proof of the feasibility of the Hydrogen-Lithium Fusion Device. The experiments used a beam of protons, a lithium target, and a specially designed target holder. The equipment is summarized in the table below:

[0049] EQUIPMENT FOR EXPERIMENTAL PROOF

FACILITY

- Space Environmental Effects Facility, Marshall Space Flight Center, Huntsville, Alabama.

Ion Accelerator

- Pelletron series ion accelerator.
- Proton beam from commercially available hydrogen gas.
- Beam energy up to 400 keV.
- Beam current between 10 and 40 μA.
- Target area ending in a steel six-way cross vacuum chamber.

Targets

- 99.9% pure commercially available lithium foils.
- 1.75 x 1.75 inches in area.
- 50, 100, and 250 microns thick.

Target Holders

- Two aluminum plates with circular center holes sandwich the lithium foil target.
- Circular center hole has a diameter greater than the diameter of the proton beam.
- Aluminum plates 1 and 5 mm thick.
- 5 mm thick aluminum plates have rounded or otherwise beveled edges.

Protective Shielding

- Steel six-way cross vacuum chamber provides protective shielding since fusion byproducts are helium ions (alpha particles).

[0050] During the periods March 12 to March 15, 2007 and June 7 to June 11, 2007, the inventors as well as other personnel from Unified Gravity Corporation (UGC) performed a series of hydrogen-lithium fusion experiments at NASA's Marshall Space Flight Center's Space

Environmental Effects Facility in Huntsville, Alabama. The facility was operated by personnel from Qualis Corporation, Huntsville, Alabama.

[0051] In the experiments, an ion accelerator 2, see FIGS. 1 and 2, using hydrogen gas as its ion source created a proton beam 16 with the 300 keV ion energy that was used to create proton-lithium fusion. The proton beam 16 was aimed at a target assembly 10 comprising a target support or target holder 12 supporting lithium target material 14, also recalled lithium foil 14 within a steel six-way cross vacuum chamber 6 as shown in FIG. 3.

[0052] Since the fusion byproducts of proton-lithium fusion are helium ions, no radiation shielding beyond the steel six-way cross vacuum chamber 6 was used.

[0053] The experiments explored the efficiency of the hydrogen-lithium fusion reaction as a function of the geometry of the lithium target 8 and the target holder 12.

[0054] The geometry of the lithium target 8 is important in that if the lithium target is a foil with no backing plate, an incoming proton experiences Type II gravity exerted by the lithium target nuclei in a ring on each side of the foil 14 approximately 2.4 mm from the proton. The Type II gravity results in continual small random momentum additions to the 300 keV proton's original momentum and enables the proton to sweep out a much larger area through the lithium foil than a single proton diameter. As a result, the probability that a proton will randomly walk into and initiate fusion with a lithium nucleus can be close to one.

[0055] The inventors predicted that the thickness of the lithium foil 14 should be less than 2.4 mm. If the thickness is greater than 2.4 mm, then the Type II gravity is only exerted by the lithium target nuclei in the 2.4 mm ring on the front side of the lithium target. This situation may reduce the proton energy below the threshold for proton-lithium fusion, resulting in a proton transferring its energy into heat in the lithium target, and may lead to melting of the lithium target.

[0056] The geometry of the lithium target holder 12 is important in that if the incoming protons experience Type II gravity exerted by the target holder nuclei, the protons will experience large deflections as they approach the lithium nuclei. The deflection of the protons by the target holder nuclei then results in the transfer of proton energy into heat in the lithium target 8. Significant heat transfer by protons results in the melting of the lithium target 8.

[0057] If the thickness of the target holder 12 experienced by the proton is greater than π (3.14...) mm, the proton will not experience Type II gravity exerted by the target holder nuclei.

[0058] In the experiments, three lithium foil target thicknesses and two target holders were used. The experiments group into three distinct test categories that are summarized below.

[0059] PARAMETERS FOR EXPERIMENTAL TESTS

Test	Lithium Target Thickness	Target Holder Plate Thickness	Total Test Duration	Lithium Target Disposition
1	50 microns	1 mm	1 second	Melted
2	100 microns	5 mm	35 minutes	No damage
3	250 microns	5 mm	2.6 hours	No damage

[0060] The smaller target holder 12, used for Test 1, consisted of two 7.6 cm x 7.6 cm x 1 mm aluminum plates each with a 3.8 cm diameter center hole. The larger target holder 12, used for Tests 2 and 3, consisted of two 7.6 cm x 8.9 cm x 5 mm aluminum plates each with a 3.2 cm diameter center hole. Edges of the larger target holder were rounded or otherwise beveled to remove all sharp corners.

[0061] The lithium target material 14 was foil 4.4 cm x 4.4 cm square with thicknesses of 50, 100, and 250 microns. The lithium target material 14 was placed between the front and back members 18, 20 of the target holder 12.

[0062] In the first fusion test, the smaller target holder with a 1 mm plate thickness was used with a lithium target thickness of 50 microns. A proton beam 16 measuring 1 cm diameter and having 307 keV proton energy and 10, 15, and 20 μA beam currents was used for initial beam alignment. During this alignment protocol, the proton beam melted a large hole in the lithium target 8, destroying it.

[0063] Since 1 watt of power is delivered per 100 keV proton energy and per 10 μA beam current, the alignment protocol delivered 3, 4.5, and 6 watts of power into the lithium target 8. Since the melting point of lithium is 180 degrees C, the maximum temperature rise in the lithium can be only 160 degrees C. If all beam energy is delivered as heat to the lithium target 8, a beam diameter of 1 cm for the proton beam 16 results in a 150 degree C temperature rise per second per watt of beam power delivered into the 1 cm beam cylinder. The corresponding heat diffusion rate from the 1 cm beam cylinder to the target holder 12 is 0.1 watts per 20 degree C temperature rise in the beam cylinder 16, giving a maximum diffusion rate of 0.8 watts (0.1 x 160/20) from the beam cylinder 16 to the target holder 12. If a very low level of fusion occurs, the lithium target 8 melts in less than a second. This happens since even the lowest alignment power level of 3 watts will result in a potential 330 (2.2 x 150) degrees C temperature rise per second in the portion of the lithium target 8 covered by proton beam 16 and extending the thickness of the target, sometimes called the beam cylinder.

[0064] These first test results are then consistent with the work of Herb who found very low levels of fusion taking place. Following Herb, one expects that a test generates heat instead of fusion and melts the target. Herb avoided melting the lithium in his target by using an extremely low beam current (10^9 protons/second or 0.00016 uA) and a backing plate to dissipate heat from the target.

[0065] In our second fusion test, the larger target holder 12 with a 5 mm plate thickness was used with a lithium target material 14 having a thickness of 100 microns. A proton beam 16 measuring 1 cm diameter, having 307 keV proton energy and having 10, 15, and 20 μA beam currents, was used for initial beam alignment. During this alignment, the proton beam 16 did not damage the lithium target 8. The proton beam diameter was then increased to 2.5 cm and the beam current to 40 μA. The lithium target 8 was bombarded with protons for 35 minutes without damage.

[0066] For the 100 micron lithium target 8 used in the second fusion test, an alignment beam diameter of 1 cm was expected to produce a 75 degrees C temperature rise per second per watt of beam power delivered into the beam cylinder. The corresponding heat diffusion rate from the 1 cm beam cylinder to the target holder 12 was calculated to be 0.3 watts per 20 degree C temperature rise in the beam cylinder. Allowing a maximum 160 degree C rise in temperature, the maximum heat diffused from the beam cylinder to the target holder 12 is 2.4 watts (0.3 x 160/20). Since the alignment protocol at 300 keV and 20 μA delivers 6 watts to the 1 cm beam cylinder, a maximum of 40% (2.4 watts/6 watts) of the beam power can be dissipated as heat. This means that 60% or more of the beam protons, based on these heat flow calculations, must undergo fusion or the target melts.

[0067] In our third fusion test, the larger target holder 12 with a 5 mm plate thickness was used with a lithium target 8 having a thickness of 250 microns. A proton beam 16 measuring 1 cm diameter and having 307 keV proton energy and 15 μA beam current was used for initial beam alignment. During this alignment, the proton beam 16 did not damage the lithium target 8. The proton beam diameter was then increased to 2.5 cm and the beam current to 36 μA. The lithium target was used for a total proton bombardment time of 2 hours and 35 minutes with some discoloration but without damage. The front and back of the 250 micron lithium foil used during the third test in the larger target holder before and after proton beam bombardment is shown in FIGS. 4 and 5 and illustrates the lack of damage to lithium target 8.

[0068] Since the thickness of the lithium target 8 in the third fusion test is 250 microns with the same target holder as in the second fusion test, the heat flow calculations do not require a larger efficiency than the 60% required by the second fusion test.

FURTHER DESCMPTION OF TARGET ASSEMBLY

[0069] FIGS. 6 and 7, which are simplified, schematic illustrations of target assembly 10, are provided to help explain the construction parameters for the target assembly. Like elements may be referred to with like reference numerals. Target assembly 10 includes a target support 12 supporting lithium target material 14. Target support 12, in this example, includes front and back members 18, 20 which capture the peripheral edge 22 of target material 14 therebetween. Front and back members 18, 20 have aligned circular openings 24, 26 to create exposed front and back target surfaces 28, 30 and thus a target area 32 for proton beam 16 which is coextensive with front target surface 28. The edges of target support 12, especially the outer edges, are rounded or otherwise beveled with a radius of π (3.14. ..) mm for enhanced efficiency

[0070] Proton beam 16 has an average transverse dimension 34 centered on beam axis 36. Beam axis 36 is typically generally centered within target area 32 and is also generally perpendicular to target area 32. As discussed herein, protons impacting target area 32 undergo fusion and the resulting helium ions are influenced by lithium ions within 9.6 mm. Accordingly, exit of the helium ions is enhanced, and therefore it is preferred, that lithium target material 14 extends at least 9.6 mm from the periphery of proton beam 16. This creates what is called an exit ring 38 centered on axis 36. Exit ring 38 has a diameter 40 equal to transverse diameter 34 plus 2 times 9.6 mm. For example, assume a circular target area 32 having a diameter of 32 mm and a proton beam 16 having a diameter of 9.5 mm, exit ring diameter 40 would equal 28.7 mm. Therefore, so long as proton beam 16 is generally centered within target area 32, the entire exit ring 38 will lie on target area 32. Exit ring 38 can extend onto target support 12 so long as the exit ring lies on target material 14.

[0071] FIG. 15 illustrates an alternative example in which target support 12 comprises circular, ring-like front and back members 18, 20 instead of the rectangular front and back members 18, 20 of FIGS. 1 and 2.

[0072] FIG. 9 shows another example of a target assembly 10 similar to that of FIGS. 6 and 7 but in which target material 14 is mounted to the front of target support 12. In this case exposed front target surface 28 is larger than exposed back target surface 30. The front and back target surfaces 28, 30 define an intersection, the intersection defining target area 32 along front target surface 28. Accordingly, it is the projected intersection of exposed front and back target surfaces 28, 30 that define target area 32 in the manner of a Venn diagram.

[0073] FIG. 10 shows a further example in which target support 12 does not circumscribe target area 32. Rather, target support 12 includes pickup and supply spindles 42, 44 on which

target material 14 is wound. This type of target support 12 may be useful to permit new target material to be quickly and easily provided by simply unrolling new, unused target material 14 from supply spindle 44 and rolling used target material 14 onto pickup spindle 42. Additional target support structure may be used in conjunction with spindles 42, 44 to provide the necessary or desirable support for target material 14.

[0074] Other types of and configurations for target supports 12 can also be used. Typically, target supports are configured to create exposed, generally aligned front and back target surfaces 28, 30 that are free of target support material.

[0075] As discussed elsewhere herein, the thickness of target material 14, measured generally parallel to axis 36, at target area 32 has been determined to be less than 2.4 mm. It is believed that it is important that the thickness of support 12, or at least that portion of support 12 adjacent to target area 32, be greater than 3.14 mm; the determination of this minimum thickness of support 12 is based upon the maximum distance between zeros of the J_0 Bessel function. However a smaller minimum thickness of less than 3.14 mm but at least 2.4 mm may be used with some reduction in efficiency, but in certain configurations may lead to melting of the lithium target. This smaller minimum thickness is based upon the minimum distance between zeros of the J_0 Bessel function.

DISCUSSION OF EXPERIMENTAL RESULTS

[0076] In general, each fusion reaction results in one of the two helium ions passing through the lithium target. The classical, predicted stopping distance of an 8.6 Mev helium ion in lithium is 180 microns. In the second fusion test in which the lithium target is 100 microns thick, conventional theory predicts that about ⅘ (100/180) of the fusion energy (or ⅘ of the total fusion energy) will be transferred to the target as heat. If this happened, the lithium target would melt in less than a second since ⅘ of the total fusion energy of a 300 keV 40 μA beam at 0.6 fusion efficiency is 100 watts and results in a 270 degrees C temperature rise per second. In the third fusion test in which the lithium target is 250 microns thick, conventional theory predicts that about ⅘ of the total fusion energy will be transferred to the target as heat. Again, the lithium target would melt in less than a second since ⅘ of the total fusion energy of a 300 keV 36 μA beam at 0.6 fusion efficiency is 200 watts and results in a 220 degrees C temperature rise per second.

[0077] According to conventional theory, the lithium target will melt either because the proton energy is transferred to the lithium foil as heat since the fusion efficiency is small or

because the helium ion fusion byproduct energy is transferred to the lithium foil as heat if the fusion efficiency is large.

[0078] The longevity of the lithium target at such a high proton beam current provides experimental evidence for the feasibility of the Hydrogen-Lithium Fusion Device.

FURTHER EXPERIMENTAL VERIFICATION

[0079] An additional experimental test (#4) was performed in October, 2007 to provide positive evidence of the production of helium ions by the HLFD prototype. The method was to capture helium ions emitted by the HLFD in a shielded Faraday Cup and measure the helium ion DC current in the Faraday Cup.

[0080] The inventors constructed a shielded aluminum Faraday Cup in which the thicknesses of all aluminum, ceramic, and Teflon components were greater than about 3.14 mm as suggested by the inventors' gravity theory to enable high fusion efficiency. The Faraday Cup had an inner length to diameter ratio of 5:1 due to size limitations of the vacuum chamber. The 5.1 cm inner diameter of the Faraday Cup was larger than the 3.2 cm diameter of the exposed lithium target and supports capture of half of the helium ions expelled in a spherically symmetric manner resulting from the 2.5 cm diameter proton beam impinging the lithium foil target.

[0081] The Faraday Cup was positioned horizontally behind the HLFD by an aluminum frame constructed of bars whose thicknesses also exceeded about 3.14 mm. The Faraday Cup was placed directly behind the HLFD and in close proximity to the lithium foil so that the lithium foil and target holder blocked any protons in the proton beam from entering the Faraday Cup.

[0082] The inner collection cylinder of the Faraday Cup was connected to an electrical feed-through connector in a vacuum chamber flange and then to ground through an ammeter located next to the six-way cross vacuum chamber. The outer shield cylinder was directly grounded to the exterior of the six-way cross vacuum chamber.

[0083] The display of the ammeter during the test was recorded by a video camera. The test used a proton beam with a 330keV proton energy and 32μA beam current striking the HLFD' s 250 micron thick lithium foil target. The October 2007 testing parameters and results are summarized below.

[0084] PARAMETERS AND RESULTS FOR OCTOBER 2007 EXPERIMENTAL TEST

Test	Lithium Target	Target Holder	Total Test	Faraday	Lithium Target

	Thickness	Plate Thickness	Duration	Current	Disposition
#4	250 microns	5 mm	10.3 minutes	9.9μA	Discolored, intact

[0085] A Residual Gas Analyzer (RGA) was used to measure the relative amounts of helium in the vacuum chamber when the proton beam was not incident on the foil compared to when the proton beam was impinging the foil.

DISCUSSION QF EXPERIMENTAL RESULTS

[0086] The capture of the helium ion fusion byproducts in the Faraday Cup is hypothesized to produce a measurable DC current. If the proton-lithium fusion reaction is 100% efficient, a proton beam current of 32μA produces a 128μA helium ion current (32μA x 2 helium ions x 2 helium charges / 1 proton charge). Assuming the helium ions are expelled in a spherically symmetric distribution, the maximum current in the Faraday Cup at 100% collection efficiency is 64μA (128μA x 0.5 coverage). The DC current obtained in the Faraday Cup from the recorded data as a function of elapsed time is shown in FIG. 1.

[0087] There are several results to be noted in FIG. 1. The current dropped to zero at an elapsed time of 294 seconds when the beam was blocked by an upstream Faraday Cup to refocus the proton beam. Thereafter, the current rose as the proton beam was incident on the center of the target. The current reached a plateau at an elapsed time of 448 seconds once the proton beam was centered on the foil.

[0088] The maximum current recorded by the ammeter connected to the Faraday Cup was 11.6μA, see FIG. 2, and the average current at the plateau was 9.9μA. This average current results in a lower bound of approximately 15.5% (9.9μA / 64μA) for the proton-lithium fusion efficiency. We hypothesize that the large 5.1 cm inner diameter of the Faraday Cup decreased its collection efficiency.

[0089] In addition to the DC current measured by the Faraday Cup, fusion was also indicated by a fivefold rise in helium levels within the vacuum chamber as recorded by the RGA. It is unclear how the interaction of helium ions with the vacuum chamber walls affects the concentration of helium in the vacuum chamber, so the RGA data was used only as an indicator that fusion was occurring.

[0090] When the test was completed and the Faraday Cup removed from the ion accelerator, it was hot to the touch, confirming the transfer of fusion energy into heat.

[0091] The total time of proton bombardment during test #4 was 10 minutes and 20 seconds. The lithium target in the HLFD showed signs of discoloration due to proton

bombardment, but remained intact (FIG. 3) as in tests #2 and #3. For that reason, as discussed in international patent application # PCT/US07/0 18256, heat flow calculations indicate that proton-lithium fusion efficiency exceeds 60%.

[0092] Therefore the results of experimental test #4 as well as tests #2 and #3 provide evidence that the proton-lithium fusion efficiency using the inventors' HLFD is far greater than the experiments of Herb and others have indicated. These experimental results then provide proof of the feasibility of the HLFD and lend support to the inventors' gravity theory based on mass-energy equivalence.

[0093] In addition, the results of experimental test #4 provide proof of the feasibility of the Fusion Heat Engine. The capture of each helium ion fusion byproduct by the Faraday Cup transfers fusion kinetic energy into heat in the Faraday Cup. Using the lower bound of 15.5% for the fusion efficiency, a proton beam current of 32 μA (32 * 6.2 10^{12} protons/sec), and an average fusion event energy of 16.2 MeV, the fusion kinetic energy transferred into heat exceeded 5.0 10^{14} MeV/sec (0.155 * 32 * 6.2 10^{12} * 16.2) = 80 joules/sec = 80 watts. Since the experimental results demonstrate that the proton-lithium fusion efficiency can be close to 100% and that the fusion energy can be transferred into heat, the Fusion Heat Engine device described below can achieve and surpass the break-even point of energy production.

ADDITIONAL EXPERIMENTAL VERIFICATION

[0094] In April 2008 under a Space Act Agreement with NASA, UGC performed 4 additional experimental tests referred to as tests #5-8. In test #5, the Faraday Cup used in test #4 and subsequently in test #8 was calibrated. In tests #6-7, control experiments were performed that included components used in the previous tests #1-4. In test #8, the Faraday Cup was used to measure both current and heat from fusion byproducts.

[0095] Tests #5-8 provide additional experimental proof of the feasibility of the Hydrogen-Lithium Fusion Device (HFLD) and its applications. The facility, ion accelerator, targets, target holders and protective shielding were substantially as described above, except that the beam energy and current were increased in some runs to 700 keV and 42 μA. In addition, the following measurement appartus were used:

Faraday Cup

- 10.2 cm diameter aluminum cylinder as outer shield, 1.3 cm sidewalls, 26.7 cm long with beveled edges
- 6.4 cm diameter aluminum cylinder as inner collector, 0.64 cm sidewalls, 25.4 cm long with beveled edges
- Ceramic bars to isolate the inner cylinder from the outer cylinder

- Outer cylinder grounded
- Inner cylinder connected to ground through an ammeter

Measurement Devices

- Fluke Ammeter
- Fluke Infrared Thermometer

[0096] In tests #5-8, an ion accelerator using hydrogen gas as its ion source created a proton beam with an energy between 300 and 700 keV in order to produce proton-lithium fusion. In test #5, the proton beam was directed into the Faraday Cup used in test #4 but without any target. In test #6, the target was a lithium foil contained between two 1 mm thick aluminum plates and was similar in dimensions to the target used by Herb. In tests #7-8, the target satisfied our specifications for a Hydrogen-Lithium Fusion Device (HFLD).

[0097] When used, the Faraday Cup was placed horizontally directly behind and close to the lithium foil and target holder, which completely shielded the inner cylinder of the Faraday Cup from the proton beam. The inner cylinder was connected to a BNC electrical feed through connector in the side flange of the six-way cross vacuum chamber and then to an ammeter and to ground. The outer shield cylinder of the Faraday Cup was also connected to a BNC electrical feed through connector and then directly to ground. The ammeter display was recorded with a digital video camera during the entire test.

[0098] Since the byproducts of hydrogen-lithium fusion are helium ions, no radiation shielding beyond the six-way cross vacuum chamber was used.

[0099] Test #5 involved the calibration of the UGC Faraday Cup as compared to the National Electrostatics Corporation (NEC) Faraday Cup which is used to measure the proton beam current inside the Pelletron ion accelerator. The UGC Faraday Cup that was used in the previous test #4 was placed horizontally within the vacuum chamber such that the proton beam impinged on the back of the UGC Faraday Cup since there was no lithium target or holder. An aluminum frame constructed of bars whose thicknesses exceeded about 3.14 mm supported the UGC Faraday Cup.

[00100] The UGC Faraday Cup current reading was taken with the same ammeter used in the control room to view the proton beam current of the Pelletron ion accelerator. When the upstream NEC Faraday Cup was moved from the path of the proton beam, the readings on the meter switched from the upstream NEC Faraday Cup to the UGC Faraday Cup.

[00101] Test #5 was performed in three steps with the proton beam energy set to 310 keV for all steps. The first step used a 1 cm diameter proton beam with an 11.8 μA current as detected by the upstream NEC Faraday Cup. The UGC Faraday Cup indicated a proton beam

current of 11.8 μA. The second step used a 2.5 cm diameter proton beam with a 21.1 μA current as detected by the upstream NEC Faraday Cup. The UGC Faraday Cup indicated a proton beam current of 21.1 μA. The third step used a 2.5 cm diameter proton beam with a 30.1 μA current as detected by the upstream NEC Faraday Cup. In this case, the UGC Faraday Cup indicated a proton beam current of 30.3 μA.

[00102] The results of the UGC Faraday Cup calibration test show that the UGC Faraday Cup is 100% efficient. The difference in step three of test #5 can be attributed to the proton beam not being completely centered on the smaller upstream NEC Faraday Cup at high current.

[00103] Test #6 was a control experiment for test #3 and used a 250 micron thick lithium foil in a thin target holder similar to the one used by Herb. Test #3 also used a 250 micron thick lithium foil, but in a target holder conforming to the HLFD specifications. To produce an exact control of test #3, copper conducting elements with ceramic holders were placed in four flanges of the vacuum chamber as to comply with a secondary experiment that was performed in conjunction with test #3. The beam alignment protocol used for test #3 was used in test #6 with the proton beam energy set to 307 keV.

[00104] The first impingement used a 1 cm proton beam diameter and a 10 μA proton beam current and lasted for 1 minute. A visual inspection then revealed that the proton beam left a visible discoloration on the lithium foil but the lithium foil did not blister. The second impingement used a 1 cm diameter proton beam and a 15 μA proton beam current and also lasted for 1 minute. A second visual inspection then revealed that the lithium foil had visible blistering. The third impingement used a 1 cm diameter proton beam and a 20 μA proton beam current and lasted for 10 minutes. A third visual inspection then revealed that the lithium foil had increased visible blistering, but was intact.

[00105] The proton beam diameter was then increased to 2.5 cm and the proton beam current to 26 μA for a period of 41 minutes. A visual inspection then revealed that the lithium foil was blistered but intact.

[00106] If no fusion occurs, heat flow calculations indicate that for a 250 micron thick target with a 1 cm proton beam diameter, the lithium foil target melts if the proton beam current exceeds 25 μA. To test that little or no fusion was occurring, the proton beam diameter was decreased to 1 cm while the proton beam current remained at 26 μA. After a period of 5 minutes, a visual inspection revealed that the target indeed had a large hole melted through the area where the proton beam impinged the lithium foil. These results are also consistent with results of test #1 which also used a thin target holder and the low fusion efficiency values obtained by Herb that

indicate the lithium target melts as a result of proton heating. Figure 1 shows the remains of the lithium foil after completion of test #6.

[00107] Test #7 was as a control experiment for test # 1 in which the 50 micron lithium foil melted in less than a second during the beam alignment protocol. As opposed to the thin target holder used in test #1, test #7 used a 50 micron lithium foil in the HLFD that was used in the 2007 experiments. To comply with the conditions of test #1, copper conducting elements supported by ceramic frames were placed in the four horizontal flanges.

[00108] As in test #1, the proton beam diameter was set to 1 cm, the proton beam energy to 307 keV, and the proton beam current to 10 μA. The proton beam impinged the lithium foil for 5 minutes without any sign of a hole or melting. Figure 2 was taken after this first beam impingement and shows no visible damage.

[00109] The proton beam diameter was then increased to 2.5 cm and the proton beam current to 29 μA. The proton beam impinged the foil for 11 minutes. The lithium foil was found to only be discolored with no indication of a hole or tear. Figure 3 shows the experimental setup inside the vacuum chamber.

[00110] The proton beam energy was then increased to 330 keV while the proton beam current remained at 29 μA. The beam impinged the foil for another 5 minutes. After completion of experimental test #7, the 50 micron lithium foil was extracted from the vacuum chamber and was found to have no holes. Figure 4 is a picture of the foil immediately after being removed from the vacuum chamber.

[00111] Test #8 was a reproduction of test #4 and was performed using the HLFD, a 250 micron lithium foil, and the UGC Faraday Cup. The method was to capture helium ions emitted by proton-lithium fusion in the Faraday Cup and measure the DC current resulting from the helium ions collected in the Faraday Cup. The proton beam energy was set to 700 keV and the proton beam current to 20 μA. The proton beam current averaged 21.4 μA and the proton impingement time was 9 1 minutes.

[00112] If the proton-lithium fusion reaction is 100% efficient, a proton beam current of 21.4μA produces a 85.6 μA helium ion current (21.4μA x 2 helium ions x 2 positive charges / 1 proton charge). Assuming the helium ions are expelled in a spherically symmetric distribution, the maximum helium ion current in the UGC Faraday Cup at 100% collection efficiency is 42.8μA (85.6μA x 0.5 coverage).

[00113] During all tests performed with the UGC Faraday Cup measuring helium ions created by proton-lithium fusion, the DC current detected by the ammeter was in fact always negative. This negative Faraday current can be explained by the dynamics of the fusion reaction.

[00114] When a proton fuses with a lithium nucleus, the result is the temporary creation of a beryllium ion. The increased charge of the beryllium ion is sufficient to capture an additional electron present in the conduction band of the lithium target. The beryllium nucleus then splits into two energetic helium ions that travel in opposite directions and leaves a total of four free electrons with forward momentum as imparted by the former beryllium nucleus. The momentum imparted to the electrons enables the electrons to randomly walk through the lithium foil in the same way as the helium ions and be collected in the Faraday Cup.

[00115] With half of the helium ions each having a double positive charge and four electrons with a quadruple negative charge collected in the Faraday Cup, a negative current double the proton beam current should be detected when 100% fusion efficiency is achieved. This was the case during test #8 in which a negative current close to double the proton current was measured but never exceeded.

[00116] The Faraday Cup during test #8 detected a measurable DC current in the high -μA range throughout the entire 91 minute period of proton impingement with two negative current plateaus that were close to double the proton current. The graph of the Faraday Cup current versus elapsed time is shown in Figure 5.

[00117] The maximum current in the Faraday Cup was -42.1 μA as documented in Figure 6, and the average Faraday current was -24.4 μA. This average current indicates an average proton-lithium fusion efficiency of 57% (24.4 μA / 42.8 μA). Figure 7 shows that the lithium foil target remained intact after the completion of test #8.

[00118] There are several results to be noted in Figure 5. The first plateau occurred at an elapsed time of 15 minutes reaching a Faraday current of -42.1 μA with a proton beam current of 21.6 μA. This reading indicates 97% fusion efficiency. Thereafter, the Faraday current dropped while the proton beam was still impinging the target. The Faraday current dipped to -16 μA but then steadily climbed during the remainder of the test. The Faraday current increased to -40 μA at 86 minutes and to -40.2 μA at 89 minutes, indicating fusion efficiencies of 99% and 99.5 % as the proton beam current was 20.1 μA. The parameters and results of tests #6-8 are summarized in the following table.

PARAMETERS AND RESULTS FOR APRIL 2008 EXPERIMENTAL TESTS

Test	Lithium Target Thickness	Target Holder	Total Test Duration	Lithium Target Disposition
#6	250 microns	Thin Holder < 2.4 mm	58 minutes	Melted
#7	50 microns	HLFD	21 minutes	No damage

#8	250 microns	HLFD	91 minutes	Slight crack

[00119] The temperature of the inner cylinder of the Faraday Cup was also recorded after the vacuum chamber was opened. Using a Fluke IR thermometer, the temperature of the Faraday Cup after test #8 was found to be 90 °C resulting in a temperature change $\Delta T = 70$ °C.

[00120] For a 24.4 μA average current in the Faraday Cup, the heat energy transferred by the helium ions to the aluminum inner cylinder is 98.7 watts. With an inner cylinder mass of 886.6 gm, the expected temperature change after 91 minutes is calculated to be 675 degrees C compared to the measured 70 degrees C. We suggest that the heat loss occurred through an electrically insulating Teflon disk, three Macor ceramic bars used to separate the cylinders, and a single steel screw insulated with Kapton tape between the inner and outer aluminum cylinders of the Faraday Cup. The heat energy was then transferred from the outer cylinder through the large aluminum Faraday Cup support to the vacuum chamber housing.

[00121] The properties of the four electrically insulating objects within the Faraday Cup are as follows. The PTFE Teflon disk had a 6.35 cm diameter contact area and 0.635 cm thickness with a thermal conductivity of 0.003 W/cm-K. The three Macor ceramic bars between the inner and outer cylinders were each 2.54 cm x 0.635 cm x 0.635 cm with a thermal conductivity of 0.014 W/cm-K. The steel screw had a 0.325 cm diameter shaft with 0.325 cm depth thread contact area with a thermal conductivity of 0.26 W/cm-K, and the strip of electrically insulating Kapton tape over the screw and the exposed current wire had a contact area of 0.63 cm2 and a thickness of 0.005 cm with a thermal conductivity of 0.0046 W/cm-K. As a result, the heat energy transfer from the inner to outer cylinder is calculated to be $dQ/dt = 0.96 * \Delta T$ watts.

[00122] Using a heat energy transfer of 98.7 watts from the helium ions to the inner cylinder and a 0.96 [watts/degree C] value for heat energy transfer from the inner to outer cylinder of the Faraday Cup, Figure 8 shows the calculated temperature change ΔT in the inner Faraday Cup as a function of elapsed time. The confirmation of the 70 degrees C temperature change about 5 minutes after the completion of the test #8 lends support to high fusion efficiency and heat energy transfer from the helium ion fusion byproducts to the inner cylinder of the Faraday Cup.

SOME INCONCLUSIVE EXPERIMENTS

[00123] During experiments in September 2008, several tests yielded inconclusive results. These tests were performed under a Space Act Agreement with NASA. The goal of these tests

was to produce additional successful results similar to those in April 2008. The primary equipment of the tests involved the HLFD and the UGC designed Faraday Cup. As in previous tests, the Faraday Cup was used to measure both a DC current and heat from the fusion byproducts created in the HLFD.

Result Summary of Inconclusive Tests

[00124] In all experimental tests that were performed with the UGC Faraday Cup in September 2008, a Faraday cup current in the low -nA range was indicated at the start of each test, then after about an hour of proton impingement the current would rapidly rise to the -μA range. Shortly after reaching the -μA range, an area on the lithium target began to illuminate with an intense white and quickly changed to a black spot. After each instance where an illuminated spot developed on the target, the target was visually examined and in all cases was found to have a hole. This behavior occurred in a similar location on all lithium targets used in September 2008.

[00125] Upon completion of the September 2008 test series, the interior components of the UGC Faraday Cup were examined. Examination showed that a Teflon spacer, used to isolate the inner cylinder from the outer shield cylinder, rotated 45 degrees from its original position and resulted in an exposed edge to the HLFD.

Hypothesis for Reduction of Efficiency in Fusion Initiation and Byproduct Exit

[00126] The inconclusive tests are believed to be explained by two main factors that were not anticipated by the UGC personnel and that caused the reduction in both fusion efficiency and helium ion exit efficiency.

[00127] The first factor was contamination of the lithium target surface area by oxygen and nitrogen from the laboratory atmosphere during its removal from the argon environment of the shipping container. The build up of an oxygen and nitrogen overburden created a very thin front and back plate composed of oxygen and nitrogen. The HLFD patent application predicts that an overburden layer can reduce fusion efficiency to Herb's level. The -nA Faraday cup current indicated that low levels of fusion occurred during September 2008. However, after approximately an hour of proton impingement, the current rapidly rose into the -μA range shortly before an illuminated spot would appear. This behavior of the Faraday cup current indicated that the proton beam slowly removed the overburden, which then allowed for fusion efficiency to increase to a high level.

[00128] The second factor was created by geometry of an exposed edge, which suggests edge effects play a significant role in efficiency of fusion initiation and byproduct exit from the HLFD. When an increase in fusion occurred, the ammeter rose into the -μA range shortly before the lithium developed a hole. The exposed edge of the Teflon spacer reduced the exit efficiency of the helium ions and resulted in heat transfer to the lithium target. The location of the hole in the lithium targets corresponded to the exposed edge from the Teflon spacer inside the Faraday Cup.

GENERAL DISCUSSION OF HYDROGEN-LITHIUM FUSION PRODUCTION

[00129] A proton beam derived from hydrogen gas is accelerated though well-known methods to create proton-lithium fusion. The beam of protons can be produced by an ion accelerator, ion implanter, Van de Graff accelerator, RF Quadruple accelerator, or other such device. The term ion accelerator is used as a generic term for any device that accelerates ions by any method.

[00130] The accelerated protons are aimed at a lithium target. The term lithium target is used subsequently as a generic term for a target of a specific shape, dimension, or composition that contains lithium. For example, the target can be metallic lithium, lithium oxide, or a lithium alloy. The lithium target should be a lithium foil whose thickness should be less than 2.4 mm.

[00131] The lithium target can be replenished by well-known methods. For example, a spool of lithium or lithium alloy strip can be cycled through the target holder; see, for example, FIG. 10. Another method of fuel replenishment is to turn off the device and replace lithium targets.

[00132] The target holder typically includes two plates with center holes that sandwich the lithium foil target. The thickness of each plate should exceed π (3.14…) mm and the edges of each plate should be rounded or otherwise beveled to remove sharp corners. The thickness of the target holder plates as well as the beveled edges allow the incoming protons and exiting helium ions to experience only Type II gravity exerted by the lithium target nuclei and not the target holder nuclei. The target holder can be aluminum, nickel, or any other material that can be used in a vacuum chamber and preferably conduct heat away from the lithium target.

[00133] As the protons approach the lithium target, the proton experiences Type II gravity exerted by lithium nuclei in a ring of each side of the lithium foil approximately 2.4 mm from the proton. The Type II gravity causes the proton to experience continual random momentum additions in the direction of the lithium nuclei. As a result, the probability that a proton will randomly walk into and initiate fusion with a lithium nucleus can be close to one.

[00134] A proton-lithium fusion event results in the production of two high energy helium ions. Similar to the movement of the protons in the lithium target, the helium ions also experience the continual random momentum additions from the Type II gravity exerted by the lithium nuclei, but in a ring on each side of the lithium foil approximately 9.6 mm from the helium ion. As a result, the probability that a helium ion will randomly walk out of the lithium foil can be close to one and the helium ion will exit the lithium target without transferring heat to the lithium target.

[00135] The resulting helium ions can **be** utilized as a power source for applications such **as** an electrogravity generator, gravity portal, or gravity propulsion engine.

[00136] After transferring their kinetic energy, the helium ions can be collected by well-known methods such as vacuum pump.

APPLICATION OF GRAVITY THEORY TO THE HYDROGEN-LITHIUM FUSION DEVICE

[00137] The Hydrogen-Lithium Fusion Device is predicated on a gravity theory described in a technical paper by the inventors Stephen A. Lipinski and Dr. Hubert M. Lipinski, Unified Gravity Corporation, Gravity Theory Based on Mass-Energy Equivalence, June 2007 and September 2008, much of which was submitted with provisional applications and the PCT application. This paper can be found below, preceding the claims.

[00138] According to the gravity theory based on mass-energy equivalence, the Type II gravity potential V_Q exerted by an object A on an equal or smaller size object B (e.g. a lithium nucleus on a proton, a lithium nucleus on a helium ion, a helium ion on an electron, or a helium ion on an unit of the fabric of space) is given by:

$$V_0(r_B) = -GM_A m_B \lambda_A / \lambda_B J_o(r_B/\lambda_B)/r_B (1 - v_A^2/c^2)^{-1/2} (1 - v_B^2/c^2)^{1/2} 1/\pi (1/\varepsilon |_{\varepsilon=0}),$$

where r_B is the distance of object A from object B, G is the gravitational constant, m_A is the rest mass of object A, m_B is the rest mass of object B, λ_A is the gravity wavelength of object A, λ_B is the gravity wavelength of object B, J_0 is the 0^{th} order Bessel function of the first kind, v_A is the speed of object A, v_B is the speed of object B, c is the speed of light, and $(1/\varepsilon |_{\varepsilon=0})$ is a first-order singularity.

[00139] The gravity wavelength λ_G of an object is given by $\lambda_G = N_{AG} M$ where $N_{AG} \approx 6.0 \times 10^{23}$ m/kg and M is its rest mass. For example, a helium ion has a gravity wavelength ≈ 4 mm, a proton has a gravity wavelength ≈ 1 mm, an electron has a gravity wavelength ≈ 0.55 microns, and a unit of the fabric of space has a gravity wavelength ≈ 2 mm.

[00140] Since the Type II gravity potential has a first-order singularity, the Type II gravity force experienced by object B is zero for distances less than its gravity wavelength. For distances greater than its gravity wavelength, a very large gravity force F_G occurs whenever $J_0(r_{BA}/\lambda_B)$ changes sign:

$F_{G(TB)} = Gm_A^2/\lambda_B \, Ji(r_B/\lambda_B)/r_B \, (1 - vA^2IC^2)^{JA} \, (1 - v_B^2/c^2 f \quad 1/\pi \, (1/\varepsilon \mid \varepsilon=0),$

where J_1 is the 1st order Bessel function of the first kind and $r_B/\lambda B$is a zero of the J_0 Bessel function. For example, the first zero of the J_0 Bessel function occurs at a value of $r\beta/\lambda\beta \approx 2.4$.

[00141] Since a force results in a change in momentum, the Type II gravity force imparts a momentum addition to object B in the direction of the Type II gravity force as object B moves through the zeros of the J_0 Bessel function.

[00142] Hydrogen gas and lithium are the preferred fuels for the Hydrogen-Lithium Fusion Device. The hydrogen gas is delivered to an ion accelerator 2 FIG. 1 that is aimed at a lithium target 14. The creation of a beam of ions, that is proton beam 16, is a well-known process and can be achieved with an ion accelerator, ion implanter, Van de Graff accelerator, RF Quadruple accelerator, or other such device.

[00143] As an incoming proton nears and then enters the lithium foil of the target, it experiences a Type II gravity force from each lithium nucleus on the side of the target at a distance ≈ 2.4 mm (2.4 x 1 mm) corresponding to the first zero of the Bessel function. If the distance to the side is greater than 2.4 mm, then the Type II gravity potential will include both positive and negative values, and no Type II gravity force will occur.

[00144] As a result, the proton receives momentum additions from each lithium nucleus in a ring approximately 2.4 mm from the proton on both sides of the lithium foil. Since the lithium nuclei occur at random locations in both 2.4 mm rings, the continual small random momentum additions to the 300 keV proton's original momentum enable the proton to sweep out a much larger area through the lithium foil than a single proton diameter. As a result, the probability that a proton will randomly walk into and initiate fusion with a lithium nucleus can be predicted as close to one.

[00145] Type II gravity also enables helium ions to exit the lithium target without transferring heat energy to the target. As the helium ion traverses the target, it experiences a Type II gravity force exerted by each lithium nucleus on either side of the lithium foil at a distance ≈ 9.6 mm (2.4 x 4 mm) corresponding to the first zero of the Bessel function. If the

distance to the side is greater than 9.6 mm, then the Type II gravity potential will include both positive and negative values, and no Type II gravity force will occur.

[00146] As a result, the helium ion receives a momentum addition from each lithium nucleus in a ring approximately 9.6 mm from the helium ion on both sides of the lithium foil. Since the lithium nuclei occur at random locations in both 9.6 mm rings, a helium ion will randomly walk out of the lithium target due to the continual small random momentum additions to the 8.6 Mev helium ion's original momentum.

[00147] The target holder 12 of the Hydrogen-Lithium Fusion Device does not affect an incoming proton if the Type II gravity potential exerted on the proton by the nuclei of the target holder that are in the same direction includes both positive and negative values.

[00148] This situation occurs if the thickness of the target holder in any direction as experienced by the proton is greater than the distance between two adjacent zeros of the J_0 Bessel function. The maximum distance between two adjacent zeros is π times the gravity wavelength since the J_0 Bessel function asymptotically approaches a cosine function. Hence the thickness of the target holder must be greater than approximately π mm (π x 1 mm) in order to avoid exertion of a Type II gravity force by the target holder on the proton.

GENERAL DISCUSSION OF FUSION HEAT ENGINE

CONCEPT OF FUSION HEAT ENGINE

[00149] The Fusion Heat Engine is a device that includes a thermally conductive heat collection device of specific geometric design for collecting and transferring heat, and a heat-to-energy converter that can be used with the Hydrogen-Lithium Fusion Device ("HLFD") described in international patent application # PCT/US07/0 18256,.

[00150] The HLFD enables a proton-lithium fusion efficiency that can be close to 100% with the helium ion fusion byproducts exiting the HLFD's lithium target without transferring significant fusion energy to the target as heat.

[00151] The resulting helium ions are symmetrically expelled from the target and give up their kinetic energy as heat in the heat collection device. We use the term "heat collection device" as a generic term for any device that transfers the kinetic energy of the helium ion byproducts into heat by any method.

[00152] The heat energy is then converted into other forms of energy by a heat-to-energy converter. We use the term "heat-to-energy converter" as a generic term for any device that converts heat into any form of energy including heat or lack of heat by any method.

THEORETICAL BASIS FOR GEOMETRIC CONFIGURATION

[00153] The heat collection device conforms to a set of geometric configurations derived from the gravity theory developed by the inventors, in order to preserve the high fusion efficiency that prevents the destruction of the HLFD's lithium target by heat.

[00154] According to the gravity theory based on mass-energy equivalence, the Type II gravity potential V_G exerted by an object A on an equal or smaller size object B (e.g. a lithium nucleus on a proton, an aluminum nucleus on a proton, a lithium nucleus on a helium ion, or a helium ion on an electron) is given by:

$$V_G(r_B) = - G m_A m_B \lambda_A / \lambda_B J_0(r_B/\lambda_B)/r_B (1 - v_A^2/c^2)^{1/2} (1 - v_B^2/c^2)^{1/2} 1/\pi (1/\varepsilon |_{\varepsilon=0}),$$

[00155] where r_B is the distance of object A from object B, G is the gravitational constant, m_A is the rest mass of object A, m_B is the rest mass of object B, λ_A is the gravity wavelength of object A, λ_B is the gravity wavelength of object B, J_0 is the 0^{th} order Bessel function of the first kind, v_A is the speed of object A, v_B is the speed of object B, c is the speed of light, and $(1/\varepsilon |_{\varepsilon=0})$ is a first-order singularity.

[00156] The gravity wavelength λ_G of an object is given by $\lambda_G = N A_G M$ where $N A_G \approx 6.0 \; 10^{23}$ m/kg and M is its rest mass. For example, a lithium nucleus has a gravity wavelength ≈ 7 mm, an aluminum nucleus has a gravity wavelength ≈ 27 mm, a helium ion has a gravity wavelength ≈ 4 mm, a proton has a gravity wavelength ≈ 1 mm, and an electron has a gravity wavelength ≈ 0.55 microns.

[00157] Since the Type 11 gravity potential has a first-order singularity, the Type II gravity force experienced by object B is zero for distances less than its gravity wavelength. For distances greater than its gravity wavelength, a very large gravity force F_G occurs whenever $J_0(r_B/\lambda_B)$ changes sign:

$$F_0 (r_B) = G m_A m_B \lambda_A/\lambda_B^2 J_1(r_B/\lambda_B)/r_B (1 - v_A^2/c^2)^{1/2} (1 - v_B^2/c^2)^{1/2} 1/\pi (1/\varepsilon |_{\varepsilon=0}),$$

where J_1 is the 1^{st} order Bessel function of the first kind and r_B/λ_B is a zero of the J_0 Bessel function. The first zero of the J_0 Bessel function occurs at a value of about 2.4, while the maximum distance between adjacent zeros is π which is about 3.14 since the J_0 Bessel function asymptotically approaches a cosine function.

[00158] Since a force results in a change in momentum, the Type II gravity force imparts a momentum addition to object B in the direction of the Type II gravity force as object B moves through the zeros of the J_0 Bessel function.

[00159] If the Type II gravity potential exerted on the proton in the lithium target by the nuclei of the heat collection device that are in the same direction includes both positive and negative first-order singularity values, the Type II gravity force exerted by the nuclei on the proton is zero. This same consideration applies to the nuclei of the target holder in the HLFD.

[00160] To allow the incoming protons to experience only Type II wave gravity exerted by the lithium target nuclei and not by the heat collection device nuclei, the thickness of the walls, components, and support structures of the heat collection device as experienced by an incoming proton in the beam cylinder of the lithium target should exceed about 2.4 mm (2.4 x 1 mm) or about 3.14 mm (π x 1 mm), depending on the distance between protons at the target and the nuclei of the heat collection device. Counter-intuitively (if intuition applies in this realm), we predict that a smaller thickness is sufficient in close proximity and a large thickness is used at a greater distance. Prudent design can be satisfied by choosing the greater thickness. These two thickness values are determined by the minimum and maximum distances between adjacent zeros of the J_0 Bessel function multiplied by the proton gravity wavelength.

[00161] In experimental test #1, the lithium foil target with a target holder consisting of two 1 mm plates and thus not conforming to the geometric specification melted within a second.

DETAILED DESCRIPTION OF FUSION HEAT ENGINE

[00162] Based on recent experimental observations, it is believed that energy could be harnessed by a Fusion Heat Engine in a two step process that transfers the kinetic energy released by proton-lithium fusion into heat and then from heat into energy.

[00163] Various geometric configurations can be used for the heat collection device conduits and components providing they conform to the geometric specification derived from the gravity theory. The geometric specification are that the thicknesses of all sections as experienced by an incoming proton in the beam cylinder of the lithium target exceeds about 2.4 mm, more preferably about 3.14 mm. Examples of three geometric configurations are shown in FIG. 11.

[00164] Even though the thicknesses of the conduit walls and cavity and other components may exceed about 3.14 mm, an edge effect may be produced by the thickness of a component section less than about 3.14 mm as experienced by an incoming proton in the beam cylinder of the lithium target as shown in FIG. 11. Edge effects may reduce fusion efficiency so

that the lithium target of the HLFD melts. Edge effects can be reduced or eliminated by the shape of the conduits and other components and by beveling edges that are present.

[00165] An ion accelerator 12, see FIGS. 12, 13, and 15, using hydrogen gas as its ion source creates a proton beam 16 with sufficient proton energy to produce proton-lithium fusion. The proton beam 16 is directed at a HLFD 23, see FIGS. 12, 13, and 15, within a vacuum chamber 6 as shown in FIGS. 14 and 15.

[00166] Helium ions that are produced by the HLFD travel in spherically symmetric radial trajectories from the HLFD's lithium target. Orienting the surfaces of the heat collection device 33, see FIGS. 12, 13, and 15, to cover the solid angle trajectories of the helium ions allows for maximum ion bombardment.

[00167] The helium ions bombard the exposed surfaces of the heat collection device enabling the fusion kinetic energy of the helium ions to be transferred into heat in the heat collection device. After transferring their kinetic energy, the helium ions can be collected by well-known methods such as vacuum pump.

[00168] That the kinetic energy of the helium ions is transferred to the heat collection device but not the lithium target results from their different geometries and from the relative size of the momentum additions experienced by the helium ions. The lithium target is a foil so that the Type II gravity force exerted on a helium ion by lithium nuclei in the 9.6 mm rings on each side of the foil result in small random momentum additions in the direction of the gravity force. The heat collection device on the other hand is likely to provide a different geometry in which the rings are incomplete and hence the momentum additions are not random and may not even occur.

[00169] Further, the equation for the Type II gravity force shows that the force and hence the momentum additions experienced by a helium ion are proportional to the square of the mass of the nucleus exerting the gravity force. For example, the ratio of the size of the momentum addition exerted by an aluminum nucleus in the heat collection device and to that exerted by a lithium nucleus in the target is about 15 (272 / 72). Since momentum is proportional to speed, the continual larger non-random speed changes of the helium ion in the heat collection device cause the helium ions to impact the lattice structure of the materials comprising the heat collection device and thus transfer kinetic energy to the lattice. Whereas the smaller random speed changes of helium ions in the lithium target cause the helium ions to randomly walk out of the target.

[00170] The walls, components, and support structures of the heat collection device can be aluminum, nickel, or any other heat-conducting material that can be used in a vacuum chamber.

The heat collection device is thermally insolated from the HLFD so as to not transfer heat to the lithium target.

[00171] For example, the heat collection device may include a set of conduits within the vacuum chamber that contain a liquid or liquid vapor condensate cycled through the conduits by a heat exchanger, see FIG. 15. The thermal energy of the helium ion fusion byproducts is transferred into heating the conduits that in turn heat the liquid or liquid vapor condensate. Another configuration for the heat collection device is one in which the conduits are integrated into the walls of the vacuum chamber in which the HLFD is located.

[00172] Since the conduits of the heat collection device are used in proximity to the lithium target of the HLFD, the thickness of the conduit walls and cavity and other components as experienced by a proton in the beam cylinder of the lithium target each exceeds about 2.4 mm, more preferably about 3.14 mm. This allows the walls of the conduit, the liquid or liquid vapor condensate in the conduit cavity, and other components each not to affect the fusion efficiency of the HLFD.

[00173] The heat energy transferred into the heat collection device can be converted into other forms of energy in the heat-to-energy converter. For example, the liquid or liquid vapor condensate cycled through the conduits by a heat exchanger can be converted into electrical energy by a turbine for generating electricity, as shown in FIG. 16.

[00174] In FIG. 16, an ion accelerator (A) directs a proton beam which bombards a HLFD (B) producing helium ion fusion byproducts. Surrounding the HLFD are liquid or condensate conduits (C) which may be either elliptical or circular or any other configuration that allows for the flow of liquid while minimizing edge effects. The heated fluid is cycled through the conduits towards a hot liquid/condensate conduit (D) which is directed to a nozzle (E). The heated condensate is expelled from the nozzle with sufficient energy to spin a turbine/generator (F) which converts the energy of the liquid or condensate to mechanical and then to electrical energy. The condensate flows into a condenser (G) which removes any heat energy and reintroduces the liquid or condensate back into the heating cycle by a cold liquid/condensate conduit (H).

[00175] The total fusion kinetic energy transferred into other forms of energy is determined in part by the number of individual fusion reactions taking place, the efficiency of transferring fusion kinetic energy into heat in the heat collection device, and the efficiency of the heat-to-energy converter. For example, the efficiency for converting fusion heat energy into heating or cooling by a heat exchanger that cycles liquid or liquid vapor condensate through the conduits of the heat collection device is about 60 to 85% depending on the type of heat

exchanger (e.g. rotary, sealed heat pipe, plate). (See U.S. Environmental Protection Agency, Center for Environmental Research Information, Cincinnati OH. Guide to Industrial Assessments for Pollution Prevention and Energy Efficiency. Dane Publishing. June 2001, p. 309). For the example shown in FIG. 16, the maximum efficiency for converting fusion heat energy into electricity is about 40%. (See Tipler, Paul A. 1999. Physics for Scientists and Engineers. W. H. Freeman and Company, New York. p. 603). Sample calculations appear below.

[00176] Since the ratio of average fusion event energy to incoming proton energy is about 54 (16.2 MeV / 300 keV) and the fusion efficiency can be close to 100%, the energy output by the heat-to-energy converter can be greater than the electrical energy to create the proton beam in the HLFD and to run the heat collection device and heat-to-energy converter. The energy output by the heat-to-energy converter is then able to generate the power used by the Fusion Heat Engine and generate excess power.

[00177] After the start-up or priming power consumption of the HLFD, heat collection device, and heat-to-energy converter, the Fusion Heat Engine achieves and surpasses the break¬ even point of energy production and is self sustaining as long as hydrogen gas and lithium are available to maintain the fusion reaction.

[00178] Surplus power produced by the Fusion Heat Engine can be delivered to external applications by well-known methods such as a power grid.

ELECTROGRAVITY GENERATOR APPLICATION

CONCEPT OFELECTROGRAVITY GENERATOR

[00179] The Electrogravity Generator is a device that is predicted to convert hydrogen-lithium fusion kinetic energy into DC electric power via electron vibration by gravity waves.

[00180] In the Electrogravity Generator, the fusion kinetic energy of the helium ions created by the Hydrogen-Lithium Fusion Device is first transferred into vibrating the electrons in a set of conducting elements (FIGS. 18-19) by the Type II gravity exerted by the helium ions on the electrons.

DETAILED DESCRIPTION OF ELECTROGRA VITY GENERATOR

[00181] We use the term "potential well" as a generic term for any mechanism that enables electrons to gain energy from wave gravity exerted by energetic particles. For example, potential wells can also be created by using a semiconductor material such as Silicon Carbide doped with Nitrogen or Gallium Phosphide as the conducting element. In this case, the kinetic

energy of the helium ions is transferred by Type II wave gravity to valence band electrons in quantum potential wells.

[00182] The helium ion fusion byproducts exert Type II wave gravity on electrons in the conducting elements. This occurs as Type II wave gravity interacts with particles of equal or smaller mass such as an electron and as such does not affect the larger atomic nuclei (e.g. Gallium or Phosphorous).

[00183] At each end the conducting element may have ohmic or elemental contacts that have low resistance, see FIG. 18, thus allowing the flow of electrons through the conducting element as a result of the applied DC electric field. For example for Silicon Carbide doped with Nitrogen or Gallium Phosphide, an ohmic contact may be a gold selenium alloy, while an elemental contact may be a conductor such as aluminum. (See Berger, Lev I. 1997. Semiconductor Materials. CRC Press. Boca Raton, FL. pp. 417-420, which pages are hereby incorporated by reference in whole).

[00184] By applying a prior DC electric field to the conducting element, the electrons in the conduction band of the conducting element are set in motion due to the DC electric field in the conducting element.

[00185] In a semiconductor material, the electron energy is transferred into DC electric power when the energy of a valence electron in a quantum potential well reaches the band gap energy and the electron jumps from the valence band to the conduction band. If the band gap energy equals or exceeds the energy of a photon emitted at the electron gravity wavelength, the electron can give up its energy to the DC electric field in the conducting element and drop back into the valence band. For example, the theoretical band gap energy of Gallium Phosphide is about 2.26 eV, whereas the practical band gap of commercial available Gallium Phosphide is smaller, on the order of 2.2 eV. The theoretical band gap may be larger than the practical band gap in most semiconductors.

[00186] The inventors believe that the yellow-green glow occurring in nuclear reactions and in natural phenomena such the Northern Lights corresponds to photons emitted at the electron gravity wavelength. The Type II wave gravity exerted by energetic particles in motion in these situations strongly vibrates electrons at the electron gravity wavelength and the electrons release the vibration kinetic energy as radiation at the electron gravity wavelength. The inventors' gravity theory predicts that the electron gravity wavelength is about 548 nanometers which corresponds to a photon energy of about 2.26 eV.

[00187] Accordingly, Type II wave gravity exerted by the helium ion fusion byproducts in motion strongly vibrates valence band electrons in the semiconductor at the electron gravity

wavelength. When the electron energy reaches the semiconductor band gap energy, the electron jumps from the valence band to the conduction band. If the band gap energy equals or exceeds the photon energy of about 2.26 eV which corresponds to the electron gravity wavelength, the electron may emit a photon or amplify a prior electric field and then drop back into the valence band.

[00188] An ion accelerator using hydrogen gas as its ion source creates a proton beam with a proton energy sufficient to produce proton-lithium fusion within a vacuum chamber. A nozzle 1316 in FIG. 17 directs protons at the HLFD' s lithium target 23. Gravity effects exerted by the helium ion fusion byproducts propagate in directions radial to the target, along the axes of the conducting elements 1320 in FIG. 19.

[00189] A spherical grouping of conducting elements 1320 is positioned in the vacuum chamber of the ion accelerator such that their length axes point at the lithium target. Multiple conducting elements can be used so as to distribute the fusion kinetic energy to the desired number of valence electrons in potential wells. The conducting elements can be wired in serial, parallel, or combination, and as a single circuit or as multiple circuits.

[00190] The efficiency of transferring fusion energy from a HLFD to a DC electric field in a semiconductor material depends in part on the number of valence electrons in quantum potential wells, the efficiency in transferring the kinetic energy of the helium ion fusion byproducts by Type II wave gravity to the valence electrons in quantum potential wells, the time for a valence electron in a quantum potential well to attain the band gap energy, the efficiency in transferring the band gap energy of the valence electrons to the DC electric field, the time for an electron that has jumped from the valence band to the conduction band to transfer its energy to the DC electric field, and the time for an electron in the conduction band to drop back into the valence band.

[00191] For example, for a 5.08 cm diameter wafer, either a 6.35 mm thick wafer including Silicon Carbide doped with Nitrogen or a 0.4 cm thick wafer including Gallium Phosphide and a HLFD as described in the experimental plan for proof of concept, the number of transition cycles per second to transfer a fusion power of 640 watts ($1.0 * 40 * 6.2\ 10^{12} *$ 16.2 MeV/sec) generated by the HLFD is calculated as:

Density of potential wells in undoped Gallium Phosphide = $1.9\ 10^{19}\ cm^{-3}$

Volume of the Gallium Phosphide wafer = $8.1\ 1\ cm^3$ ($\pi * 2.54^2 * 0.4$)

Number of valence electrons in potential wells = $1.54\ 10^{20}$ ($8.1\ 1 * 1.9\ 10^{19}$)

Band gap energy of Gallium Phosphide = 2.26 eV

Energy transferred in wafer per transition cycle = 3.48 10^{20} eV (1.54 10^{20} * 2.26)

Fusion power from HLFD = 640 watts = 4.00 10^{21} eV/sec

Transition cycles per second = 11.5 sec^{-1} (4.00 10^{21} / 3.48 10^{20})

[00192] The maximum number of possible transition cycles per second in transferring fusion energy from a HLFD to a DC electric field in a semiconductor material such as Silicon Carbide doped with Nitrogen or Gallium Phosphide can be determined by varying the available fusion power and/or the quantity of semiconductor material and comparing these percentage changes to the percentage changes in output electric power. When the number of transition cycles per second is less than the maximum number, the percentage changes can be expected to be similar. Once the number of transition cycles reaches the maximum number, the output electric power can be expected to remain constant. Thus for example by increasing the available fusion power until the output electric power reaches a plateau, the maximum number of possible transition cycles is determined by the ratio of the fusion power from the HLFD to the energy transferred in the semiconductor material per transition cycle.

POSSIBLE SEMICONDUCTORS FOR USE AS CONDUCTING ELEMENTS

[00193] The Electrogravity Generator may use semiconductor materials with a band gap that equals or exceeds about 2.26 eV as conducting elements in order to transfer the fusion kinetic energy released by the HLFD into amplifying an electric current.

[00194] The addition of dopants to some semiconductors not only can add or reduce valence or conduction electrons, but also increase or decrease the band gap of the semiconductor material. It is then possible for a semiconductor material with a band gap lower than about 2.26 eV to be doped with a particular element or compound to increase the band gap to equal or exceed about 2.26 eV.

[00195] A conducting element may also be a semiconductor material that is conductive. For example, while pure Gallium Phosphide is an insulator, when doped with Zinc the semiconductor becomes electrically conductive. For Gallium Phosphide doped with Zinc, an ohmic contact may be a gold selenium alloy, while an elemental contact may be a conductor such as aluminum. Another example is Silicon Carbide doped with Nitrogen. For Silicon Carbide doped with Nitrogen an elemental contact may be Nickel. The conductive property in the

conducting elements facilitates the amplification of the current and reduces heat generation in the semiconductor material as a result of the amplified electric current.

[00196] Possible N-Type and P-Type semiconductors, both intrinsic and extrinsic, **with a direct** or indirect band gap, for use **as** conducting elements **are** identified and **described** in Berger, **Lev I.** 1997. Semiconductor Materials. CRC **Press.** Boca Raton, **FL, which** reference **is** hereby incorporated in whole. Potential dopants also **are** identified and discussed in **Berger's** book.

[00197] Possible dopants may **be** elements, other semiconductors, or compounds of elements and other semiconductors. **The** dopants **are either** N-type or P-type and change **the** properties of **the** semiconductor material accordingly. **A** partial list of possible dopants **is** included below.

[00198] POSSIBLE DOPANTS FOR USE IN SEMICONDUCTORS

- Arsenic
- Arsine
- Argon
- Boron
- Boron Trichloride
- Boron Trifluoride
- Chlorine
- Germanium
- Gold
- Helium
- Hydrogen
- Hydrogen Selenide
- Indium
- Lithium
- Nitrogen
- Oxygen
- Phosphorus
- Phosphorus Pentafluoride
- Selenium
- Silicon
- Sulfur
- Sulfur Hexafluoride
- Thallium
- Tellurium
- Vanadium
- Zinc

[00199] For example, **a** semiconductor **that** may **have its** band **gap** increased to about **2.26 eV is** Zinc Telluride (ZnTe) doped **with** Vanadium. Intrinsic undoped ZnTe **has** an indirect band **gap** of 2.23-2.25 **eV. (See** Hoosain, M.S., Islam, R., Khan, **K.A. 2008.** Electrical Conduction

Mechanisms of Undoped and Vanadium Doped ZnTe Thin Films. Chalcogenide Letters VoI 5, No. 1, p. 1-9.)

[00200] For a 5.08 cm diameter by 0.4 cm thick wafer of Zinc Telluride doped with Vanadium and a HLFD as described in the experimental plan for proof of concept, the number of transition cycles per second to transfer a fusion power of 640 watts ($1.0 * 40 * 6.2\ 10^{12} * 16.2$ MeV/sec) generated by the HLFD is calculated as:

Density of potential wells in Zinc Telluride doped with Vanadium = $2.5\ 10^{16}\ cm^{-3}$

Volume of Zinc Telluride wafer doped with Vanadium = $8.11\ cm^3$ ($\pi * 2.54^2 * 0.4$)

Number of valence electrons in potential wells = $2.02\ 10^{17}$ ($8.1\ 1 * 2.5\ 10^{16}$)

Band gap energy of Zinc Telluride doped with Vanadium = 2.26 eV

Energy transferred in wafer per transition cycle = $4.56\ 10^{17}$ eV ($2.02\ 10^{17} * 2.26$)

Fusion power from HLFD = 640 watts = $4.00\ 10^{21}$ eV/sec

Transition cycles per second = $8.77\ 10^3\ sec^{-1}$ ($4.00\ 10^{21} / 4.56\ 10^{17}$)

[00201] The time for a single transition cycle and thus the maximum number of possible transition cycles per second in transferring fusion energy from a HLFD to a DC electric field in a doped semiconductor material such as Zinc Telluride doped with Vanadium is not known.

[00202] Silicon Carbide doped with Nitrogen (SiC-N) is a strong candidate for a proof of concept experiment since Silicon Carbide is commonly used for high power applications such as Schottky Diodes, Schottky Rectifiers, and High Voltage Field Effect Transistors. (See B. Jayant Baliga, Silicon Carbide Power Devices, North Carolina State University, USA)

EXPERIMENTAL PLAN FOR PROOF OF CONCEPT

[00203] This section presents an experimental plan to prove the feasibility of the Electrogravity Generator. The experiment uses a Hydrogen-Lithium Fusion Device ("HLFD"), an electric circuit, an applied DC electric field, and a conducting element made of a semiconductor material such as silicon carbide doped with nitrogen (SiC-N). The equipment is summarized in the table below.

[00204] EQUIPMENT FOR EXPERIMENTAL PROOF OF ELECTROGRAVITY GENERATOR

FACILITY

- Space Environmental Effects Facility, Marshall Space Flight Center, Huntsville, Alabama

Hydrogen-Lithium Fusion Device

- Proton beam energy 307 keV
- Proton beam current up to 40 mA
- 99.9% pure lithium foil target 250 microns thick
- Target area ending in a steel six-way cross vacuum chamber

Conducting Element

- 5.08 cm diameter, 6.35 mm thick wafer of silicon carbide doped with nitrogen

DC Power Supply

- Detection circuit connected to vacuum chamber electrical feed-through connectors

Detection Equipment

- A circuit consisting of a conducting element connected by vacuum chamber electrical feed-through connectors with a power supply and set of power resistors
- A voltmeter to measure DC voltage across the vacuum chamber electrical feed-through connectors
- An ammeter to measure DC electric current in the circuit

[00205] The conducting element is a 6.35 mm thick wafer of silicon carbide doped with nitrogen. The conducting element is centered behind the target and positioned at horizontal in close proximity to the target holder.

[00206] The conducting element circuit is connected to an electrical feed-through connector in a six-way cross vacuum chamber flange. The external section of the circuit is connected to a DC power supply and one or more power resistors.

[00207] A DC electric current is applied to the conducting element circuit. The DC electric current provides a direction for electron motion and allows the electric field to be amplified as the electrons cross the band gap of the conducting element.

[00208] A voltmeter measures the DC voltage across the conducting element and an ammeter measures the DC electric current in the conducting element circuit.

[00209] When the HLFD is turned on, the helium ions transfer energy through Type II wave gravity to the valence electrons in the conducting element. When the energy of a valence electron reaches the band gap energy, the electron jumps to the conduction band and the electron energy is added to the DC electric field in the conducting element circuit. The amplification of the DC electric current will provide experimental proof for the feasibility of the Electrogravity Generator.

ELECTRIC POWER PRODUCTION EXAMPLE

[00210] A Hydrogen-Lithium Fusion Device ("HLFD") is used as the power source for the Electrogravity Generator.

[00211] A spherical grouping of conducting elements consists of a semiconductor material such as silicon carbide doped with nitrogen. The conducting elements are centered on the target and positioned in close proximity surrounding the target holder. The conducting elements are wired to form one or more circuits.

[00212] The helium ion byproducts of the fusion reactions are expelled symmetrically with respect to the target. The movement of the helium ions creates Type II wave gravity that vibrates electrons in the conducting elements so as to enable kinetic energy transfer from the helium ions to the electrons in the conducting elements.

[00213] The kinetic energy of the helium ions is transferred by Type II wave gravity to the electrons in the valence band of a semiconductor material such as silicon carbide doped with nitrogen by means of quantum potential wells which are a characteristic of a semiconductor.

[00214] The quantum potential wells allow for a one way energy transfer without the electrons leaving the vicinity of the valence band before the electromagnetic energy of the electrons can **be** released into the electric field in the conduction band.

[00215] The arrangement, shape, volume, mass, and material of the conducting elements are designed to maximize the number of electrons in quantum potential wells which may gain energy transferred by the Type II wave gravity exerted by the helium ions. For example, a conducting element can be Silicon Carbide doped with nitrogen, Zinc Telluride doped with Vanadium, or other semiconductor materials which expose the valence electrons to quantum potential wells and have a band gap energy that equals or exceeds about 2.26 eV.

[00216] The amount of helium ion kinetic energy transferred into electric power is determined in part by the number of individual fusion reactions taking place, the efficiency of transferring fusion kinetic energy via the Type II wave gravity experienced by electrons exposed to potential wells, and the number of electrons exposed to potential wells in the conducting elements.

[00217] Since the ratio of average fusion event energy to incoming proton energy is about 54 (16.2 MeV / 300 keV) and the fusion efficiency can be close to 100%, the fusion kinetic energy transformed into electric power can be greater than the electric power to create the proton beam in the HLFD. The fusion kinetic energy that is transferred into electric power is then able to generate the used by the Electrogravity Generator while still generating excess electric power.

[00218] After the start-up or priming power consumption of the HLFD, the Electrogravity Generator achieves and surpasses the break-even point of energy production and is self sustaining as long as hydrogen gas and lithium are available to maintain the fusion reaction.

[00219] Surplus electric power produced by the Electrogravity Generator can be delivered to external applications by well-known methods such as a power grid.

ILLUSTRATIVE FUSION ENERGY PRODUCTION

[00220] In the following illustrative example, we estimate output electrical power from conversion of fusion energy generated by the HFLD. A one or two inch diameter proton beam directed at a lithium target produces energy that is converted to heat by a heat exchanger. The heat captured generates steam that drives a turbine and generates an estimated 64 kilowatts of electricity from 160 kilowatts of fusion produced energy. Other approaches to converting raw fusion produced energy into electricity may be applied.

[00221] Assumptions:

Ion type = Proton
Ion accelerator = Pelletron
Proton energy = 307 keV
Beam current = 10mA ($6.2\ 10^{16}$ protons/sec)
Standard lithium target ($_6$Li: $_7$Li) = (7.5%: 92.5%)
Average fusion event energy = 16.2 MeV (0.075 * 4.0 + 0.925 * 17.2)
Ratio of fusion event energy to proton energy = 54 (16.2 MeV / 300 keV)
Fusion efficiency of HLFD = 100%

[00222] Fusion energy generated per second

= Fusion efficiency * Protons/sec * Average fusion event energy
= 1.0 * $6.2\ 10^{16}$ * 16.2 MeV/sec
= $1.0\ 10^{18}$ MeV/sec = $1.6\ 10^5$ joules/sec = 160 kilowatts

[00223] Fusion energy transferred to other forms of energy

Fusion Heat Engine:

- Heat Exchanger only efficiency = 80%

  Output heat power = 128 kilowatts

- Steam power using Rankinβ cycle efficiency = 40%

  Output electrical power = 64 kilowatts

Electrogravity Generator:

* Semiconductor conducting element efficiency = 100%

  Output electrical power = 160 kilowatts

Some Particular Embodiments

[00224] The present invention may be practiced as a method or device adapted to practice the method. One embodiment is a target assembly for use with the proton generator capable of generating a proton beam. The proton beam is projected along an axis and has a transverse dimension at a target position. The target assembly includes a target support locatablc at the target position and a lithium target having front and back surfaces. The lithium target is supported by the target support. It has a minimum target thickness measured generally parallel to the proton beam's axis. The target support is configured so that the target has exposed front and back target surfaces that are free of target support material. A target area can be defined by projecting the exposed front surface onto the exposed back surfaces and taking the intersection between areas of the exposed front and back target areas. The target area is the target for the proton beam.

[00225] One aspect of this embodiment is limiting the maximum target thickness to less than a first zero of the Bessel J_0 function times the gravity wave length of a proton. It is estimated that the maximum target thickness, by this measure, needs to be less than approximately 2.4 mm.

[00226] Alternatively, the maximum target thickness may need to be less than the distance between successive zeros of the Bessel J_0 function times the gravity wave length of a proton. In this case, it is estimated that the maximum target thickness would need to be less than approximately 3.14 mm ("pi" mm.)

[00227] Another aspect of this embodiment is limiting the minimum target support thickness to greater than the distance between successive zeros of the Bessel J_0 function times the gravity wave length of a proton. Again, this quantity is estimated to be approximately 3.14 mm ("pi" millimeters.)

[00228] Alternatively, the minimum target support thickness may need to be greater than the first zero the Bessel J_0 function times the gravity wave length of a proton. It is estimated that this measure would corresponds to a minimum target support thickness of approximately 2.4 mm.

[00229] In the embodiments described above, the thickness of the target or target holder is measured along the axis of the proton beam.

[00230] Another aspect of this embodiment is that the target support may circumscribe the target area. It may be made of aluminum. The target support may have front and back parts with the target sandwiched between the front and back parts.

[00231] The target itself may be comprised of lithium, such as metallic lithium or a lithium containing material, such as lithium oxide or a lithium alloy. The target area of the target may be circular. With a circular target, the target may have a minimum transverse dimension of at least 19.2 mm plus the transverse dimension of the proton beam. The target may have a uniform thickness.

[00232] Another embodiment is a target assembly that recombines various features and aspects described above. This target assembly is for use with the proton generator capable of generating a proton beam directs along an axis. The proton beam has a transverse dimension at a target position. The target assembly includes a target support locatable at the target position. It has a minimum target thickness measured generally parallel to the proton beam's axis. The minimum target support thickness is greater than the distance between successive zeros of the Bessel J_0 function times the gravity wave length of a proton. Again, this quantity is estimated to be approximately 3.14 mm. The target assembly further includes a lithium target having front and back surfaces supported by the target support. The target has a maximum thickness of the first zero the Bessel Jo function times the gravity wave length of a proton. It is estimated that this measure would correspond to a minimum target support thickness of approximately 2.4 mm.

[00233] The target support in this embodiment is configured so that the target has exposed front and back target surfaces that are free of target support material. A target area can be defined by projecting the exposed front and back target surfaces along the proton beam axis and taking the intersection of the projected areas. The target area is the target for the proton beam. The target support circumscribes the target area. The target has a minimum transverse dimension of at least 19.2 mm plus the transverse dimension of the proton beam.

[00234] As a method, the corresponding embodiment is adapted to making a target assembly for use with a proton generator capable of generating a proton beam along an axis. The proton beam has a transverse dimension that target position. The method includes selecting a lithium target material having front and back surfaces, the target material to target area having a maximum thickness of less than a first zero of the Bessel Jo function times the gravity wave length of a proton, which is estimated to be approximately 2.4 mm.

[00235] An aspect of this method is selecting a target material having a uniform thickness.

[00236] Another aspect is selecting a target that includes at least one of metallic lithium, lithium oxide or a lithium alloy.

[00237] The target support may be chosen so that the target area is circular. The target support may be aluminum.

[00238] The target may be mounted between two parts of the target support so that the target material is sandwiched between the front and back of the target support. Each part of the support may have a thickness according to the criteria above or the combined parts may be sized according to the criteria above.

[00239] A related method, which optionally may be practiced using the target support described above, is a method of producing sustained hydrogen-lithium fusion. This method includes selecting a lithium target material having front and back surfaces optionally having dimensions generally described above. The method further includes mounting the target material to a target support to create a target assembly locatable at a target position, optionally having dimensions and characteristics described above. Practicing this method, the selecting and mounting actions are carried out so that the target assembly comprises a lithium target having exposed front and back surfaces free of target support material. The exposed front and back surfaces define a target area as described above. The method further includes projecting the proton beam along the axis and fusing protons in the proton beam with lithium nuclei in the target area.

[00240] An aspect of this method is sustaining the hydrogen-lithium fusion for more than 10 minutes without melting the target material.

[00241] Another aspect is realizing more than 5% and preferably more than 60% efficiency in combining protons with lithium nuclei. Efficiency may approach 100%, such as achieving 90%, 95% or 99%. The current experiments appear to indicate a high efficiency, given that the target is not melting. Further experiments using particle counting tools calibrated to the expected efficiency range may support refinement of these estimates.

[00242] Another related method, which optionally may be practiced using the target support described above or as an enhancement to the method of producing sustained hydrogen-lithium fusion, is a method of generating an amplified electrical current. This method includes projecting helium ion byproducts produced by hydrogen-lithium fusion onto a heat collection device to convert energy of the helium ion byproducts into usable heat.

[00243] According to one aspect, this method may further include projecting a proton beam onto a lithium target to produce the hydrogen-lithium fusion. Preferably, the hydrogen-lithium fusion reacts 60 percent or more of protons in the proton beam with lithium in the lithium

target. Alternatively, the lithium target undergoes fusion for more than five minutes without melting. Or, stated somewhat differently, the hydrogen-lithium fusion reacts a sufficient proportion of the protons to avoid melting the lithium target due to transfer of energy from the protons to the lithium target. It is useful, when practicing this method, for the lithium target to not be melted by exposure to the proton beam. Stated differently, the lithium target remains substantially in tact during exposure to the proton beam.

[00244] According to another aspect, this method further includes the heat collection device circulating a heated fluid and conveying thermal energy generated by collisions of the helium ion byproducts with the heat collection device. From the heat collection device, the thermal energy may be conveyed to a heat exchanger.

[00245] A device embodiment is a heat generator, including a hydrogen-lithium fusion device that projects helium ion byproducts produced by a hydrogen-lithium fusion reaction and a heat collector positioned to receive at least some of the helium ion byproducts from the hydrogen-lithium fusion device.

[00246] The heat generator can be extended to be an electrical generator, by further including a heat-to-electrical energy converter. In some embodiments of the heat generator, the walls, components, and support structures of the heat collection device have a minimum thickness of about 2.4 mm, measured in a radial direction from the lithium target of the hydrogen-lithium fusion device. Alternatively, the walls, components, and support structures of the heat collection device have a minimum thickness of about 3.14 mm, measured in a radial direction from the lithium target of the hydrogen-lithium fusion device. The heat generator's hydrogen-lithium fusion device further includes a proton beam generator and a lithium target positioned to receive a proton beam from the proton beam generator, wherein the hydrogen-lithium fusion device reacts 60 percent or more of protons in the proton beam with lithium in the lithium target. Alternatively, the heat generator's hydrogen-lithium fusion device may further include a proton beam generator and a lithium target positioned to receive a proton beam from the proton beam generator, wherein the hydrogen-lithium fusion device reacts a sufficient proportion of the protons to avoid melting the lithium target due to transfer of energy from the protons to the lithium target.

[00247] Of course, any features of the target support, HFLD or related methods can be combined with aspects of the heat generator method and/or device.

[00248] Another related method, which optionally may be practiced using the target support described above or as an enhancement to the method of producing sustained hydrogen-lithium fusion, is a method of generating an amplified electrical current. This method includes

harnessing gravity waves induced by fusion byproducts to amplify an electrical current. In one embodiment, the electrical current is a DC current.

[00249] An aspect of this method involves the fusion byproducts disbursing along vectors D and amplifying the electrical current by exposing a plurality of conducting elements to gravity waves induced by the fusion byproducts. The conducting elements are aligned to have axes generally with some of the vectors D. In this sense, conducting elements are generally aligned with surfaces normal to some of the vectors, when the vectors are taken to originate from where the fusion byproducts are generated. This alignment of conducting elements may coincidently be aligned with the gravity waves induced by the fusion byproducts.

[00250] Practicing this method may include using conducting elements that have potential wells that enable electrons to gain energy from the wave gravity induced by fusion byproducts.

[00251] A further aspect of this method includes projecting a proton beam onto a lithium target and creating hydrogen-lithium fusion collisions in said target, whereby the fusion byproducts are helium ions that move away from the target along the vectors D. This aspect of the method may be combined with any other aspects or features of the method of generating an amplified electrical current. It may be understood that the helium ions create gravity waves and the gravity waves amplify the current in the conducting elements.

[00252] A corresponding device embodiment amplifies electrical power using gravity waves produced by fusion byproducts. This device includes a beam of accelerated protons and a target comprising lithium that is exposed to the proton beam, whereby fusion collisions between the accelerated protons and lithium atoms create helium ions that move away from the target along vectors D. The device further includes one or more conducting elements in which electrons are exposed to potential wells and gain energy from wave gravity produced by the fusion byproducts, generally aligned along some of the vectors D and a primer circuit coupled to the conducting elements that induces an electrical current to be amplified. The device further includes solenoid wrappings around the conducting elements carrying a current and producing magnetic fields with lines through the cores of the conducting elements.

[00253] Further details of the conducting elements disclosed above can be utilized with this device embodiment, of course.

[00254] A further aspect of this device includes at least one ion accelerator that generates a beam of accelerated protons by ionizing hydrogen gas and accelerating the resulting ions. This aspect may be combined with the further aspect of helium ions creating gravity waves, wherein the gravity waves produce gravitational attraction and gravitational repulsion of electrons, wherein the electrons transfer gravity wave energy into the electrical current to be amplified.

[00255] It is contemplated that modifications and combinations will readily occur to those skilled in the art, which modifications and combinations will be within the spirit of the invention and the scope of the claims.

[00256] The following section reproduces a technical paper by the inventors describing their gravity theory.

GRAVITY THEORY BASED ON MASS-ENERGY EQUIVALENCE

Stephen A. Lipinski and Dr. Hubert M. Lipinski
Unified Gravity Corporation

PAPER ABSTRACT

[00257] In this theory, an object is a mass density field in the fabric of space (FS) that satisfies mass-energy equivalence. In contrast with General Relativity (GR), the theory posits a preferred reference frame - namely the reference frame in which the FS is at rest. Also in contrast with GR, gravity between two objects results from the interaction of their mass density fields integrated over the entire FS. This interaction results in two types of gravity: Type I gravity which includes classical gravity, and under certain conditions, Type II gravity which includes a very strong wave gravity. Gravity exerted by large on small objects reduces to classical gravity. Gravity exerted by small on large objects is 3x the classical value at small kinetic energies. When the small object becomes relativistic, then gravity becomes much larger. Every object has a gravity wavelength, and for the object being acted upon, classical type gravity occurs at distances less than its gravity wavelength while wave gravity occurs at distances greater than its gravity wavelength. The theory yields a set of 8 logarithmic singularities in the gravity force as well as a first-order singularity in the gravity potential. If the FS is quantized into discrete units, these singularities act on the FS to effect changes and interactions in mass density fields instantaneously. As a result, gravity acts instantaneously. We suggest that the 3 degree K cosmic background radiation results from kinetic energy released by the FS units. The theory then predicts that the rest mass of each FS unit is 2 proton masses and its characteristic length is approximately 2mm. We extend the gravity theory to photons and predict the same results as GR for the classical experimental tests as well as for the change in period of binary pulsars. Finally, we show that the gravity theory makes possible a derivation of the Coulomb force

1. INTRODUCTION

[00258] The observation of the cosmic background radiation suggests the existence of a preferred reference frame and calls into question the relativistic invariance foundation of General Relativity (GR). Even with GR's widespread acceptance and numerous precise validations (Will 1993), we can ask whether there is another gravity theory that might explain the nature of the cosmic background radiation and its preferred reference frame.

[00259] The derivation of such a gravity theory began as an attempt to answer where kinetic energy is stored and how the storage of kinetic energy affects gravity. Since we could find no answers to these questions, we started with the only equation that seemed relevant, namely that of mass-energy equivalence (Einstein 1905).

[00260] We believed that both rest mass and kinetic energy distort the fabric of space (FS) - not space-time as in GR. Accordingly, we looked for a rest mass and kinetic energy density function that when integrated over all space would give the answer predicted by mass-energy equivalence. We found only one function and that was in the table of Fourier cosine transforms of Bessel functions (Erdelyi, Magnus, Tricomi 1954). The transform was originally derived by Weber and is also called a Weber discontinuous integral.

[00261] Thus, we hypothesize that an object is the following mass density field DQ(Γ) in is the FS:

$$D_G(r) = M/4\pi\lambda G Jo(r/\lambda G) \cos(vr/c\lambda G) / r^2, \quad (1)$$

where M is the rest mass of the object, λG is its gravity wavelength, J_0 is the Oth order Bessel function of the first kind, r is the distance from the object, v is the speed of the object, and c is the speed of light. The J_0 Bessel function (also called a cylindrical harmonic) corresponds to the space distortion due to rest mass, while the cosine function corresponds to the space distortion due to kinetic energy.

[00262] The integral over all space in spherical coordinates of the mass density field D_G(Γ) reduces to the Fourier cosine transform of the Jo Bessel function (Erdelyi, Magnus, Tricomi 1954):

$$I_0^{2\pi} d\phi \}_0^{\pi} d\theta \sin\theta \, Io^{\infty} dr \, r^2 D_G(r) = M / \sqrt{(1 - v7c^2)} \quad v/c < 1 \quad (2)$$
$$= 0 \quad v/c > 1$$

[00263] The integral over all space of the mass density field DQ(Γ) now predicts mass-energy equivalence and also that the speed of an object is limited by the speed of light. The mass density field may have v = 0 since in that case the integral reduces to the Bessel function normalization integral (Wolfram 1998):

$$M/4\pi\lambda_G \, Jo^{2\pi} d\phi \, J_o^{\pi} d\theta \sin\theta \, J_0^{\infty} dr \, J_0 CrA_G) = M \, M \quad (3)$$

[00264] The mass density field differs from those in current theories of gravity since it includes negative values and must be integrated to infinity. We interpreted the negative values as

resulting from rest mass waves and kinetic energy waves in the FS. The speed of an object is defined relative to the FS since the mass density field of the object exists in the FS. Thus the reference frame in which the FS is at rest is the preferred reference frame. This conclusion is consistent with the cosmic background radiation since we suggest that this radiation results from kinetic energy being released from the FS.

[00265] In contrast with GR, gravity between two objects results from the interaction of the two individual mass density fields integrated over the entire FS. For the object being acted upon, the theory predicts either classical type gravity or wave gravity, depending upon the distance between the two objects and the object's gravity wavelength. The derivation of the gravity force is exact and the values of the constants in the theory are determined from observational data.

[00266] If gravity acts at the speed of light, the integration of the mass density fields to infinity poses a serious problem. This problem is resolved as the theory includes a set of eight logarithmic singularities (i.e. proportional to $-\log(\varepsilon)\,|_{\varepsilon=0}$) and a first-order singularity (i.e. proportional to $1/\varepsilon\,|_{\varepsilon=0}$) in the gravity force. As we develop later, if the FS is quantized into discrete units, the singularity equations show that both types of singularities act on the FS to effect any changes and interactions in the mass density fields. Since the singularities are infinite forces, the changes and interactions occur instantaneously, the integration to infinity is done instantaneously and hence gravity acts instantaneously.

[00267] We also describe the gravitational interaction of photons and compare the predictions of the gravity theory with the experimental tests of GR. Our theory predicts the same results for the classical tests as well as for the change in period of binary pulsars.

[00268] It is noteworthy that the singularities of Type I and Type II gravity display many of the same characteristics as phenomena such as Cooper pairs, Brownian motion, and Aurora Borealis whose forces are not well explained by conventional theory.

[00269] We should add what this theory is not. It is not a quantum theory of gravity but rather a classical theory, even though the FS is quantized into discrete units. This theory is not Lorentz invariant since gravity acts instantaneously. Gravity is also not symmetric in that gravity exerted by an object A on an object B is not the same as gravity exerted by object B on object A. As we show later, Newton's third law is preserved in a two-body system, but the gravity theory does violate the equivalence principle in a novel way. Also,the gravity force is not applied directly by the object exerting the gravity, but by the FS. As a result, energy and momentum are conserved if the FS is included. This is possible since the theory specifies that the FS has mass and kinetic energy and we suggest, based on observational data, that each FS unit has a rest mass

of 2 proton masses, a characteristic length of approximately 2mm, and the capability to store and transfer kinetic energy as vibration energy.

2. GRAVITY CONSTANTS

[00270] We hypothesize that the gravity wavelength λ_Q of an object is linearly proportional to its rest mass and is referenced to the gravity wavelength $\lambda_{F}s$ of a FS unit as follows:

$$\lambda_G = \lambda_{F}s\ M / m_{F}s, \quad (4)$$

where M is the object rest mass and rriFs is the rest mass of a FS unit. We use the atomic mass formula expressed in kilograms per mole to replace the rest mass of a FS unit:

$$aFs = N\,A\,nips\ [kg\ mole^{-1}], \quad (5)$$

where $a_{F}s$ is the atomic mass of a FS unit in kilograms per mole and N_A is Avogadro's number. We define a constant K and rewrite the gravity wavelength of an object as:

$$K = a_{F}s / \lambda_{FS}\ [kg\ mole^{-1}\ m^{-1}] \quad (6)$$

$$\lambda_G = N_A/\kappa\,M \quad (7)$$

[00271] The constant K is the FS atomic mass linear density since the gravity wavelength $\lambda_{F}s$ of a FS unit is its characteristic length.

[00272] To determine the constant NA/κ from observational data, we suggest that the yellow-green glow occurring in nuclear reactions (Rohringer 1968) corresponds to the electron gravity wavelength. As we show later, wave gravity exerted by fusion or fission byproducts in motion strongly vibrates electrons at the electron gravity wavelength. As a result, the electrons release the vibration kinetic energy as radiation at the electron gravity wavelength. We divide the electron gravity wavelength $\lambda_e \approx 0.55\ 10^{-6}$ m (yellow-green light) by its rest mass me and obtain:

$$\lambda_e \approx 0.55\ 10^{-6}m\ (yellow\text{-}green\ light), \quad (8)$$

$$N_A/\kappa = \lambda_e / m_e \approx 6.0\ 10^{23}\ [m\ kg^{-1}]$$

[00273] This result provides observational support that the value of NA/κ is Avogadro's number and that the value of the FS atomic mass linear density K is one.

[00274] Wave gravity can transfer kinetic energy not only to electrons, but also to FS units by strongly vibrating the units at the FS gravity wavelength. As with electrons, the units release the vibration kinetic energy as radiation which we should observe at the FS gravity wavelength. One type of radiation connected with the FS is the 3 degree K cosmic background radiation. If

we assume that this radiation results from cosmic kinetic energy stored in the FS at the instant of the Big Bang and released since that time, then the FS gravity wavelength λ_{FS} is the wavelength of the cosmic background radiation (Penzias, Wilson 1965):

$$\lambda_{FS} \approx 2.0\ 10^{-3}\ m \qquad (9)$$

[00275] We now use equation (7) for the gravity wavelength to obtain the rest mass of a FS unit:

$$m_{FS} = \lambda_{FS} / (N_A/\kappa) = 2m_p \qquad (10)$$

[00276] The result is so close to 2 proton masses that we hypothesize that the rest mass mFS of a FS unit is indeed 2 proton masses ($2m_p$). We would further hypothesize that a FS unit is, in fact, a vibrating proton-antiproton pair.

3. GRAVITY FIELDS

[00277] We show later that the gravity force exerted by an object A on an object B that reduces to classical gravity is:

$$F_{G(IB)} = A_G\, G m_A m_B\, Jo(r_B/\lambda_B) / r_B^2, \qquad (11\ 1)$$

[00278] where AG is an amplification factor independent of N_A/K, G is the gravitational constant, n_{1A} is the mass of object A, m_B is the mass of object B, r_B is the distance of object A from object B, and λ_B the gravity wavelength of object B. For example, aside from relativistic rest mass corrections, $A_G = 1$ for gravity exerted by large on small objects. The deviation of gravity from an inverse square force arises from the J_0 Bessel function.

[00279] Classical gravity corresponds to gravity in the near-zero region of the Jo Bessel function. If $r_B/\lambda_B \ll 1$, the near-zero expansion of the Bessel function $J_0(x) = 1 - x^2/4 + \ldots$ shows that $J_0(r_B/\lambda_B) \sim 1$ and we have the classical gravity force times the amplification factor. Since an object's gravity wavelength in meters is $6.0\ 10^{23}$ times its rest mass in kilograms, an object's gravity wavelength is extremely large except for elementary particles and nuclei. As a result, the near-zero region for larger objects is very large and gravity reduces to classical gravity for most objects and distances.

[00280] Wave gravity occurs in the region $r_B/\lambda_B > 11$ as the Bessel function $Jo(r_B/\lambda_B)$ becomes harmonic. For example, in the asymptotic region $r_B/\lambda_B \gg 1$ we have:

$$Jo(r_B/\lambda_B) \sim \sqrt{(2\lambda_B/\pi r_B)}\cos(r_B/\lambda_B - \pi/4) \qquad (12)$$

$$F_G(r_B) \approx A_G G m_A m_B \sqrt{(2\lambda_B/\pi)} \cos(r_B/\lambda_B - \pi/4) / r_B^{5/2} \quad (13)$$

[00281] However, the wave gravity region for planetary masses like the Earth or Sun is very far away since $\lambda_{Earth} = 3.8\ 10^{32}$ light-years and $\lambda_{sun} = 1.3\ 10^{38}$ light-years. These gravity wavelengths should be compared to the size of the observable universe - about $4.2\ 10^{10}$ light-years. Thus gravity for planetary masses as for most objects is a classical $1/r^2$ force. But, as we show later, gravity is on the average larger than classical gravity since $A_G = 3$ in the case of gravity exerted by small on large objects and A_G has a logarithmic singularity as the masses become equal. In the former case, when the small object is relativistic, $A_G \gg 3$ and gravity is also very much larger than classical gravity.

[00282] If we examine the mass density field in the asymptotic region $r/\lambda_G \gg 1$, we obtain:

$$D_G(r) \approx M/4\pi\lambda_G V(\lambda_G/2\pi) \{\cos((1 + v/c)\ r/\lambda o - \pi/4) + \cos((1 - v/c)\ r/\lambda_G - \pi/4)\} / r^{5/2} \quad (144)$$

[00283] This asymptotic behavior suggests that gravity can be best understood using wave theory. In this view, the kinetic energy creates a mass density wave that has no carrier but only two sidebands. This is an extremely efficient method to transfer information or energy. Wave theory also suggests that the mass density field of the receiving object acts as a receiving antenna and demodulator. Accordingly, we hypothesize that the gravity force occurs at the mass density field level.

[00284] The calculation of the gravity force experienced by an object follows the standard calculation of classical gravity exerted by an object with a spherically symmetric mass density. However, we use the mass density fields of both objects and a coupling constant between the two mass density fields. In order that gravity experienced by a very large object reduces to classical gravity, the coupling constant must be $G4\pi\lambda_G$ where G is the gravitational constant and λ_G is its gravity wavelength. Thus the gravity force exerted by an object A with mass ni_A, gravity wavelength λ_A, and speed V_A on an object B with mass m_B, gravity wavelength λ_B, and speed v_B is:

$$F_G(\Gamma_B) = G m_A m_B / 4\pi\lambda_A \int_o^\infty dr_A\ r_A^2 \int_o^\pi d\theta \sin\theta\ J_0 2\pi d\phi\ J_0(r_A/\lambda_A) \cos(v_A r_A/c\lambda_A) / r_A^2\ Jo((r_B^2 + r_A^2 - 2r_B r_A \cos\theta)'^2 / \lambda_B) \cos(v_B(r_B^2 + r_A^2 - 2r_B r_A\cos\theta)'^2 / c\lambda_B)\ (\Gamma_B - r_A\cos\theta) / (r_B^2 + r_A^2 - 2r_B r_A\cos\theta)^{3/2} \quad (155)$$

[00285] We integrate over ϕ and twice by parts over θ, collect terms, and then make the substitution $x = (r_B^2 + r_A^2 - 2r_B r_A\cos\theta)^{1/2}$ with the result:

$$F_G(r_B) = Gm_Am_B / 2\lambda_A r_B^2 \int_0^\infty dr_A J_0(r_A/\lambda_A) \cos(v_A r_A/c\lambda_A) \quad (166)$$
$$\{[J_o(O'B + r_A)/\lambda_B) \cos(v_B(r_B + r_A)/c\lambda_B) + J_0((r_B - r_A)/\lambda_B) \cos(v_B(r_B - r_A)/c\lambda_B)]$$
$$- 1/2\,\lambda_B \int_{r_B-r_A}^{r_B+r_A} dx/x\ (r_A^2 - r_B^2 + x^2)/r_A\ J_0'(x/\lambda_B) \cos(v_B x/c\lambda_B)$$
$$+ v_B/c2\lambda_B \int_{r_B-r_A}^{r_B+r_A} dx/x\ (r_A^2 - r_B^2 + x^2)/r_A\ J_0(x/\lambda_B) \sin(v_B x/c\lambda_B)\}$$

[00286] There are really three integrals here. The first integral which includes the two J_0 terms is gravity that arises from the density of space and is evaluated in Appendix A. The second is gravity that arises from the change in the density of space due to the rest mass and is evaluated in Appendix B. The third is gravity that arises from the change in the density of space due to kinetic energy and is evaluated in Appendix C. The integration shows that there are two types of gravity which we call Type I and Type II gravity.

4. TYPE I GRAVITY

[00287] We now calculate what we call Type I gravity which reduces to classical gravity in the classical limit. We bring the integrals back together, grouping them by whether they contain a "$\cos(r_A\ldots)$" or "$\sin(r_A\ldots)\,r_A$" term. We evaluate the "$\cos(r_A\ldots)$" integrals first. If we define $s = r_B/\lambda_B$ and the functions A(s), B(s), and C(s), we then have:

$$F_{GI}(r_B) = Gm_Am_B\lambda_B / 4\lambda_A r_B^2\ A(s) \quad (177)$$

$$A(s) = 1/\lambda_B \int_o^\infty dr_A\ Jo(r_A/\lambda_A)\ 1/\pi \int_o^\pi d\theta \quad (18)$$
$$\{\exp(iys)\ [\cos(r_A(y/\lambda_B + v_A/c\lambda_A)) + \cos(r_A(y/\lambda_B - v_A/c\lambda_A))]$$
$$+ \exp(izs)\ [\cos(r_A(z/\lambda_B + v_A/c\lambda_A)) + \cos(r_A(z/\lambda_B - v_A/c\lambda_A))]\},$$
$$\text{where } y = \cos\theta + v_B/c$$
$$z = \cos\theta - v_B/c$$

$$F_{G22}(r_B) = Gm_Am_B\lambda_B / 4\lambda_A r_B^2\ B(s) \quad (19)$$

$$B(s) = 1/\lambda_B \int_0^\infty dr_A\ J_0(r_A/\lambda_A)\ 1/\pi \int_o^\pi d\theta\ (1 - \cos^2\theta) \quad (20)$$
$$\{\exp(iys)\ (s/iy - 1/(iy)^2)\ [\cos(r_A(y/\lambda_B + v_A/c\lambda_A)) + \cos(r_A(y/\lambda_B - v_A/c\lambda_A))]$$
$$+ \exp(izs)\ (s/iz - 1/(iz)^2)\ [\cos(r_A(z/\lambda_B + v_A/c\lambda_A)) + \cos(r_A(z/\lambda_B - v_A/c\lambda_A))]\},$$

$$F_G3i(r_B) = Gm_Am_B\lambda_B / 4\lambda_A r_B^2\ C(s) \quad (21\,1)$$

$$C(s) = - i\,v_B/c\ 1/\lambda_B \int_o^\infty dr_A\ J_0(r_A/\lambda_A)\ 1/\pi \int_o^\pi J_o d\theta \quad (222)$$
$$\{\exp(iys)\ [\cos(r_A(y/\lambda_B + v_A/c\lambda_A)) + \cos(r_A(y/\lambda_B - v_A/c\lambda_A))]\ /iy$$
$$- \exp(izs)\ [\cos(r_A(z/\lambda_B + v_A/c\lambda_A)) + \cos(r_A(z/\lambda_B - v_A/c\lambda_A))]\ /iz\}$$

[00288] We now now reverse the order of integration, noting that the integrals over r_A are the same Weber discontinuous integrals as for the mass density integral. However, as we show in Appendix D, the "$\sin(r_A\ldots)\,r_A$" terms cancel the integrals when the resulting inverse square root terms are imaginary. The integration over r_A gives:

$$A(s) = 1/\pi \int_0^{\pi} d\theta \exp(iys) \quad (233)$$
$$[(\lambda_B^2/\lambda_A^2 - (y + v_A\lambda_B/c\lambda_A)^2)^{-1/2} + (\lambda_B^2/\lambda_A^2 - (y - v_A\lambda_B/c\lambda_A)^2)^{3/2}]$$
$$+ 1/\pi \int_0^{\pi} d\theta \exp(izs)$$
$$[(\lambda_B^2/\lambda_A^2 - (z + v_A\lambda_B/c\lambda_A)^2)^{-1/2} + (\lambda_B^2/\lambda_A^2 - (z - v_A\lambda_B/c\lambda_A)^2)^{3/2}],$$

$$B(s) = 1/\pi \int_0^{\pi} d\theta (1 - \cos^2\theta) \exp(iys) (s/iy - 1/(iy)^2) \quad (244)$$
$$[(\lambda_B^2/\lambda_A^2 - (y + v_A\lambda_B/c\lambda_A)^2)^{3/2} + (\lambda_B^2/\lambda_A^2 - (y - v_A\lambda_B/c\lambda_A)^2)^{3/2}]$$
$$+ 1/\pi \int_0^{\pi} d\theta (1 - \cos^2\theta) \exp(izs) (s/iz - 1/(iz)^2)$$
$$[(\lambda_B^2/\lambda_A^2 - (z + v_A\lambda_B/c\lambda_A)^2)^{3/2} + (\lambda\beta^2/\lambda_A^2 - (z - v_A\lambda_B/c\lambda_A)^2)^{3/2}],$$

$$C(s) = - i v_B/c \; 1/\pi \int_0^{\pi} d\theta \exp(iys) / iy \quad (25)$$
$$[(\lambda_B^2/\lambda_A^2 - (y + v_A\lambda_B/c\lambda_A)^2)^{3/2} + (\lambda_B^2/\lambda_A^2 - (y - v_A\lambda_B/c\lambda_A)^2)^{3/2}]$$
$$+ i v_B/c \; 1/\pi \int_0^{\pi} d\theta \exp(izs) / iz$$
$$[(\lambda_B^2/\lambda_A^2 - (z + v_A\lambda_B/c\lambda_A)^2)^{3/2} + (\lambda_B^2/\lambda_A^2 - (z - v_A\lambda_B/c\lambda_A)^2)^{1/2}]$$

[00289] The integrals are non-zero for all values of λ_B/λ_A, but the integration limits may be reduced so that the inverse square root terms are real. For the most part, when $\lambda_B/\lambda_A > 1$ (i.e. gravity exerted by object A on object B that has larger mass), the integral limits are 0 to π as the zeros of the Weber terms lie outside the integration interval. As λ_B/λ_A approaches one, the zeros of the Weber terms approach the integration interval and the limits must be carefully specified. When $\lambda_B/\lambda_A < 1$ (i.e. gravity exerted by object A on an object B that has smaller mass), then the integration limits are the zeros of the Weber inverse square root terms even though we may display the limits as 0 to π.

[00290] We first show, however, that the Type I gravity force experienced by object B is an amplification factor multiplied by $Jo(r_B/\lambda_B) / r_B^2$. We do this by showing that the Type I gravity force satisfies Bessel's equation of order zero. If we add the function A(s) and its second derivative, we obtain:

$$d^2/ds^2 A(s) + A(s) = 1/\pi \int_0^{\pi} d\theta \exp(iys) [(I - \cos^2\theta) - yv_B/c - \cos\theta v_B/c] \quad (266)$$
$$[(\lambda_B^2/\lambda_A^2 - (y + v_A\lambda_B/c\lambda_A)^2)^{3/2} + (\lambda_B^2/\lambda_A^2 - (y - v_A\lambda_B/c\lambda_A)^2)^{3/2}]$$
$$+ 1/\pi \int_0^{\pi} d\theta \exp(izs) [(I - \cos^2\theta) + zv_B/c + \cos\theta v_B/c]$$
$$[(\lambda_B^2/\lambda_A^2 - (z + v_A\lambda_B/c\lambda_A)^2)^{3/2} + (\lambda_B^2/\lambda_A^2 - (z - v_A\lambda_B/c\lambda_A)^2)^{3/2}]$$

[00291] Taking the derivative of B(s) and dividing by s gives:

$$1/s \; d/ds \; B(s) = 1/\pi \int_0^{\pi} d\theta \exp(iys) (1 - \cos^2\theta) \quad (277)$$
$$[(\lambda_B^2/\lambda_A^2 - (y + v_A\lambda_B/c\lambda_A)^2)^{3/2} + (\lambda_B^2/\lambda_A^2 - (y - v_A\lambda_B/c\lambda_A)^2)^{3/2}]$$
$$+ 1/\pi \int_0^{\pi} d\theta \exp(izs) (1 - \cos^2\theta)$$
$$[(\lambda_B^2/\lambda_A^2 - (z + v_A\lambda_B/c\lambda_A)^2)^{3/2} + (\lambda_B^2/\lambda_A^2 - (z - v_A\lambda_B/c\lambda_A)^2)^{3/2}]$$

[00292] The function C(s) is the kinetic energy correction term that contributes to the second derivative of A(s) to remove the first of its kinetic energy terms. Thus we take the second derivative of C(s) to obtain:

$$d^2/ds^2\ C(s) = 1/\pi \int_0^{\pi} d\theta \exp(iys)\ yv_B/c \quad (28)$$
$$[(\lambda_B^2/\lambda_A^2 - (y + v_A\lambda_B/c\lambda_A)^2)^{-1/2} + (\lambda_B^2/\lambda_A^2 - (y - v_A\lambda_B/c\lambda_A)^2)^{-1/2}]$$
$$- 1/\pi \int_0^{\pi} d\theta \exp(izs)\ zv_B/c$$
$$[(\lambda_B^2/\lambda_A^2 - (z + v_A\lambda_B/c\lambda_A)^2)^{-1/2} + (\lambda_B^2/\lambda_A^2 - (z - v_A\lambda_B/c\lambda_A)^2)^{-1/2}]$$

[00293] We show in Appendix E that the remaining kinetic energy term in the second derivative of A(s) integrates to zero and so the Type I gravity force satisfies an equation that we compare to Bessel's equation:

$$d^2/ds^2\ \{A(s) + C(s)\} - 1/s\ d/ds\ B(s) + A(s) = 0, \quad (29)$$

$$d^2/ds^2\ J_n(s) + 1/s\ d/ds\ J_n(s) + (1 - n^2/s^2)\ J_n(s) = 0 \quad (300)$$

[00294] Thus the Type I gravity force is a Bessel function of order zero and the functions A(s) and C(s) are proportional to $J_0(s)$ and B(s) to $-J_0(s)$. By grouping together the terms in s and noting that $\exp(is\cos\theta)$ is a Bessel generating function, we can replace the terms in s by Jo(s). We begin with the A(s) term, changing the integration variable to $t = \cos\theta$:

$$\exp(is\cos\theta) = Jo(s) + 2\sum_{n=1}^{\infty} i^n J_n(s)\cos(n\theta), \quad (31)$$

$$A(s) = J_0(S)\ 1/\pi \int_{-1}^{1} dt\ (1 - t^2)^{-1/2} \quad (322)$$
$$\{((t + v_B/c + \alpha)(\beta - 1 - v_B/c))^{1/2} + ((t + v_B/c + \beta)(\alpha - t - v_B/c))^{-1/2}$$
$$+ ((t - v_B/c + \alpha)(\beta - 1 + v_B/c))^{-1/2} + ((t - v_B/c + \beta)(\alpha - 1 + v_B/c))^{1/2}\},$$
$$\text{where } \alpha = \lambda_B/\lambda_A\,(1 + v_A/c)$$
$$\beta = \lambda_B/\lambda_A\,(1 - v_A/c)$$

[00295] When the integral limits are -1 to 1 or the Weber zeros, each integral has the following form where K(m) is the complete elliptic integral K of the first kind (Wolfram 1996):

$$\int_{-1}^{1} (1 - t^2)^{-1/2} (a + 1)^{-1/2} (b - 1)^{-1/2} = 2/((1 + a)(1 + b))^{-1/2})\ K(m), \quad (333)$$
$$\text{where } m = 2(a + b) / ((1 + a)(1 + b))$$

[00296] When object A is much smaller than object B (i.e. $r_B/\lambda_B \ll 1$), then $a \gg 1$ and $b \gg 1$, and the argument of the complete elliptic integral K(m) is very small. We can then use the identity $K(0) = \pi/2$ to approximate each of the 4 integrals:

$$A(s) \approx 4\ J_0(s)\ (\alpha\beta)^{1/2}, \quad (34,4)$$

$$F_G i(r_B) \approx Gm_A m_B\,(1 - v_A^2/c^2)^{1/2}\ J_0(r_B/\lambda_B)\ /\ r_B^2, \quad (355)$$
$$\text{where } \lambda_B/\lambda_A \gg 1$$

[00297] Now we take the classical limit in which the mass of object B is large (i.e. $\lambda_B \gg 1$) and recover classical gravity with a rest mass increase for object A relativistic:

$$F_{G\,classical\ 0"B)} = G m_A m_B (1 - v_A^2/c^2)^{-1/2} I r_B^2, \quad \text{where } \lambda_B A_{,A} \gg 1, r_B/\lambda_B \ll 1 \tag{366}$$

[00298] When object A is much larger than object B (i.e. $\lambda_B A_{,A} \ll 1$), then $\alpha \ll 1$ and $\beta \ll 1$. If $\lambda_B/\lambda_A \ll (1 - V_B^2/C^2)$, then $m \ll 1$, $K(m) \approx \pi/2$, and $A(s) \approx 4 J_0(s) (1 - v_B^2/c^2)^{-1/2}$. Therefore the contribution of A(s) to the gravity of a larger object on a smaller object is negligible.

[00299] We now examine the 8 logarithmic singularities in the functions A(s) and C(s) which occur whenever λ_A, $\lambda\beta$, v_A, and V_B satisfy one of the 4 following conditions:

$$\lambda_B/\lambda_A = (1 \pm v_B/c) / (1 \pm v_A/c) \tag{377}$$

[00300] The singularities occur when the zeros of the Weber terms are coincident with the zeros at the edge of the Bessel integration region and result in a factor 1/(1 - 1) or 1/(1+ 1). Since the singularities are at the integration limits, this results in Type I gravity having two logarithmic singularities from each of its four terms..

[00301] For example, we evaluate the first A(s) term in eq. (32) when the Weber zeros in eq. (33) occur at $a = 2\lambda\beta/\lambda_A - 1$ and $b = 1$, corresponding to $\lambda\beta/\lambda_A = (1 + v_B/c) / (1 - v_A/c)$. The integration region is from -1 to 1 since $\lambda\beta/\lambda_A \geq 1$ and we have:

$$A_{11}(S) = J_0(S)\, 2/\pi\, ((I + a)(l + b))^{J/2} K(m), \quad \text{where } m = 2(a + b) / ((I + a)(l + b)) \tag{38}$$
$$a = \lambda_B/\lambda_A (1 + v_A/c) + v_B/c$$
$$b = \lambda_B/\lambda_A (1 - v_A/c) - v_B/c$$

[00302] The argument of the complete elliptic integral K(m) is close to 1 so $K(m) \sim -\frac{1}{4}$ log(l - m) + log(4) and we obtain at the singularity:

$$Foii(rb) = G m_A m_B J_0(IBAB) / r_B^2 \quad \text{l/8 } \pi (\lambda_B/\lambda_A)^{1/2} \{\log(3_{\,2}\ \lambda_{B}/\lambda_{A} / (\lambda_{B}/\lambda_{A} - I)))) - \text{l}\log g((bb - 1)) \text{ I } b\text{==i.)}\}, \quad \text{where } \lambda_B/\lambda_A = (1 + v_B/c) / (1 - v_A/c) \tag{39}$$

[00303] The other singularity in the first term occurs at a = 1 and $b = 2\lambda_B/\lambda_A - 1$, corresponding to $\lambda_B/\lambda_A = (1 - v_B/c) / (1 + v_A/c)$. The integration region is from -1 to b since $\lambda_B/\lambda_A \leq 1$. Such integrals with mixed limits have the following form (Wolfram 1996):

$$J\text{-}i^{b} dt\ (1\text{-}\ 1^2)^{"1/2} (a + t)^{"1/2} (b - 1)^{-1/2} = 2/(2(a + b)f\ \ K(I/m) \tag{40}$$

[00304] The argument of the complete elliptic integral K(I /m) is again close to 1 and we obtain:

Foil (TB) = $G m_A m_B$ Jo(r_B/λ_B) / $r_B^2 r_B^2$
(41 1)

l/8 π (λ_B/λ_A)$^{\gamma 2}$ {log(32 λ_B/λ_A / (1 - λ_B/λ_A)) - log(a - 1) | $_a$=i},
where λ_B/λ_A = (1 - v_B/c) / (1 + v_A/c) where λ_B/λ_A = (1 - v_B/c) / (1 + v_A/c)

[00305] The singularities in the B(s) terms give rise both to gravity exerted by a larger object A on a smaller object B and to gravity exerted by a smaller object A on a larger object B. We also show that this gravity reduces to classical gravity in the classical limit. We first note that the singularities in B(s) are removed by differentiation so that its J_0 (s) nature arises from the combination of both the 1/iy and l/(iy) ^{2} terms. As a result, we replace the common terms in s and the Bessel generating functions (i.e. "(s - 1/iy) exp(iys)" and "(s - 1/iz) exp(izs)") by -Jo(s). In addition, we change the integration variable to t = cos:

B(s) = -Jo(s) l/i π J_{-1}^{1} dt (l - t^2)$^{\gamma 2}$ (422)
{[(t + v_B/c + α)$^{\gamma 2}$(β - 1 - v_B/c)$^{1/2}$ + (t + v_B/c + β)$^{J/2}$(α - 1 - v_B/c)$^{\gamma 2}$]/(t+v_B/c)
+[(t - V_B/C + α)$^{\gamma 2}$(β - 1 + v_B/c)$^{J/2}$ + (t - V_B/C + β)$^{\gamma 2}$(α - 1 + v_B/c)$^{1/2}$]/(t-v_B/c)}

[00306] For gravity exerted by a larger object A on a smaller object B, the zeros of the Weber terms lie inside the integration interval 0 to π and so the integration interval is really between the zeros of each Weber term. We shift the integration variable so that each integral has the following form where II(n | m) is the complete elliptic integral Il of the third kind (Wolfram 1996):

J_{-a}^{b} dt (e + 1)$^{\gamma 2}$ (d - t)$^{1/2}$ (a + 1)$^{\gamma 2}$ (b - 1)$^{\gamma 2}$ / 1 (433)
= 2(d-b)((a+d)(b+e))$^{1/2}$ {n((a+bb))//((aa++dd)) | m)) + e/bb n((dd((aa++bb))//((bb(a+d)) | m)},
where m = 2(a+b)/((a+d)(b+e))

[00307] If λ_B/λ_A « 1, then a « 1 and b « 1. If (a + b) « ed, then m « 1 and we can use the identity $\ddot{u}$ (n | 0) = (1—n)$^{1/2}$$\pi$/2 to approximate the terms. The integral evaluates to {π(d-b)$^{1/2}$(b+e)$^{-1/2}$ (1 - i e(ab)$^{\gamma 2}$)}. Thus the gravity exerted by a much larger object A on a smaller object B is:

B(s) $\approx$ 4 Jo(s) ($\alpha\beta$y$^{1/2}$ (ed)$^{\prime /2}$, (444)

F_G22(r_B) ~ $G m_A m_B$ (1 - v_A^2/c^2y$^{\gamma 2}$ (1 - v_B^2/c^2)$^{\gamma 2}$ J_0(r_B/λ_B) / r_B^2, (455)
where λ_B/λ_A « (1 —v_B^2/c^2)

[00308] We note that the gravity exhibits a rest mass increase for object A relativistic, but a rest mass decrease for object B relativistic. We now take the classical limit in which the mass of object B is large (i.e. $\Gamma_B/\lambda_B \ll 1$) and we obtain classical gravity with a rest mass increase for object A relativistic, but with a rest mass decrease for object B relativistic:

$$F_{G\,classical}(r_B) = Gm_Am_B(1 - v_A^2/c^2)^{J/2}(1 - v_B^2/c^2)^{\gamma/2}/r_B^2, \quad (46)$$
where $\lambda\beta/\lambda_A \ll (1 - VB^2/C^2)$, $r\beta/\lambda\beta \ll 1$

[00309] When object A is smaller than object B, the integration limits are the Bessel limits. We shift the integration variable so that each integral has the following form (Wolfram 1996):

$$L^d dt\,(e + tf\ (d - tf\ (a + ty^{'1/2}(b - t)^{-\gamma^2}/1 \quad (47)$$
$$= 2(b-d)((a+d)(b+e))^{J/2}\{-(b+e)/b\ K(m) + \pi(2/(b+e)\ |m)$$
$$+ e/b\ \pi(2b/((b+e)d))\ |m)\},$$
where $m = 2(a+b)/((a+d)(b+e))$

[00310] If $\lambda\beta_{A\text{-}A} \gg 1$, then $a \gg 1$, $b \gg 1$, $m \ll 1$, and we can use the identities $K(O) = \pi/2$ and $n(n\ I0) = (l\text{-}n)^{-\gamma 2}\pi/2$ to approximate the terms. Consequently the K(m) term cancels the first $n(n\ Im)$ term and we have:

$$B(s) \approx 4\,J_0(s)\,(\alpha\beta)^{-1/2}\,(ed)^{1/2}, \quad (,48)$$

$$F_G2_2(r_B) \approx Gm_Am_B(1 - v_A^2/c^2)^{-\gamma 2}(1 - v_B^2/c^2)^{\gamma 2}J_0(r_B/\lambda_B)/r_B^2, \quad (49)$$
where $\lambda_B/\lambda_A \gg 1$

[00311] While this result implies that gravity exerted by a smaller object A on a much larger object B is now twice the classical value, it is in fact three times the classical value since we show later that Type II gravity also gives the same result. However, in the case of Type II gravity, the gravity is only the same for $v_A/c \ll 1$. As object A becomes relativistic, Type II gravity becomes much larger than just a relativistic increase in the rest mass of object A.

[00312] We conclude Type I gravity by evaluating the kinetic energy correction term C(s). We show that C(s) is negligible in the classical limit when object A is larger than object B and integrates to zero when object A is smaller than object B. As with A(s), we replace the terms in s by Jo(s) and change the integration variable to $t = \cos\theta$ to obtain:

$$C(s) = -v_B/c\ J_0(s)\ l/\pi J_{-1}^{1}\,dt\,(1 - t^2)^{-12} \quad (500)$$
$$\{[(t + v_B/c + \alpha)^{-\gamma 2}(\beta - 1 - v_B/c)^{-12} + (t + v_B/c + \beta)^{-\gamma 2}(\alpha - 1 - v_B/c)^{-\gamma 2}]/(t+v_B/c)$$
$$-[(t - V_B/C + \alpha)^{-\gamma 2}(\beta - 1 + v_B/c)^{-12} + (t - v_B/c + \beta)^{-\gamma 2}(\alpha - 1 + v_B/c)^{-\gamma 2}]/(t-v_B/c)\}$$

[00313] For gravity exerted by a larger object A on a smaller object B, the zeros of the Weber terms lie inside the integration interval 0 to π and so the integration interval is between

the zeros of each Weber term. We shift the integration variable so that each integral has the following form (Wolfram 1996):

$$L^{b}\, dt\, (e+1)^{-1/2}\, (d-1)^{J/2}\, (a+t)^{-1/2}\, (b-1)^{-1/2} / 1 \qquad (51)$$
$$= 2/((a+d)(b+e))^{-1/2}\{1/d\ K(m) + (d-b)/bd\ \pi\,(d(a+b)/(b(a+d)))\ |\ m)\},$$
$$\text{where } m = 2(a+b)/((a+d)(b+e))$$

[00314] If $\lambda\beta/\lambda_A$ « 1, then a « 1 and b « 1. If (a + b) « de then m « 1, and we can use the identities K(O) = $\pi/2$ and FI(n | 0) = (l-n) $^{-1/2}\pi/2$ to approximate the terms. The integral evaluates to $\{\pi(de)^{-1/2}(1/d - i\,(ab)^{-1/2})\}$ with the result that the imaginary part of the 4 terms in C(s) cancel and the real part is negligible.

[00315] When object A is smaller than object B, the integration limits are the Bessel limits. The first and fourth terms and the second and third terms cancel as they are mirror images with respect to the integration interval and occur with opposite sign. Thus the kinetic energy correction term C(s) integrates to zero.

5. TYPE II GRAVITY

[00316] We can follow a similar procedure for Type II gravity and find that this gravity is far stronger than classical gravity in all regions. For Type II gravity, we evaluate the "sin(rA…) / Γ_A" integrals. We define $s = r_B/\lambda_B$ and the functions E(s) and F(s) as follows:

$$F_{G}23(r_B) = Gm_Am_B\lambda B/\ 4\lambda_A r_B^{\,2}\ E(s) \qquad (522)$$

$$E(s) = I_o^{\infty}\, dr_A/r_A\ Jo(r_A/\lambda_A)\ i/\pi\ J_o^{\pi} d\theta\ (1 - \cos^2\theta) \qquad (533)$$
$$\{\exp(iys)\ (l/(iy)^3 - s/(iy)^2)[\sin(r_A(y/\lambda_B + v_A/c\lambda_A)) + \sin(r_A(y/\lambda_B - v_A/c\lambda_A))]$$
$$+\exp(izs)\ (l/(iz)^3 - s/(iz)^2)[\sin(r_A(z/\lambda_B + v_A/c\lambda_A)) + \sin(r_A(z/\lambda_B - v_A/c\lambda_A))]\},$$
$$\text{where } y = \cos\theta + v_B/c$$
$$z = \cos\theta - v_B/c$$

$$F_{G3}2(r_B) = Gm_Am_B\lambda_B / 4\lambda_A r_B^{\,2}\ F(s) \qquad (544)$$

$$F(s) = iv_B^{\,2}/c^2\ J_o^{\infty}\, dr_A/r_A\ Jo(r_A/\lambda_A)\ 1/\pi\ J_o^{\pi} d\theta\ J_0^{1} dt \qquad (55)$$
$$\{\exp(iy_t s)\ (l/(iy_t)^3 - s/(iy_t)^2)$$
$$[\sin(r_A(y_t/\lambda_B + v_A/c\lambda_A)) + \sin(r_A(y_t/\lambda_B - v_A/c\lambda_A))]$$
$$+ \exp(iz_t s)\ (l/(iz_t)^3 - s/(iz_t)^2)$$
$$[\sin(r_A(z_t/\lambda_B + v_A/c\lambda_A)) + \sin(r_A(z_t/\lambda_B - v_A/c\lambda_A))]\},$$
$$\text{where } y_t = \cos\theta + v_B t/c$$
$$z_t = \cos\theta - v_B t/c$$

[00317] The F(s) term is the kinetic energy correction term and has the same functional form as E(s). When object A is the same size or larger than object B or the same size (i.e. $\lambda\beta_{A\text{-}A} \leq$

I)$_5$ E(s) has a first-order singularity while F(s) does not, so we neglect the F(s) term in that region. When object A is smaller than object B (i.e. $\lambda_B/\lambda_A > 1$), we show later that F(s) integrates to zero.

[00318] To determine the functional form of E(s), we first define the functions P(s) and Q(s) as:

$$E(s) = P(s) - s\,Q(s), \tag{56}$$

$$P(s) = \int_0^\infty dr_A/r_A\, Jo(r_A/\lambda_A)\, i/\pi \int_0^\pi d\theta\,(1 - \cos^2\theta) \{\exp(iys)\, l/(iy)^3 [\sin(r_A(y/\lambda_B + v_A/c\lambda_A)) + \sin(r_A(y/\lambda_B - v_A/c\lambda_A))] + \exp(izs)\, l/(iz)^3 [\sin(r_A(z/\lambda_B + v_A/c\lambda_A)) + \sin(r_A(z/\lambda_B - v_A/c\lambda_A))]\}, \tag{57}$$

$$Q(s) = \int_0^\infty dr_A/r_A\, J_0(r_A/\lambda_A)\, i/\pi \int_0^\pi d\theta\,(1 - \cos^2\theta) \{\exp(iys)\, l/(iy)^2 [\sin(r_A(y/\lambda_B + v_A/c\lambda_A)) + \sin(r_A(y/\lambda_B - v_A/c\lambda_A))] + \exp(izs)\, l/(iz)^2 [\sin(r_A(z/\lambda_B + v_A/c\lambda_A)) + \sin(r_A(z/\lambda_B - v_A/c\lambda_A))]\} \tag{58}$$

[00319] We can then write the following equation which removes the singularities in E(s), add and subtract Q(s), and use that Q(s) = d/ds P(s) to obtain:

$$d/ds\,(1/s\; d/ds\,(P(s) - s\,Q(s))) = -\,d/ds\,(P''(s)), \tag{59}$$

$$d/ds\,(P''(s) + 1/s\,P'(s) + P(s)) - (Q''(s) + 1/s\,Q'(s) + (1 - 1/s^2)\,Q(s)) = 0 \tag{60}$$

[00320] Since Q(s) = d/ds P(s), this equation is zero only if both the equations in P(s) and Q(s) are zero. Thus P(s) is the $J_0(s)$ Bessel function and Q(s) is the $J_1(S)$ Bessel function. To try to simplify E(s), we use that P(s) satisfies Bessel's equation of order zero, Q(s) = P'(s), and Q(s) satisfies Bessel's equation of order one to obtain:

$$E(s) = -2/s\,Q(s) + sQ''(s) \tag{61}$$

[00321] Rather than evaluate the Type II gravity force at this time, we calculate the Type II gravity potential as seen by object B. We integrate the second term in E(s) twice by parts and find that the resulting integral cancels the first term in E(s):

$$V_{G23}(r_B) = Gm_Am_B/4\lambda_A\, V_E(s), \tag{62}$$

$$V_E(S) = Ids\; E(s)\,/\,s^2 = -\,P(s)\,/\,s \tag{633}$$

[00322] Thus the Type II gravity potential is proportional to $-Jo(r_B/\lambda_B)\,/\,r_B$. We replace the Bessel generating functions in the P(s) integrals by $J_0(s)$ as follows:

$$P(s) = J_0(S) \int_0^{\infty} dr_A/r_A\, Jo(r_A/\lambda_A)\, i/\pi \int_o^{\pi} d\theta\, (1 - \cos^2\theta) \quad (644)$$
$$\{1/(iy)^3 [\sin(r_A(y/\lambda_B + v_A/c\lambda_A)) + \sin(r_A(y/\lambda_B - v_A/c\lambda_A))]$$
$$+ 1/(iz)^3 [\sin(r_A(z/\lambda_B + v_A/c\lambda_A)) + \sin(r_A(z/\lambda_B - v_A/c\lambda_A))]\}$$

[00323] We reverse the order of integration and note that the integrals over rA are the Fourier sine transform ($a > 0$):

$$\int_0^{\infty} dt/t\, Jo(at)\, \sin(xt) = -\pi/2 \quad -\infty < \chi < -a \quad (655)$$
$$= \sin^{-1}(x/a) \quad -a < x < a$$
$$= \pi/2 \quad a < x < \infty$$

[00324] We now examine the P(s) integrals. When $\lambda_B/\lambda_A \leq 1$, the Fourier transform provides three regions of integration. There is the region of the inverse sine with the limits of the inverse sine, and $-\pi/2$ and $\pi/2$ regions with the limits from the inverse sine to the Bessel limits. When $\lambda_B/\lambda_A > 1$, the integration limits are 0 to π from the Bessel limits and the inverse sine is incomplete. We examine this case later.

[00325] When object A is the same size or larger than object B or the same size (i.e. $\lambda_B/\lambda_A \leq 1$), all the P(s) integrals have a first-order singularity in the region of the inverse sine so we can neglect the other two regions:

$$P(s) = -J_0(s)\, 1/\pi \int_0^{\pi} d\theta\, (1 - \cos^2\theta) \quad (66)$$
$$\{1/y^3 [\sin^{-1}(y\lambda_A/\lambda_B + v_A/c) + \sin^{-1}(y\lambda_A/\lambda_B - v_A/c)]$$
$$+ 1/z^3 [\sin^{-1}(z\lambda_A/\lambda_B + v_A/c) + \sin^{-1}(z\lambda_A/\lambda_B - v_A/c)]\}$$

[00326] If we change the integration variable to argument of the inverse sine, all the P(s) integrals have the following form:

$$\int_{-1} dt\, (a + t)^{\Lambda} (b - t)^{1/2} \sin^{-1}(t) / (t - d)^3 \quad (67)$$

[00327] We then set the square root terms to their value at the singularity, evaluate the resulting integrals (Wolfram 1996), and keep only the term with the singularity which we express as $(1/\varepsilon \mid_{\varepsilon=0})$. As with B(s) in Type I gravity, P(s) exhibits a rest mass increase for object A relativistic and a rest mass decrease for object B relativistic:

$$P(s) = J_0(S)\, \lambda_A^2/\lambda_B^2\, (1 - v_A^2/c^2)^{-1/2}\, (1 - v_B^2/c^2)^{1/2}\, 4/\pi\, (1/\varepsilon \mid_{\varepsilon=0}), \quad (68)$$

$$V_G 2_3(r_B) = - Gm_A m_B \lambda_A/\lambda_B\, Jo(r_B/\lambda_B)/rB\, (1 - v_A^2/c^2)^{1/2}\, (1 - v_B^2/c^2)^{1/2}\, 1/\pi\, (1/\varepsilon \mid_{\varepsilon=0}),$$
$$\text{where } \lambda_B/\lambda_A \leq 1 \quad (69)$$

[00328] Since the Type II gravity potential has a first-order singularity, the Type II gravity force experienced by object B is zero for distances less than its gravity wavelength. For distances

greater than its gravity wavelength, a very large gravity force occurs whenever $J_0(r_B/\lambda_B)$ changes sign:

$$F_{023}(r_B) = Gm_Am_B\lambda A/\lambda BV \quad Ji(iW\lambda_B)/r\& (I - v_A^2/c^2)^{-r2} (1 - v_B^2/c^2)^{r^2} 1/\pi (1/\varepsilon |_{\varepsilon=o}), \quad (700)$$

where J_1 is the 1st order Bessel function of the first kind and r_B/λ_B is a zero of the J_0 Bessel function. For example, the first zero of the J_0 Bessel function occurs at a value of $r_B/\lambda_B \approx 2.4$.

[00329] Since a force results in a change in momentum, we hypothesize that the Type II gravity force imparts a momentum addition to object B in the direction of the Type II gravity force as object B moves through the zeros of the J_0 Bessel function. For example, an alpha particle emitted from a fusion reaction transfers kinetic energy into vibrating electrons in the surrounding environment at the electron gravity wavelength.

[00330] As shown earlier, the electron gravity wavelength is —0.55 10^{-6}m. Thus at atomic distances which are about 10^{-10}m, gravity experienced by an electron is the small classical force andand does not appear to affect atomic quantum mechanical phenomena.

[00331] We now examine Type II gravity when object A is smaller than object B (i.e. $\lambda_{BA,A} > 1$). In this region, the integration limits are 0 to π from the Bessel limits and the inverse sine is incomplete. We change the integration variable to $t = \cos\theta$ and obtain:

$$\begin{aligned} P(s) \quad &= -J_0(s)\, 1/\pi \int_{-1}^{1} dt\, (1 - t^2)^{1/2} \\ &\{[\sin^{-1}(\lambda_A/\lambda_B(t + v_B/c) + v_A/c) + \sin^{-1}(\lambda_A/\lambda_B(t + v_B/c) - v_A/c)] / (t + v_B/c)^3 \\ &+ [\sin^{-1}(\lambda_A/\lambda_B(t - v_B/c) + v_A/c) + \sin^{-1}(\lambda_A/\lambda_B(t - v_B/c) - v_A/c)] / (t - v_B/c)^3\} \end{aligned} \quad (71)$$

[00332] Each integral has the following form (Wolfram 1996):

$$\begin{aligned} &J_{-I}^{1}{}_{CIt} (1 - t^2)^{1/2} \sin^{-1}\{a(t + d) + b\} / (t + d)^3 \\ &\quad = 1/2 \sin^{-1}\{-a\pi + (b - 2ad(1 - d^2)) \\ &\qquad \log[-4(1 - d^2)^{1/2}/(b - 2ad(1 - d^2))] / (1 - d^2)^{3/2}\} \\ &\quad -1/2 \sin^{-1}\{a\pi + (b - 2ad(1 - d^2)) \\ &\qquad \log[4(1 - d^2)^{1/2}/(b - 2ad(1 - d^2))] / (1 - d^2)^{3/2}\} \end{aligned} \quad (722)$$

[00333] If $V_A/C \ll 1$ and $v_B/c \ll 1$, then P(s) is nearly independent of V_A/C and v_B/c and we have:

$$P(s) \quad \approx\approx 4/\pi\, Jo(s)\, \sin^{-1}(\pi\lambda A/\lambda\beta), \quad (73)$$

$$Vo_{23}(r_B) \approx -Gm_Am_B\lambda_B/\lambda_A\ 1/\pi \sin^{-1}(\pi\lambda_A/\lambda_B)\, Jo(r_B/\lambda_B) / r_B, \quad (74)$$

where $\lambda_B/\lambda A > 1$, $V_A/C \ll 1$, $v_B/c \ll 1$

[00334] In the classical limit for object A much smaller than object B (i.e. $\lambda\beta/\lambda_A$ » **1,** $r\beta/\lambda_B$ « 1), the Type II gravity potential reduces to the classical gravity potential:

$$V_{Q23}(\Gamma_B) \sim -Gm_A m_B / r_B, \quad \text{where } \lambda\beta/\lambda_A \gg 1,\ r\beta/\lambda\beta \ll 1,\ V_{A/C} \ll 1,\ V\beta/c \ll 1 \tag{75}$$

[00335] For object A much smaller than object B (i.e. $\lambda\beta/\lambda_A \gg 1$), object A highly relativistic (i.e. $V_A/C \approx 1$), and $V\beta/c \ll 1$, each integral contributes the same real part while the imaginary parts cancel, andand the factor $\lambda\beta/\lambda_A$ no longer cancels in the Type II gravity potential. As a result, the Type II gravity potential and the gravity force in the classical limit are very large since the mass of object A is effectively replaced by the mass of object B:

$$P(s) \approx 2/\pi\, J_0(S)\, \mathrm{Re}\{\sin^{-1}(\log 4) - \sin^{-1}(\log 4 + i\pi)\}, \tag{76}$$

$$V_{G23}(r_B) \approx -Gm_A m_B/r_B\, \lambda_B/\lambda_A\, l/2\pi\, \mathrm{Re}\{\sin^{-1}(\log 4) - \sin^{-1}(\log 4 + i\pi)\}, \quad \text{where } \lambda_B\Lambda_A \gg 1,\ r\beta/\lambda\beta \ll 1,\ V_A/C \approx 1,\ v_B/c \ll 1 \tag{77}$$

[00336] Thus a relativistic small object or FS unit is able to exert a very large classical type force on a large object.

[00337] We conclude Type II gravity by showing that the contribution of the kinetic energy correction term F(s) integrates to zero when object A is smaller than object B (i.e. $\lambda_B\Lambda_A > 1$). As with E(s), we define $F(s) = P_{KE}(S) - s\, Q_{KE}(S)$, show that the gravity potential $V_{G32}(\Gamma_B)$ is proportional to $-P_{KE}(S)/S$, evaluate the integral over Γ_A, and replace the Bessel generating functions in $P_{KE}(S)$ by Jo(s) to obtain:

$$V_{G32}(r_B) = -Gm_A m_B\, \lambda_B/4\lambda_A\, P_{KE}(S) / r_B, \tag{78,78}$$

$$P_{KE}(S) = -v_B^2/c^2\, J_0(s)\, 1/\pi \int_0^{\pi} d\theta \int_0^1 dt \{[\sin^{-1}(y_t\lambda_A/\lambda_B + v_A/c) + \sin^{-1}(y_t\lambda_A/\lambda_B - v_A/c)] / y_t^3 + [\sin^{-1}(z_t\lambda_A/\lambda_B + v_A/c) + \sin^{-1}(z_t\lambda_A/\lambda_B - v_A/c)] / z_t^3\} \tag{79}$$

[00338] In evaluating the integrals over t, the values at the lower limits cancel, and as a result each integral over t has the following form which we substitute in the $P_{KE}(S)$ integrals (Wolfram 1996):

$$\mathbf{Vdt}\ \sin^{-1}(at + b) / (et + d)^3 = -l/2e \{\sin^{-1}(b+a) / (d+e)^2 + \lambda_A/\lambda_B\, (1 - V_A^2/c^2)^{-1}\, (1 - (b+a)Y^2 / (d+e) + (\lambda_A/\lambda_B)^2\, (b-ad/e)\, (1 - v_A^2/c^2)^{-3/2} \log[(l - (b-ad/e)\, (b+a) + (1 - v_A^2/c^2)^{\Lambda}\, (l-(b+a)^2)^{1/2}) / (d+e)]\}, \tag{800}$$

$$P_{KE}(S) = \tfrac{1}{2}\, V_B/C\, J_0(S)\, 1/\pi\, J_o^{\pi} d\theta\, \{ \tag{81}$$

$$\{[\sin^{-1}(y\lambda_A/\lambda_B + v_A/c) + \sin^{-1}(y\lambda_A/\lambda_B - v_A/c)] / y^2$$
$$- [\sin^{-1}(z\lambda_A/\lambda_B + v_A/c) + \sin^{-1}(z\lambda_A/\lambda_B - v_A/c)] / z^2\}$$
$$+ \lambda_A/\lambda_B (1 - v_A^2/c^2)^{-1}$$
$$\{[(1 - (y\lambda_A/\lambda_B + v_A/c)^2)^{1/2} + (1 - (y\lambda_A/\lambda_B - v_A/c)^2)^{1/2}] / y$$
$$- [(1 - (z\lambda_A/\lambda_B + v_A/c)^2)^{1/2} + (1 - (z\lambda_A/\lambda_B - v_A/c)^2)^{1/2}] / z\}$$
$$+ (\lambda_A/\lambda_B)^2 v_A/c (1 - v_A^2/c^2)^{-3/2}$$
$$\{\log[(1 - v_A/c (y\lambda_A/\lambda_B + v_A/c) + (1 - v_A^2/c^2)^{1/2} (1-(y\lambda_A/\lambda_B + v_A/c)^2)^{1/2}) / y]$$
$$-\log[(1 + v_A/c (y\lambda_A/\lambda_B - v_A/c) + (1 - v_A^2/c^2)^{1/2} (1-(y\lambda_A/\lambda_B - v_A/c)^2)^{1/2}) / y]$$
$$-\log[(1 - v_A/c (z\lambda_A/\lambda_B + v_A/c) + (1 - v_A^2/c^2)^{1/2} (1-(z\lambda_A/\lambda_B + v_A/c)^2)^{1/2}) / z]$$
$$+\log[(1 + v_A/c (z\lambda_A/\lambda_B - v_A/c) + (1 - v_A^2/c^2)^{1/2} (1-(z\lambda_A/\lambda_B - v_A/c)^2)^{1/2}) / z]\}\}$$

[00339] In the first two sets of integrals, the first and fourth terms and the second and third terms cancel as they are mirror images with respect to the integration interval and occur with opposite sign. In the third set of integrals, the log(y) and log(z) factors cancel. Then the first and fourth terms and the second and third terms are negative mirror images and cancel as well.

6. GRAVITY ACTS INSTANTANEOUSLY

[00340] In this section we show that if the FS is quantized into discrete units, the mass density fields in the FS are created or changed instantaneously by both the logarithmic and first-order singularities in the gravity force since the singularities are infinite forces. We suggest that each FS unit has a rest mass equal to 2 proton masses, a characteristic length equal to its gravity wavelength (2mm), and a speed parameter that corresponds to its kinetic energy. The mass density field of an arbitrary object is then defined by its density value at each FS unit.

[00341] We first consider the gravity force exerted by a FS unit denoted as unit A on a FS unit denoted as unit B. The rest mass of each FS unit is twice the proton mass and the kinetic energy of each FS unit is the same. As a result, the Type I gravity force has 4 logarithmic singularities according to equation (377) since the gravity wavelengths λ_{Fs} of the two FS units are identical and the speed parameters are also identical. Thus the Type I gravity force exerted by unit A on unit B is:

$$F_G i(r_B) = A_{GIFS}\, G(2m_p)^2\, J_0(r_B/\lambda_{FS})\, Zr_B^2, \qquad (822)$$

where the FS amplification factor $A_{G_{IFS}}$ contains the four logarithmic singularities of the Type I gravity force exerted on unit B.

[00342] The net Type I gravity force exerted by all units A in a radial line on unit B is:

$$\int_0^\infty dr_B\, r_B^2\, F_{GI}(r_B) = A_G i_{FS}\, G(2m_p)^2 \int_0^\infty dr_B\, J_0(r_B/\lambda_{FS}) = A_G i_{FS}\, G(2m_p)^2\, \lambda_{FS} \qquad (83)$$

[00343] What is important is that the value of the integral is positive and thus the net force from all units A along the radial line is proportional to the amplification factor A_{GIFS} and hence is infinite. This net force, however, is exactly balanced by the net Type I gravity force exerted by the units A in the opposite radial direction. The same is true for every radial direction for every unit B of the arbitrary object mass density field.

[00344] The same calculation can be done for Type II gravity. Because the gravity wavelengths for both unit A and unit B are identical, the Type II gravity force has a first-order singularity according to equation (700) at the zeros of the J_0 Bessel function:

$$F_G ii(r_B) = AGIIFS\ G(2m_p)^2 / \lambda_{FS}\ J_1(r_B/\lambda_{FS}) / r_B, \quad (84)$$

where the FS amplification factor A_{GIIFS} contains the first-order singularity of Type II gravity, J_1 is the 1st order Bessel function of the first kind, and r_B/λ_{FS} is a zero of the J_0 Bessel function.

[00345] The net Type II gravity force exerted by all units A in a radial line on unit B is the sum of the Type II gravity force at the zeros of the J_0 Bessel function:

$$\sum Zeros\ of\ JO\ FGH(\Gamma B) = AGHFS\ G(2m_p)^2 / \lambda_{FS} \sum Zeros\ of\ JO\ JIO\ ''B/\lambda FS) / I'B \quad (855)$$

[00346] The value of the sum is positive and thus the net force from all units A along the radial line is proportional to the amplification factor A_{GIFS} and hence is infinite. This net force, however, is exactly balanced by the net Type II gravity force exerted by the units A in the opposite radial direction. The same is true for every radial direction for every unit B of the arbitrary object mass density field. We note that Type II singularities occur at the points in the FS where the Type I singularities are zero, i.e. at the zeros of the J_0 Bessel function. We also note that the Type I and Type II forces on the FS are symmetric in that the gravity force exerted by unit A on unit B is the same as the gravity force exerted by unit B on unit A.

[00347] Thus when an arbitrary object mass density field is created or changed, every part of the mass field is acted on by the singularities in all directions and at all distances to bring the mass density field to its new state. Since the singularities are infinite forces that act at all distances, any changes or interactions in the mass density fields occur instantaneously and gravity acts instantaneously.

7. CONTRACTION AND EXPANSION OF THE FABRIC OF SPACE

[00348] We show that if kinetic energy is transferred into or released from the FS, then the FS contracts or expands. Again we assume that the FS is quantized into discrete units with each

FS unit having a rest mass of 2 proton masses, a characteristic length equal to its gravity wavelength (2mm), and a speed parameter v that corresponds to its kinetic energy KE according to mass-energy equivalence:

$$KE = 2m_p c^2 ((I - v^2/c^2)^{J/2} - 1) \quad (86)$$

[00349] Since the gravity wavelengths for any two units are identical, the Type II gravity force has a first-order singularity according to equation (70) at the zeros of the J_0 Bessel function. Consider the following units in which the central unit and all units to the left have a speed parameter V_1 and all units to the right have a speed parameter v_2:

$$\begin{array}{ccccccccccc} \ldots & D & D & D & D & D & D & O & \ldots \\ & V_1 & V1 & V_1 & V1 & V2 & V_2 & V_2 & \\ & & \leftarrow & r_i & I & r_{1,}\ r_2 & \rightarrow & & \end{array} \quad (87)$$

[00350] The Type II gravity forces exerted on the central unit by the units on the left and right of the central unit are as follows where the FS amplification factor $A_{G\Pi FS}$ includes the first-order singularity, Ji is the 1st order Bessel function of the first kind, ri is the unit of radial distance, λ_{FS} is the FS gravity wavelength, and r_1/λ_{FS} is a zero of the Jo Bessel function:

$$F_{GII\,LEFT}(ri) = A_{G\Pi FS}\, G(2m_p)^2 / \lambda_{FS}\, Ji(ri/\lambda_{FS}) / ri, \quad (88)$$

$$F_{G\Pi RIGHT}(n) = A_{G\Pi FS}\, G(2m_p)^2 / \lambda_{FS}\, (1 - V_1V)'^{72} (1 - v_2^2/c^2y'^2\, Ji(n/\lambda_{FS}) / n, \quad (89)$$

and the forces are zero if ΠA_{FS} is not a zero of the J_0 Bessel function. The only way that these forces balance exactly for all radial distances is if the FS on the right is contracted or expanded and the new unit of distance r_2 in the FS on the right is related to the old unit of distance r_1 as follows:

$$r_2 = n\ (1 - V_2V\ f^2 (1 - vi^2/c^2)^{-'/2} \quad (900)$$

[00351] Thus as kinetic energy is transferred into the FS, its speed parameter increases and the FS contracts. The opposite is also true, namely as kinetic energy is released from the FS, its speed parameter decreases and the FS expands. Thisis contraction and expansion of the FS are unrelated to the mass or distribution of mass in the FS.

[00352] We Wmay then hypothesize that the universe was created with such a large amount of kinetic energy stored in the FS that space was immensely contracted with all mass concentrated in a small volume. When time began, the cosmic kinetic energy began to be released from the FS and the FS and mass began to expand and are still is expanding today. The

cosmic kinetic energy released from the FS units is in fact the 3 degree K cosmic background radiation. This gravity theory suggests that the universe expands once.

8. GRAVITY FOR PHOTONS AND OTHER ZERO MASS PARTICLES

[00353] The gravity theory can also describe the gravitational interactions of photons, other zero mass particles, or any type of gravitating energy. We hypothesize that an object without mass is a mass density field DQ(Π) in the FS without the kinetic energy cosine term:

$$D_G(r) = E/c^2 \; l/4\pi\lambda_G \; Jo(r/\lambda G) / r^2, \qquad (91)$$

where E is its energy, E/c^2 is its effective mass, X_G is its gravity wavelength, J_0 is the O^{th} order Bessel function of the first kind, and r is the distance from the object. We also hypothesize that the gravity wavelength X_G of a gravitating energy or other zero mass particle is given by eq. (7) as for objects with mass, but proportional to its effective mass.

[00354] For a photon, however, we hypothesize that its gravity wavelength is equivalent to that of a bound particle-antiparticle pair with the same energy. For example, particle A has mass m_A, gravity wavelength X_A, and speed V_A, and its antiparticle B has mass m_B, gravity wavelength λ_B, and speed V_B. The non-singular gravity force exerted by particle A on its antiparticle B is given by eq. (19) and the function B(rβ/λβ) by eq. (42).

[00355] We further hypothesize that the gravity wavelength X_G of a photon is its energy E divided by the gravity force experienced by the particle or antiparticle at a distance equal to its gravity wavelength. Since this force does not include Type II gravity, photons experience only Type I gravity and not Type II gravity. Using that $\Pi_A = \Pi_B$, λA = λβ, $\lambda\beta = N_A/K$ me, $V_A = V_B$, and B(rβ/λβ) = 4 Jo(rB/λβ) when $X_A = X_B$ and $V_A = V_B$, we obtain:

$$\lambda_G = E / F_G(\lambda_B) = E / [Gm_B^2/\lambda_B^2 \; J_0(I)] = E \; (N_A/\kappa)^2 / [G \; J_0(I)], \qquad (92)$$

where NA is Avogadro's number, K is the FS atomic mass linear density, and JO(I) is the value of the JO Bessel function at unit argument.

[00356] If a photon is isolated, its gravity wavelength is proportional to its own energy. However, if the photon is a constituent of an electromagnetic wave, then its gravity wavelength is proportional to the energy of the electromagnetic wave. This behavior of the gravity wavelength for photons is comparable to an isolated particle with mass and the same particle bound within a larger object or wave.

9. COMPARISON WITH EXPERIMENTAL TESTS

[00357] The gravity theory specifies the mass density fields are integrated to infinity to obtain mass-energy equivalence and the gravity forces, and as a result specifies that the FS to extend to infinity. Since the FS and the mass in the universe are not related, the size and age of the visible universe as measured by the Hubble radius are unaffected, except that the FS units expand according to eq. (90) as the FS units release cosmic kinetic energy. As we show elsewhere, by comparing the Hubble radius to an object's gravity wavelength, we can determine if and when gravity changes from classical to wave gravity.

[00358] As a classical gravity test, we consider two experimental situations —the measurement of gravity on a beam of neutrons and on a single neutron. If a neutron is isolated, its gravity wavelength $\lambda_G \approx$ lmm and the neutron experiences wave gravity exerted by objects at distances greater than lmm. However, if a neutron is part of a beam of neutrons, it experiences the first-order singularities of Type II gravity exerted by the other neutrons in the beam. Since the neutron is now a constituent of a wave, its gravity wavelength is proportional to the mass of all the neutrons in the beam. As a result, each neutron in the beam experiences classical gravity, as exerted by the Earth for example.

[00359] In an experimental situation that measures gravity on a single neutron, gravity is measured quantum mechanically. Hence the single neutron is not isolated, but is part of the quantum mechanical system that includes the measurement apparatus. Thus the neutron's gravity wavelength includes the mass of the measurement apparatus and the neutron again experiences classical gravity.

[00360] Also, if gravity exerted by small on large objects is 3x classical gravity, the Earth's tides (which result primarily from gravity exerted by the Moon) should be much larger than what is actually observed. Why then does classical gravity accurately predict the Earth's tides? The answer lies in the fact that tidal water particles, unlike particles that comprise the solid Earth, have very different speeds. Thus, whereas the mass density fields of solid particles that comprise the Earth are collectively combined by the fabric of space units that exert gravity, the mass density fields of tidal water particles combine separately. As a result, the gravity wavelength of tidal water particles is proportional only to the mass of tidal water particles with similar speeds, and the gravity force exerted by the Moon on tidal waters is the large on small gravity force, which is equal to classical gravity.

[00361] We now compare the predictions of the gravity theory based on mass-energy equivalence with the experimental tests of General Relativity (GR). With the mass density field

given by eq. (91), a photon experiences gravity according to eq. (11) in which object B is now a photon, m_B is its effective mass, and $\lambda\beta$ is its gravity wavelength. Using that a photon energy E = hf where h is Planck's constant and f is its frequency, we can rewrite the photon gravity wavelength λ_G in eq. (92) as:

$$\lambda o = f\,(N_A/\kappa)^2 / [G/h\,J_0(I)] = 4.7\ 10^{24}\ f \ \text{[meters]} \qquad (93)$$

[00362] For example, an isolated photon with frequency f = 5.5 10^{14} cps (yellow-green light) has a gravity wavelength λ_Q = 2.6 10^{39} m or 2.7 10^{23} light-years. Since the size of the observable universe is about 4.2 10^{10} light-years, we have $r\beta/\lambda\beta \ll 1$ and the Bessel function $J_0(r_B/\lambda_B) \approx 1$ in eq. (11). As a result, for this example as well as for most photon frequencies, the photon experiences classical type gravity.

[00363] The first comparison test with GR is gravitational redshifting. For example, we consider a star such as our Sun whose gravity wavelength λs_{un} = 1-3 10^{38} light-years and a yellow-green photon. Since $\lambda_G/\lambda s_{un} \ll 1$, we have large object on small object gravity and $A_G = 1$ in eq. (11). Thus the gravity exerted by a star on an emitted photon is classical gravity and the photon experiences gravitational redshifting in agreement with GR.

[00364] The second comparison test with GR is the bending of light by a massive object. The degree of bending of light predicted by the gravity theory depends on the ratio of the gravity wavelengths of the massive object and the photon gravity wavelength. If the photon or parent wave gravity wavelength is much less than the gravity wavelength of the massive object (i.e. $\lambda\beta/\lambda_\Lambda \ll 1$), then we have large on small gravity from B(s) in eq. (46). As a result, $A_G = 1$ in eq. (11) and the bending of light is the classical Newtonian value.

[00365] However, if the photon is a constituent of an electromagnetic wave whose gravity wavelength is very much larger than that of the massive object (i.e. $\lambda\beta/\lambda A \gg 1$), the small on large gravity receives equal Type I gravity contributions from A(s) in eq. (36) and B(s) in eq. (49). As a result, $A_G = 2$ in eq. (11) and the bending of light is twice the classical Newtonian value.

[00366] For example, assuming an average sunlight frequency of 5.5 10^{14} cps and intensity of 1400 W/m^2 at the Earth's surface, the number of photons impacting a square meter per second is 3.8 10^{21}. Thus the gravity wavelength of a one light-second long, one square meter cylinder of photons is λ_G = 1.1 10^{45} light-years. Even this gravity wavelength for such a small volume of the parent light wave is much larger than the gravity wavelength of the Sun which is λs_{un} = 1.3 10^{38} light-years. Since $\lambda_G/\lambda s_{un} \gg 1$, the bending of light is twice the classical Newtonian value in agreement with GR.

[00367] The third comparison test with GR is the related Shapiro time delay which results from the additional distance traveled due to bending of a parent wave by a massive object such as the Sun. For example (MIT 2008), with a radar pulse energy E = 15 J (150 KW pulse power, 100 μs pulse width), the gravity wavelength of photons in the pulse according to eq. (92) is λ_G = 1.07 10^{59} m or 1.13 10^{43} light-years. Since the photon gravity wavelength is very much larger than that of the Sun (i.e. $\lambda_G/\lambda_{sun} \gg 1$), the small on large gravity exerted by the Sun on the photons in the radar pulse receives equal Type I gravity contributions from A(s) in eq. (36) and B(s) in eq. (49). As a result, $A_G = 2$ in eq. (11) and the time delay of the radar signal is twice the classical Newtonian value, again in agreement with GR.

[00368] The fourth comparison test with GR is the precession of the perihelion of Mercury. We consider the Sun and Mercury as a two-body gravitational system, denoting the larger object (Sun) as object 1 with inertial mass m_i and the smaller object (Mercury) as object 2 with inertial mass m_2. When two non-relativistic objects have inertial masses that are very unequal, the small on large gravity force is 3x the large on small gravity force. If we assume that the gravitational mass (g-mass) of the smaller object is equal to 3x its inertial mass, then Newton's third law is preserved as we show in eqs. (94)-(99).

[00369] Accordingly, we define the distances r_1 and r_2 of each object from the center of g-mass. We then include the relativistic increases of the inertial masses in the acceleration terms and the relativistic corrections to the gravity force from eqs. (36), (46), (49), and (75) in the equations of motion about the center of g-mass:

$$r_1 = 3m_2 r / M,\ r_2 = m_i r / M,\ r = r_i + r_2,\ M = m_i + 3m_2, \tag{94}$$

$$m_i(1 - v_i^2/c^2)^{-1/2}\, d^2n/dt^2 = -Gm_1m_i/r^2\, \underline{n}\, [(1 - v_2^2/c^2)^{-1/2} + (1 - V_1^2/C^2)^{1/2}(1 - V_2^2/C^2)^{-1/2} + 1], \tag{95}$$

$$In_2(1 - v_2^2/c^2)^{-1/2}\, d^2r_2/dt^2 = -Gmim_2/r^2\, \underline{\mathbf{r}}_2\, (1 - v_2^2/c^2)^{1/2}(1 - v_i^2/c^2)^{-1/2}, \tag{96}$$

where V_1 and V_2 are the speeds of objects 1 and 2 relative to the FS (or CMBR) at rest and c is the speed of light. We expand the relativistic factors and obtain to order $1/c^2$:

$$m_i\, d^2n/dt^2 = -GHI_1HI_2/r^2\, \underline{r}_i\, (3 - 2v_i^2/c^2 + v_2^2/c^2), \tag{97}$$

$$m_2\, d^2r_2/dt^2 = -Gmim_2/r^2\, \underline{\mathbf{r}}_2\, (1 + \tfrac{1}{2} V_1V - v_2^2/c^2) \tag{98}$$

[00370] The motion of the center of g-mass relative to the FS at rest is then specified by only relativistic terms:

$$m_i\, d^2n/dt^2 + 3m_2\, d^2r_2/dt^2 = F_{CM} = -G\pi n m_2/r^2\, \underline{\mathbf{r}}_2\, (7/2v_i^2/c^2 - 4v_2^2/c^2) \tag{99}$$

[00371] These equations result in the conservation of energy, linear momentum, and angular momentum that follow from Newton's third law. While the ratio between g-mass and inertial mass of the smaller object is 3 when the inertia! masses are very unequal and non-relativistic, the ratio decreases to 1 as the inertial masses becomes equal as we show in eq. (114). The observance of Newton's third law by the gravity theory does imply, however, that the gravity theory violates the equivalence principle in a novel way.

[00372] Since r_2 is defined relative to the center of g-mass, the force on the center of g-mass is the negative of the same force on object 2. Thus corrected for the motion of the center of g-mass, the equation of motion for r_2 in the reference frame that is the FS at rest is:

$$m_2 d^2r_2/dt^2 = - Grmm_2 / r^2 \underline{\mathbf{r_2}} (1 - 3v,^2/c^2 + 3v_2^2/c^2) \quad (100)$$

[00373] The speeds V_1 and v_2 are each vector combinations of the velocity of the center of g-mass relative to the FS at rest and the velocity relative to the center of g-mass. The terms proportional to V_{CM}^2/C^2 in vi^2/c^2 and v_2^2/c^2 cancel, where V_{CM} is the speed of the center of g-mass relative to the FS at rest. In addition, we neglect the remaining speed terms in V_1^2/c^2 since they are much smaller for the Sun than the corresponding terms in v_2^2/c^2 for Mercury. We then write the equations of motion for Mercury in polar coordinates about the center of g-mass in the reference frame that is the FS at rest:

$$d^2r_2/dt^2 - r_2 (d\phi/dt)^2 = - GmKm_1M)^2 / r_2^2 \{1 + 3/c^2 [(dr_2/dt)^2 + r_2^2(d\phi/dt)^2] + 6V_{CM}/C^2 (\cos\theta\, dr_2/dt - \sin\theta\, r_2 d\phi/dt)\}, \quad (101)$$

$$r_2^2\, d\phi/dt = h_2, \quad (102)$$

where θ is the angle between position vector of Mercury relative to the center of g-mass and the velocity vector of the center of g-mass relative to the FS at rest and h_2 is the angular momentum of Mercury per unit mass around the center of g-mass. We make the usual $u_2 = l/r_2$ substitution where $\alpha = Gm_1(m_1/M)^2/h_2^2$ and $\lambda = 3h_2^2/c^2$, and obtain:

$$d^2u_2/d\phi^2 + U_2 = \alpha\{1 + \lambda[(du_2/d\phi)^2+u_2^2] - 6v_{CM}h_2/c^2 (\cos\theta\, du_2/d\phi + \sin\theta\, u_2)\} \quad (103)$$

[00374] We then expand the periodic solutions of eq. (103) in a Fourier cosine series (see for example (Bergmann 1942)) and add a term proportional to $\sin\theta$:

$$u_2 = \alpha + \lambda\beta_0 + \alpha\varepsilon \cos p\phi + \alpha k \sin\theta + \lambda \sum_{n=}2^{\infty} \beta n \cos np\phi, \quad (104)$$

where ε is Mercury's eccentricity and $\theta = p\alpha_{vi}\phi + \Delta$. We substitute eq. (104) into eq. (103), use that $p \approx 1$ and $p_{cM} \approx 1$, and obtain to first order:

$$\alpha\varepsilon(1 - p^2)\cos p\phi + \alpha k(1 - pcM^2)\sin\theta + \alpha + \lambda\beta o \quad (105)$$
$$= \alpha\{1 + \lambda\alpha^2(1 + \varepsilon^2 + 2\varepsilon\cos p\phi + k^2 + 2\varepsilon k\sin\Delta + 2k\sin\theta)$$
$$- 6\alpha v c_M h_2/c^2 (k + \varepsilon\sin\Delta + \sin\theta)\}$$

[00375] In eq. (105), we compare the terms proportional to cos $p\phi$, $\sin\theta$, and a constant, and obtain the following equations:

$$(1 - p^2) = 2\lambda\alpha^2, \; p \approx 1 - \lambda\alpha^2, \quad (106)$$

$$(1 - PCM^2)\, k = -6\alpha v_{CM} h_2/c^2 + 2\lambda\alpha^2 k, \quad (107)$$

$$\beta_0 = \alpha^3(1 + \varepsilon^2 + k^2 + 2\varepsilon k\sin\Delta) - 2\alpha^2 v_{CM}/h_2\,(k + \varepsilon\sin\Delta) \quad (108)$$

[00376] Eq. (106) is the identical equation to that derived in GR. Thus the gravity theory based on mass-energy equivalence contributes the same 43 seconds of arc per century for the precession of the perihelion of Mercury as does GR.

[00377] In eq. (107), the constant k is dimensionless and thus the parameters of the $\sin\theta$ term are:

$$k = VCM/C,\; pcM \approx 1 + 3\alpha h_2/c - \lambda\alpha^2 \quad (109)$$

[00378] As a result, the gravity theory based on mass-energy equivalence, like GR, is consistent with lunar laser ranging measurements of the Moon's orbit. In these measurements there is no preferred reference frame effect, since they are undertaken in the reference frame that is the center of g-mass at rest, where the $\sin\theta$ term in eq. (104) is zero.

[00379] The fifth comparison test with GR is the geodetic precession of a gyroscope orbiting the Earth as measured by Gravity Probe B. As derived for gravity exerted by a large on small object, the increased gravity force in eq. (100) results in a smaller circumference for the gyroscope orbit than would occur in Newtonian gravity. The velocities of object 1 (Earth) and object 2 (gyroscope) are $V_1 = V_E$ and $V_2 = V_E + v$, where V_E is the velocity of the Earth relative to the FS at rest and v is the velocity of the gyroscope relative to the Earth. Then in the reference frame that is the Earth at rest, the contracted radial distance R specified by eq. (100) is $R = r(1 — 3/2\ v^2/c^2)$. Thus in this gravity theory, geodetic precession is entirely due to a novel gravito-electric field which is larger than in GR (i.e. 3/2 rather than 1/2), and results in the same geodetic precession as GR.

[00380] The sixth comparison test with GR is the change in period of a binary pulsar. We show that this change in period can be explained by energy loss due to the motion of the center of g-mass. In a binary pulsar such as PSR 1913 + 16, the two stars are approximately the same

size. Thus in the equations of motion, we use the gravity force from eqs. (32), (42), and (74) for approximately equal masses:

$$\text{In}_1(\text{I} - v^2/c^2)^{\text{J/2}}\, d^2\text{n}/dt^2 = -\, Gm_1\text{In}_2/r^2\, \underline{n} \qquad (110)$$
$$[(\text{I} - v^2/c^2)^{-\text{i}^2}\, K(z(\text{l} - v^2/c^2)^{-}\text{V}\, 2\pi + K(z)/2\pi + 3/2],$$

$$m_2(\text{l} - v^2/c^2)^{-\text{12}}\, d^2r_2/dt^2 = -\, Gmim_2/t^2\, \underline{\mathbf{r}}_2 \qquad (111)$$
$$[(\text{I} - v^2/c^2)^{-\text{y}^2}\, K(z(\text{l} - v^2/c^2)^{-1})/2\pi + K(z)/2\pi + 1],$$

where $\text{mi} \approx m_2$, $\text{mi} > m_2$, $V_1 \approx V_2 = v$, K(z) is the complete elliptic integral K of the first kind, and its argument $z = (4m_2/\text{nii})/(\text{l} + m_2/\text{mi})^2 = (4\text{mi}/m_2)/(\text{l}+ \text{mj}/\text{ma})^2$. We expand the relativistic factors and obtain to order $1/c^2$:

$$\text{nndVi}/dt^2 = -\, Gm_1\text{Hi}_2/r^2\, \underline{\mathbf{r}}_\text{l}\, [(K(z)/\pi + 3/2)(\text{l} - V_2V^2/c^2) + \tfrac{1}{2}v^2z_c^2\, (\text{1-z})^{-1}], \qquad (112)$$

$$m_2d^2r_2/dt^2 = -\, Gm_1\text{In}_2/r^2\, \underline{\mathbf{r}}_2\, [(K(z)/\pi + \text{I})(\text{I} - v_2w^2Ic^2) + \tfrac{1}{2}v^2z_c^2\, (\text{1-z})^{-1}] \qquad (113)$$

[00381] As a result, the motion of the center of g-mass is given by:

$$\text{m}_1\text{dVi}/dt^2 + \text{X}\, m_2d^2r_2/dt^2 = F_{CM} = -\, Gm_1m_2Zr^2\, \underline{\mathbf{r}}_2\, v^2/c^2\, [\text{^(l-z)}^{-1}(\text{X} - \text{I})], \qquad (114)$$
$$\text{where X} = (K(z)/\pi + 3/2)\ /\ (K(z)/\pi + 1)$$

[00382] We define the total mass $M = \text{mi} + m_2$, reduced mass $\mu = \text{mim}_2/M$, angular momentum per unit mass $h = r^2d\phi/dt$, and effective gravitational constant $G_E = (K(z)/\pi + \text{I})G$. We next make the substitutions $r = a(\text{l} - \varepsilon^2)/(\text{l} + \varepsilon\cos\phi)$, $h^2 = GEMa(\text{I} - \varepsilon^2)$, and $v^2 = \text{V4G}_E\text{M}/(a(\text{l} - \varepsilon^2))\ [(\text{I} + \varepsilon\cos\phi)^2 + \varepsilon^2\sin^2\phi]$, where a is the semi-major axis and ε is the orbital eccentricity. We then write the relativistic force F_{CM} on the center of g-mass as:

$$Fc_M = -\, \underline{\mathbf{r}}_2\, G^2\mu M^2/(a^3(\text{l} - \varepsilon^2)\text{V})\ \ (16(\text{1-Z}))^{-1} \qquad (115)$$
$$(\text{1} + \varepsilon\cos\phi)^2\ [(\text{I} + \varepsilon\cos\phi)^2 + \varepsilon^2\sin^2\phi]$$

[00383] We change to polar coordinates in the equation of motion and find that the motion of the center of g-mass is almost circular. The equation of motion, the radius r_{CM}, and the period PcM of the center of g-mass are:

$$Mh^2/r^2\, [d/d\phi(\text{l}/r^2\, dr_{CM}/d\phi) - r_{CM}/r^2] = F_{CM}, \qquad (116)$$

$$rc_M \approx G\mu/c^2\, (K(z)/\pi + \text{I})^{-1}\, (16(\text{1-Z}))^{-1}, \qquad (117)$$

$$Pc_M \approx 2\pi\, G\mu/c^3\, (K(z)/\pi + \text{I})^{-2}\, (16(\text{l-z}))^{-3/2} \qquad (118)$$

[00384] If we consider the center of g-mass as revolving around the objects, then the distance D_{CM} traversed by the center of g-mass relative to the objects per unit time of the center of g-mass is:

$$D_{CM} = r\, d\phi/dt\ P_{CM}/2\pi = h/r\ P_C M/2\pi \qquad (119)$$

[00385] The distance traversed by the center of g-mass is always parallel to the force on the center of g-mass. As a result, the energy E transferred per unit time by the force F_{CM} in moving the center of g-mass a distance $D_C M$ is given by:

$$dE/dt = -(K(z)/\pi + 1)^{-3/2} (16(l-z))^{-5/2} G^{7/2}\mu^2 M^{5/2} c^{-5} a^{-7/2} (1 - \varepsilon^2)^{-7/2} (1 + \varepsilon\cos\phi)^3 [(I + \varepsilon\cos\phi)^2 + \varepsilon^2 \sin^2\phi] \qquad (120)$$

[00386] We average the change in energy $E = -\frac{1}{2} GeM\mu/a$ and period $P_b = 2\pi a^{3/2}[G_E M]^{-1/2}$ over an orbit with the result:

$$\langle dE/dt\rangle = -\mathbf{(K(z)/\pi + I)^{-1}} (16(l-z))^{-5/2} G^4\mu^2 M^3 c^{-5} a^{-5} (l - \varepsilon^2)^{-7/2} (l + ll/2\ \varepsilon^2 + 9/4\ \varepsilon^4), \qquad (121)$$

$$\mathbf{P_b^{-1} dP_b/dt} = -3 (K(z)/\pi + I)^{-2} (16(l-z))^{-5/2} G^3\mu M^2 c^{-5} a^{-4} (l - \varepsilon^2)^{-7/2} (l + l\,l/2\ \varepsilon^2 + 9/4\ \varepsilon^4) \qquad (122)$$

[00387] This change in period should be compared to the GR prediction (see for example (Will 1993)):

$$P_b\text{-}'dP_b/dt = -96/5\ G^3\mu M^2 c^{-5} a^{-4} (1 - \varepsilon^2)^{-7/2} (1 + 73/24\ \varepsilon^2 + 37/96\ \varepsilon^4) \qquad (123)$$

[00388] Assuming an identical pulsar mass mi and eccentricity ε, and a mass ratio $m_2/mi \approx 0.963$ in eq. (123), the changes in period are equal if the mass ratio $m_2/mi \approx 0.768$ in eq. (122). With this value, the gravity theory predicts the same change in period for the binary pulsar PSR 1913 + 16 as does GR. However, the change in period results from the circular motion of the center of g-mass rather than unobserved gravitational radiation.

[00389] We can then use eqs. (117) and (118) to obtain the radius $\Gamma_{CM} \approx 1.6\ 10^3$ m and period $P_{CM} \approx 3.1\ 10^{-5}$ s of the circular motion of the center of g-mass. Since orbital energy is transferred to the motion of the system as a whole as a result of gravity applied by the FS units, the energy loss is transferred to the FS units.

10. DEMVATION OF THE COULOMB FORCE

[00390] The gravity theory makes possible a derivation of the Coulomb force. We hypothesize that the Coulomb force exerted by a charged object A with electric charge q_A, mass m_A, and gravity wavelength λ_A on a charged object B with electric charge q_B and mass m_B results from the interaction of the mass density fields of object A without a kinetic energy term and an equivalent mass *Coulomb photon* B in place of object B, integrated over the entire fabric of space (FS). In the same way as the gravity force is applied by the units of the FS, the Coulomb force is also applied by the units of the FS.

[00391] The mass density field $D_G(r_B)$ of *Coulomb photon* B is obtained from eq. (91):

$$D_G(r_B) = m_B/4\pi\lambda_B \, Jo(r_B/\lambda_B) / r_B^2, \quad (124)$$

where m_B is its effective mass, λ_B is its gravity wavelength, J_0 is the 0^{th} order Bessel function of the first kind, and r_B is the distance from object B. The gravity wavelength λ_B of *Coulomb photon* B is obtained from eq. (92):

$$\lambda_B = m_B c^2 (N_A/K)^2 / [G \, J_0(I)], \quad (125)$$

where N_A is Avogadro's number, K is the FS atomic mass linear density, G is the gravitational constant, and $J_0(I)$ is the value of the J_0 Bessel function at unit argument.

[00392] We hypothesize that the coupling constant between the mass density fields of object A and *Coulomb photon* B is $C4\pi\lambda_B$, where C is given by:

$$C = - (k/2) (q_A/m_A) (q_B/m_B), \quad (126)$$

and where k is the Coulomb constant. The Coulomb force $Fc(r_B)$ exerted by object A on object B is then:

$$F_c(r_B) = (C4\pi\lambda_B) (m_A/4\pi\lambda_A) (m_B/4\pi\lambda_B) \quad (127)$$
$$\int_0^{\infty} dr_A \, r_A^2 \int_0^{\pi} d\theta \sin\theta \int_0^{2\pi} d\varphi \, J_0(r_A/\lambda_A) / r_A^2$$
$$J_0((r_B^2 + r_A^2 - 2r_B r_A \cos\theta)^{1/2} / \lambda_B) (r_B - r_A\cos\theta) / (r_B^2 + r_A^2 - 2r_B r_A \cos\theta)^{3/2}$$

[00393] As indicated previously, a photon experiencing gravity and hence a charged object experiencing the Coulomb force experiences only the Type I force and not the Type II force. Since the *Coulomb photon* gravity wavelength λ_B is very much larger than the gravity wavelength λ_A of object A (i.e. $\lambda_B/\lambda_A \gg 1$), the Coulomb force receives equal contributions from the A(s) and B(s) terms in eqs. (35) and (49):

$$F_c(r_B) \approx 2Cm_A m_B J_0(r_B/\lambda_B) / r_B^2 = - kq_A q_B Jo(rB/\lambda_B) / r_B^2, \quad (128)$$
where $\lambda\beta/\lambda\Lambda \gg 1$

[00394] In the region where $r_B/\lambda_B \ll 1$, $Jo(r_B/\lambda_B) \approx 1$ and we obtain the classical Coulomb force:

$$Fc\ ciassicai(r_B) = - kq_A q_B / r_B^2, \quad (129)$$
where $\lambda_B/\lambda_A \gg 1$, $r_B/\lambda_B \ll 1$

[00395] For example, the gravity wavelength of a *Coulomb photon* corresponding to an electron is $\lambda_B = 5.8\ 10^{44}$ m or $6.1\ 10^{28}$ light-years. As a result, electrons and protons experience the classical Coulomb force. Since the singularities in the gravity force act on the FS to effect any changes and interactions in the mass density fields instantaneously, the Coulomb force also acts instantaneously. This derivation of the Coulomb force suggests that elementary particles do not have an electric charge density since the electric charge appears only in the coupling constant between the two mass density fields.

ACKNOWLEDGMENTS

[00396] The authors gratefully acknowledge Dr. H. Pierre Noyes, Professor Emeritus at Stanford Linear Accelerator Center (SLAC) for his advice, patience, and willingness to serve as a sounding board for the theories in this paper.

APPENDIX A: GRAVITY FROM DENSITY OF SPACE

[00397] We evaluate the first integral that is the contribution to gravity arising from the density of space:

$$FGI(\Gamma B) = Gm_A m_B / 2\lambda_A r_B^2 \int_0^\infty dr_A J_0(r_A/\lambda_A) \cos(v_A r_A/c\lambda_A) \quad (Al)$$
$$[J_0(O_B + r_A)/\lambda_B) \cos(v_B(r_B + r_A)/c\lambda_B) + J_0((r_B - r_A)/\lambda_B) \cos(v_B(r_B - r_A)/c\lambda_B)]$$

[00398] We use the integral representation of the Bessel function, expand the cosine functions in terms of exponential functions, and collect terms to obtain:

$$J_n(x) = i^{-n}/\pi \int_0^\pi d\theta \exp(ix \cos\theta) \cos(n\theta) \quad (A2)$$

$$Foi(ib) = Gm_A m_B / 4\lambda_A r_B^2 \int_0^\infty dr_A J_0(r_A/\lambda_A) 1/\pi \int_0^\pi d\theta \quad (A3)$$
$$\{\exp(iy\ r_B/\lambda_B) [\cos(r_A(y/\lambda_B + v_A/c\lambda_A)) + \cos(r_A(y/\lambda_B - v_A/c\lambda_A))]$$
$$+ \exp(iz\ r_B/\lambda_B) [\cos(r_A(z/\lambda_B + v_A/c\lambda_A)) + \cos(r_A(z/\lambda_B - v_A/c\lambda_A))]\},$$
where $y = \cos\theta + v_B/c$
$z = \cos\theta - v_B/c$

These terms with "cos(r_A...)" contribute to Type I gravity.

APPENDIX B: GRAVITY FROM CHANGE DUE TO REST MASS

[00399] We evaluate the second integral that is the contribution to gravity arising from the change in the density of space due to the rest mass:

$$F_{G2}(r_B) = -Gm_Am_B / 4\lambda_A\lambda_B r_B^2 \int_0^\infty dr_A\, J_0(r_A/\lambda_A) \cos(v_A r_A/c\lambda_A) \quad \text{(B1)}$$
$$\int_{r_B-r_A}^{r_B+r_A} dx/x\ (r_A^2 - r_B^2 + x^2)/r_A\, J_0'(x/\lambda_B) \cos(v_B x/c\lambda_B)$$

[00400] We use the Bessel function identities $J_0'(x/\lambda_B) = -J_1(x/\lambda_B)$ and $J_1(x/\lambda_B) = \frac{1}{2}(J_0(x/\lambda_B) + J_2(x/\lambda_B))$, and the integral representation of the Bessel functions to obtain:

$$F_{G2}(r_B) = Gm_Am_B / 8\lambda_A\lambda_B^2 r_B^2 \int_0^\infty dr_A\, J_0(r_A/\lambda_A) \cos(v_A r_A/c\lambda_A) \quad \text{(B2)}$$
$$1/\pi \int_0^\pi d\theta\ (1 - \cos^2\theta)$$
$$\int_{r_B-r_A}^{r_B+r_A} dx\ \exp(i\cos\theta\, x/\lambda_B)\ (r_A^2 - r_B^2 + x^2)/r_A \cos(v_B x/c\lambda_B)$$

[00401] We now expand the cosine terms, perform the integration over x, and collect terms in r_A:

$$F_{G2}(r_B) = Gm_Am_B / 4\lambda_A\lambda_B^2 r_B^2 \int_0^\infty dr_A\, J_0(r_A/\lambda_A)\ 1/\pi \int_0^\pi d\theta\ (1 - \cos^2\theta) \quad \text{(B3)}$$
$$\{\exp(iy\ r_B/\lambda_B)\ [i \sin(r_A(y/\lambda_B + v_A/c\lambda_A))\ r_A\lambda_B/iy$$
$$+ i \sin(r_A(y/\lambda_B - v_A/c\lambda_A))\ r_A\lambda_B/iy$$
$$+ \cos(r_A(y/\lambda_B + v_A/c\lambda_A))\ (r_B\lambda_B/iy - \lambda_B^2/(iy)^2)$$
$$+ \cos(r_A(y/\lambda_B - v_A/c\lambda_A))\ (r_B\lambda_B/iy - \lambda_B^2/(iy)^2)$$
$$+ i \sin(r_A(y/\lambda_B + v_A/c\lambda_A))\ (\lambda_B^3/(iy)^3 - r_B\lambda_B^2/(iy)^2) / r_A$$
$$+ i \sin(r_A(y/\lambda_B - v_A/c\lambda_A))\ (\lambda_B^3/(iy)^3 - r_B\lambda_B^2/(iy)^2) / r_A]$$
$$+ \exp(iz\ r_B/\lambda_B)\ [i \sin(r_A(z/\lambda\beta + v_A/c\lambda_A))\ r_A\lambda_B/iz$$
$$+ i \sin(r_A(z/\lambda_B - v_A/c\lambda_A))\ r_A\lambda_B/iz$$
$$+ \cos(r_A(z/\lambda_B + v_A/c\lambda_A))\ (r_B\lambda_B/iz - \lambda_B^2/(iz)^2)$$
$$+ \cos(r_A(z/\lambda_B - v_A/c\lambda_A))\ (r_B\lambda_B/iz - \lambda_B^2/(iz)^2)$$
$$+ i \sin(r_A(z/\lambda_B + v_A/c\lambda_A))\ (\lambda_B^3/(iz)^3 - r_B\lambda_B^2/(iz)^2) / r_A$$
$$+ i \sin(r_A(z/\lambda_B - v_A/c\lambda_A))\ (\lambda_B^3/(iz)^3 - r_B\lambda_B^2/(iz)^2) / r_A]\},$$
$$\text{where } y = \cos\theta + v_B/c$$
$$z = \cos\theta - v_B/c$$

[00402] The terms with "cos(r_A...)" and "sin(r_A...) r_A" contribute to Type I gravity while the terms with "sin(r_A...) / r_A" contribute to Type II gravity.

APPENDIX C: GRAVITY FROM CHANGE DUE TO KINETIC ENERGY

[00403] We evaluate the third integral that is the contribution to gravity arising from the change in the density of space due to kinetic energy:

$$FG3(\Gamma B) = v_B/c\ Gm_A m_B / 4\lambda_A\lambda_B r_B^2 \int_o^\infty dr_A\ Jo(rA/\lambda A)\ \cos(v_A rA/c\lambda_A) \quad (C\ 1)$$
$$J_{rB-rA}^{rB+rA} dx/x\ (r_A^2 - r_B^2 + x^2)/\tau_A\ J_0(x/\lambda_B)\ \sin(v_B x/c\ \lambda_B)$$

[00404] We use the integral representation of the sine function and reverse the order of integration to obtain:

$$FG3<TB) = v_B^2/c^2\ Gm_A m_B / 4\lambda_A\lambda_B^2 r_B^2 \int_o^\infty dr_A\ Jo(r_A/\lambda_A)\ \cos(v_A rA/c\lambda_A)\ Jo'dt$$
$$JrB\text{-}rA^{rB+rA} dx\ (r_A^2 - r_B^2 + x^2)/r_A\ Jo(x/\lambda_B)\ \cos(v_B xt/c\ \lambda_B) \quad (C2)$$

[00405] This is similar to the integral in Appendix B. We make the substitution $s = r_B/\lambda_B$ so that:

$$F_{G3}(r_B) = VB^2/C^2\ Gm_A m_B / 4\lambda_A r_B^2 \int_o^\infty dr_A\ Jo(r_A/\lambda_A)\ 1/\pi \int_o^\pi d\theta \int_0^1 dt \quad (C3)$$
$$\{\exp(iy_t s)\ [i\ \sin(r_A(y_t/\lambda_B + v_A/c\lambda_A))\ r_A/iy_t\lambda_B$$
$$+ i\ \sin(r_A(yt/\lambda_B - v_A/c\lambda_A))\ r_A/iy_t\lambda_B$$
$$+ \cos(r_A(y_t/\lambda_B + v_A/c\lambda_A))\ (s/iy_t - l/(iy_t)^2)$$
$$+ \cos(r_A(y_t/\lambda_B - v_A/c\lambda_A))\ (s/iy_t - l/(iyt)^2)$$
$$+ i\ \sin(r_A(yA_B + v_A/c\lambda_A))\ (\lambda_B/(iy_t)^3 - s\lambda_B/(iy_t)^2)\ /\ r_A$$
$$+ i\ \sin(r_A(yt/\lambda_B - v_A/c\lambda_A))\ (\lambda_B/(iy_t)^3 - s\lambda_B/(iy_t)^2)\ /\ r_A]$$
$$+ \exp(iz_t s)\ [i\ \sin(r_A(z_t/\lambda_B + v_A/c\lambda_A))\ r_A/iz_t\lambda_B$$
$$+ i\ \sin(r_A(zt/\lambda_B - v_A/c\lambda_A))\ r_A/iz_t\lambda_B$$
$$+ \cos(r_A(z_t/\lambda_B + v_A/c\lambda_A))\ (s/iz_t - l/(iz_t)^2)$$
$$+ \cos(r_A(z_t/\lambda_B - v_A/c\lambda_A))\ (s/izt - l/(iz_t)^2)$$
$$+ i\ \sin(r_A(z_t/\lambda_B + v_A/c\lambda_A))\ (\lambda_B/(iz_t)^3 - s\lambda_B/(iz_t)^2)\ /\ r_A$$
$$+ i\ \sin(r_A(z_t/\lambda_B - v_A/c\lambda_A))\ (\lambda_B/(iz_t)^3 - s\lambda_B/(iz_t)^2)\ /\ r_A]\},$$
$$\text{where}\quad y_t = \cos\theta + v_B t/c$$
$$Zt = \cos\theta - V_B t/c$$

[00406] For the terms that contribute to Type I gravity, we evaluate the integrals over t by taking the derivative with respect to s and then integrating by parts. For example:

$$d/ds\ \{v_B^2/c^2 \int_0^1 dt\ \exp(iy_t s)\ [i\ \sin(r_A(y_t/\lambda_B + v_A/c\lambda_A))\ r_A/iyt\lambda_B \quad (C4)$$
$$+ \cos(r_A(y_t/\lambda_B + v_A/c\lambda_A))\ (s/iy_t - l/(iyt)^2)]\}$$
$$= - iv_B/c\ \{\exp(iys)\ \cos(r_A(y/\lambda_B + v_A/c\lambda_A))$$
$$- \exp(is\ \cos\theta)\ \cos(r_A(\cos\theta/\lambda s + v_A/c\lambda_A))\}$$

[00407] The lower limit of the integral is cancelled by the lower limit of the corresponding term in z_t and we then integrate with respect to s to obtain:

$$F_G3(r_B) = Gm_A m_B / 4\lambda_A r_B^2 \int_o^\infty dr_A\ Jo(r_A/\lambda_A)\ 1/\pi \int_o^\pi d\theta \quad (C55)$$
$$\{- iv\beta/c\ (\exp(iys)\ [\cos(r_A(y/\lambda_B + v_A/c\lambda_A)) + \cos(r_A(y/\lambda_B - v_A/c\lambda_A))]\ /\ iy$$
$$- \exp(izs)\ [\cos(rA(z/\lambda s + v_A/c\lambda_A)) + \cos(rA(z/\lambda_B - v_A/c\lambda_A))]\ /\ iz\}$$
$$+ iv_B^2/c^2 \int_0^1 dt\ \{\exp(iy,s)\ (\lambda_B/(iy_t)^3 - s\lambda_B/(iy_t)^2)$$
$$[\sin(r_A(y_t/\lambda_B + v_A/c\lambda_A)) + \sin(r_A(y_t/\lambda_B - v_A/c\lambda_A))]\ /\ r_A$$
$$+ \exp(iz_t s)\ (\lambda_B/(iz_t)^3 - s\lambda_B/(iz_t)^2)$$

$$[\sin(r_A(zt/\lambda_B + v_A/c\lambda_A)) + \sin(r_A(z_t/\lambda_B - v_A/c\lambda_A))] / r_A \}\}$$

[00408] The terms with "$\cos(r_A\ldots)$" contribute to Type I gravity while the terms with "$\sin(r_A\ldots) / r_A$" contribute to Type II gravity.

APPENDIX D: TYPE I GRAVITY CANCELLATION

[00409] We evaluate the "$\sin(r_A\ldots)\, r_A$" integrals and show that they cancel the Type I gravity that would arise from the "$\cos(r_A\ldots)$" integrals when the Weber arguments are imaginary. If we define $s = r_B/\lambda_B$ and the function D(s), we have:

$$F_G 2i(r_B) = Gm_A m_B \lambda_B / 4\lambda_A r_B^2\, D(s) \quad \text{(D 1)}$$

$$D(s) = 1/\lambda_B^2 \int_0^\infty dr_A\, J_0(r_A/\lambda_A)\; 1/\pi \int_0^\pi d\theta\, (1 - \cos^2\theta) \quad \text{(D2)}$$
$$\{\exp(iys)/y\, [\sin(r_A(y/\lambda_B + v_A/c\lambda_A)) + \sin(r_A(y/\lambda_B - v_A/c\lambda_A))]\, r_A$$
$$+ \exp(izs)/z\, [\sin(r_A(z/\lambda_B + v_A/c\lambda_A)) + \sin(r_A(z/\lambda_B - v_A/c\lambda_A))]\, r_A]\}$$

[00410] At this point, if we reverse the order of integration and evaluate the integrals over rA, we find that the integrals are Weber discontinuous integrals but with a sine instead of a cosine argument. As a result, the four integrals are respectively non-zero when:

$$(y/\lambda_B + v_A/c\lambda_A) > 1/\lambda_A \text{ or } (y/\lambda_B + v_A/c\lambda_A) < -1/\lambda_A \quad \text{(D3)}$$
$$(y/\lambda_B - v_A/c\lambda_A) > 1/\lambda_A \text{ or } (y/\lambda_B - v_A/c\lambda_A) < -1/\lambda_A$$
$$(z/\lambda_B + v_A/c\lambda_A) > 1/\lambda_A \text{ or } (z/\lambda_B + v_A/c\lambda_A) < -1/\lambda_A$$
$$(z/\lambda_B - v_A/c\lambda_A) > 1/\lambda_A \text{ or } (z/\lambda_B - v_A/c\lambda_A) < -1/\lambda_A$$

[00411] Rather than put the limits on each integral, we leave the limits 0 and π in place, but with the understanding that the integrals are really over an annular region bounded by 0 and π whose width is determined by the above conditions. To evaluate the integrals, we first take the derivative of D(s) to remove the 1/y and 1/z factors and then integrate by parts:

$$d/ds\, D(s) = i/\pi\, 1/\lambda_B \int_0^\infty dr_A\, J_0(r_A/\lambda_A) \quad \text{(D4)}$$
$$\{\sin\theta\, [\exp(iys)\, [\cos(r_A(y/\lambda_B + v_A/c\lambda_A)) + \cos(r_A(y/\lambda_B - v_A/c\lambda_A))]$$
$$+ \exp(izs)\, [\cos(r_A(z/\lambda_B + v_A/c\lambda_A)) + \cos(r_A(z/\lambda_B - v_A/c\lambda_A))]] \Big|_{\theta=o}^{\pi}$$
$$+ is \int_0^\pi d\theta\, (1 - \cos^2\theta)$$
$$[\exp(iys)\, [\cos(r_A(y/\lambda_B + v_A/c\lambda_A)) + \cos(r_A(y/\lambda_B - v_A/c\lambda_A))]$$
$$+ \exp(izs)\, [\cos(r_A(z/\lambda_B + v_A/c\lambda_A)) + \cos(r_A(z/\lambda\beta - v_A/c\lambda_A))]]$$
$$- \int_o^\pi d\theta \cos\theta$$
$$[\exp(iys)\, [\cos(r_A(y/\lambda_B + v_A/c\lambda_A)) + \cos(r_A(y/\lambda_B - v_A/c\lambda_A))]$$
$$+ \exp(izs)\, [\cos(r_A(z/\lambda_B + v_A/c\lambda_A)) + \cos(r_A(z/\lambda_B - v_A/c\lambda_A))]]\}$$

[00412] The first term is zero. We then use that $y = \cos\theta + v_B/c$ and $z = \cos\theta - v_B/c$ to rewrite the last integral and note that the integrals are the same integrals as arose in the "$\cos(\Gamma_A \ldots)$" terms in Type I gravity, except for the integration limits:

$$d/ds\ D(s) = -\{d/ds\ B(s) + d/ds\ A(s) + d/ds\ C(s)\} \quad (D5)$$

$$D(s) = -\{B(s) + A(s) + C(s)\} \quad (D6)$$

[00413] Thus the D(s) term cancels the integration region in Type I gravity for which the Weber argument is imaginary.

APPENDIX E: REMAINING KINETIC ENERGY TERM CANCELLATION

[00414] The remaining kinetic energy term occurring from the second derivative of A(s) is:

$$\text{Rem}\ \kappa E = -V_B/c\ \{1/\pi \int_{Jo}^{\pi} d\theta\ \exp(iys)\ \cos\theta \quad (El)$$
$$[(\lambda_B^2/\lambda_A^2 - (y + v_A\lambda_B/c\lambda_A)^2)^{-1/2} + (\lambda_B^2/\lambda_A^2 - (y - v_A\lambda_B/c\lambda_A)^2)^{-1/2}]$$
$$- 1/\pi \int_{0}^{\pi} d\theta\ \exp(izs)\ \cos\theta$$
$$[(\lambda_B^2/\lambda_A^2 - (z + v_A\lambda_B/c\lambda_A)^2)^{-1/2} + (\lambda_B^2/\lambda_A^2 - (z - v_A\lambda_B/c\lambda_A)^2)^{J/2}]\}$$

[00415] f the solution is a Bessel function of order zero, we can replace the terms in s in the remainder integrals by Jo(s) to obtain:

$$\text{Rem}_{KE} = -v_B/c\ J_0(s)\ 1/\pi \int_{o}^{\pi} d\theta\ \cos\theta \quad (E2)$$
$$\{(\lambda_B^2/\lambda_A^2 - (y + v_A\lambda_B/c\lambda_A)^2)^{-1/2} + (\lambda_B^2/\lambda_A^2 - (y - v_A\lambda_B/c\lambda_A)^2)^{-1/2}$$
$$- (\lambda_B^2/\lambda_A^2 - (z + v_A\lambda_B/c\lambda_A)^2)^{-1/2} - (\lambda_B^2/\lambda_A^2 - (z - v_A\lambda_B/c\lambda_A)^2)^{J/2}\}$$

[00416] The first and fourth integrals and the second and third integrals cancel as they are mirror images with respect to the integration interval and occur with opposite sign. Thus the remaining kinetic energy term integrates to zero and the solution is indeed a Bessel function of order zero.

REFERENCES

Bergmann, P.G., *Introduction to the Theory of Relativity,* Prentice-Hall, New York 1942.

Einstein, A., *On the Electrodynamics of Moving Bodies, Ann. Phys.* 17, 891 (1905).

Erdelyi, W., Magnus, F., Tricomi, F.G., *Tables of Integral Transforms, Volume II,* in *Bateman Manuscript Project,* McGraw-Hill, New York 1954.

Massachusetts Institute of Technology (MIT), 2008 MIT Haystack Observatory Incoherent Scatter Radar (ISR), http://www.haystack.mit.edu/atrn/mho/instruments/isr

Penzias, A.A., Wilson, R.W., *A Measurement of the Flux Density of CAS A at 4080 Mc/s. Astrophys. J. Lett.* 142, 1149 (1965).

Rohringer, G., The Yellow-Green-Infrared Glow Following Nuclear Detonations, Report, General Electric Company, Santa Barbara, CA 1-7, 1968.

Will, CM., *Theory and Experiment in Gravitational Physics,* Cambridge University Press, New York 1993.

Wolfram 1996-2006 The Wolfram Integrator, Wolfram Research Inc., http://integrals.wolfram.com

Wolfram 1998-2006 The Wolfram Functions Site, Wolfram Research Inc., http://functions.wolfram.com

* * *

[00417] We claim as follows:

CLAIMS

1. A method of generating heat to power a heat engine, including projecting helium ion byproducts produced by hydrogen-lithium fusion onto a heat collection device to convert energy of the helium ion byproducts into usable heat.

2. The method of claim 1, further including projecting a proton beam onto a lithium target to produce the hydrogen-lithium fusion.

3. The method of claim 2, wherein the hydrogen-lithium fusion reacts 60 percent or more of protons in the proton beam with lithium in the lithium target.

4. The method of claim 3, wherein the lithium target undergoes fusion for more than five minutes without melting.

5. The method of claim 2, wherein the hydrogen-lithium fusion reacts a sufficient proportion of the protons to avoid melting the lithium target due to transfer of energy from the protons to the lithium target.

6. The method of claim 2, wherein the lithium target is not melted by exposure to the proton beam.

7. The method of claim 2, wherein the lithium target remains substantially in tact during exposure to the proton beam.

8. The method of claim 1, further including the heat collection device circulating a heated fluid and conveying thermal energy generated by collisions of the helium ion byproducts with the heat collection device.

9. The method of claim 8, further including conveying the thermal energy from the heat collection device through a heat exchanger.

10. A heat generator, including:

a hydrogen-lithium fusion device that projects helium ion byproducts produced by a hydrogen-lithium fusion reaction; and

a heat collector positioned to receive at least some of the helium ion byproducts from the hydrogen-lithium fusion device.

11. An electrical generator, including the heat generator of claim 10, and further including a heat-to-electrical energy converter.

12. The device of claim 10, wherein walls, components, and support structures of the heat collection device have a minimum thickness of about 2.4 mm, measured in a radial direction from the lithium target of the hydrogen-lithium fusion device.

13. The device of claim 10, wherein walls, components, and support structures of the heat collection device have a minimum thickness of about 3.14 mm, measured in a radial direction from the lithium target of the hydrogen-lithium fusion device.

14. The heat generator of claim 10, wherein the hydrogen-lithium fusion device further includes a proton beam generator and a lithium target positioned to receive a proton beam from the proton beam generator, wherein the hydrogen-lithium fusion device reacts 60 percent or more of protons in the proton beam with lithium in the lithium target.

15. The heat generator of claim 10, wherein the hydrogen-lithium fusion device further includes a proton beam generator and a lithium target positioned to receive a proton beam from the proton beam generator, wherein the hydrogen-lithium fusion device reacts a sufficient proportion of the protons to avoid melting the lithium target due to transfer of energy from the protons to the lithium target.

16. A method of generating an amplified electrical current, including harnessing wave gravity induced by fusion byproducts to amplify an electric current.

17. The method of claim 16, wherein:

the fusion byproducts are dispersed along vectors D; and

amplifying the electric current further includes exposing a plurality of conducting elements, which include semiconductor materials and have axes generally aligned with some of the vectors D, to the wave gravity induced by the fusion byproducts.

18. The method of claim 17, further including potential wells in the conducting elements that enable electrons to gain energy from the wave gravity induced by fusion byproducts.

19. The method of claim 16, further including:

projecting a proton beam onto a lithium target and creating hydrogen-lithium fusion collisions in said target, whereby the fusion byproducts are helium ions that move away from the target along the vectors D.

20. The method of claim 17, further including:

projecting a proton beam onto a lithium target and creating hydrogen-lithium fusion collisions in said target, whereby the fusion byproducts are helium ions that move away from the target along the vectors D.

21. The method of claim 18, further including:

projecting a proton beam onto a lithium target and creating hydrogen-lithium fusion collisions in said target, whereby the fusion byproducts are helium ions that move away from the target along the vectors D.

22. The method of claim 21, whereby the helium ions create the wave gravity that amplifies the current in the conducting elements.

23. A device for amplifying electric power using wave gravity produced by fusion byproducts, including:

a beam of accelerated protons;

a target comprising lithium that is exposed to the proton beam, whereby fusion collisions between the accelerated protons and lithium atoms create helium ions that move away from the target along vectors D;

at least one conducting element in which electrons are exposed to potential wells and gain energy from wave gravity produced by the fusion byproducts, positioned along at least one of the vectors D; and

a primer circuit coupled to the conducting elements that induces an electrical current to be amplified.

24. The device of claim 23, further including at least one ion accelerator that generates the beam of accelerated protons by ionizing a hydrogen gas and accelerating the resulting ions.

25. The device of claim 24, wherein the helium ions create wave gravity, wherein the wave gravity produces gravitational momentum additions to the electrons, wherein said electrons gain wave gravity energy, wherein said electrons release electromagnetic energy to an electrical current, wherein said electrical current is amplified.

26. The device of claim 23, further including a plurality of conduction elements positioned along a plurality of the vectors D.

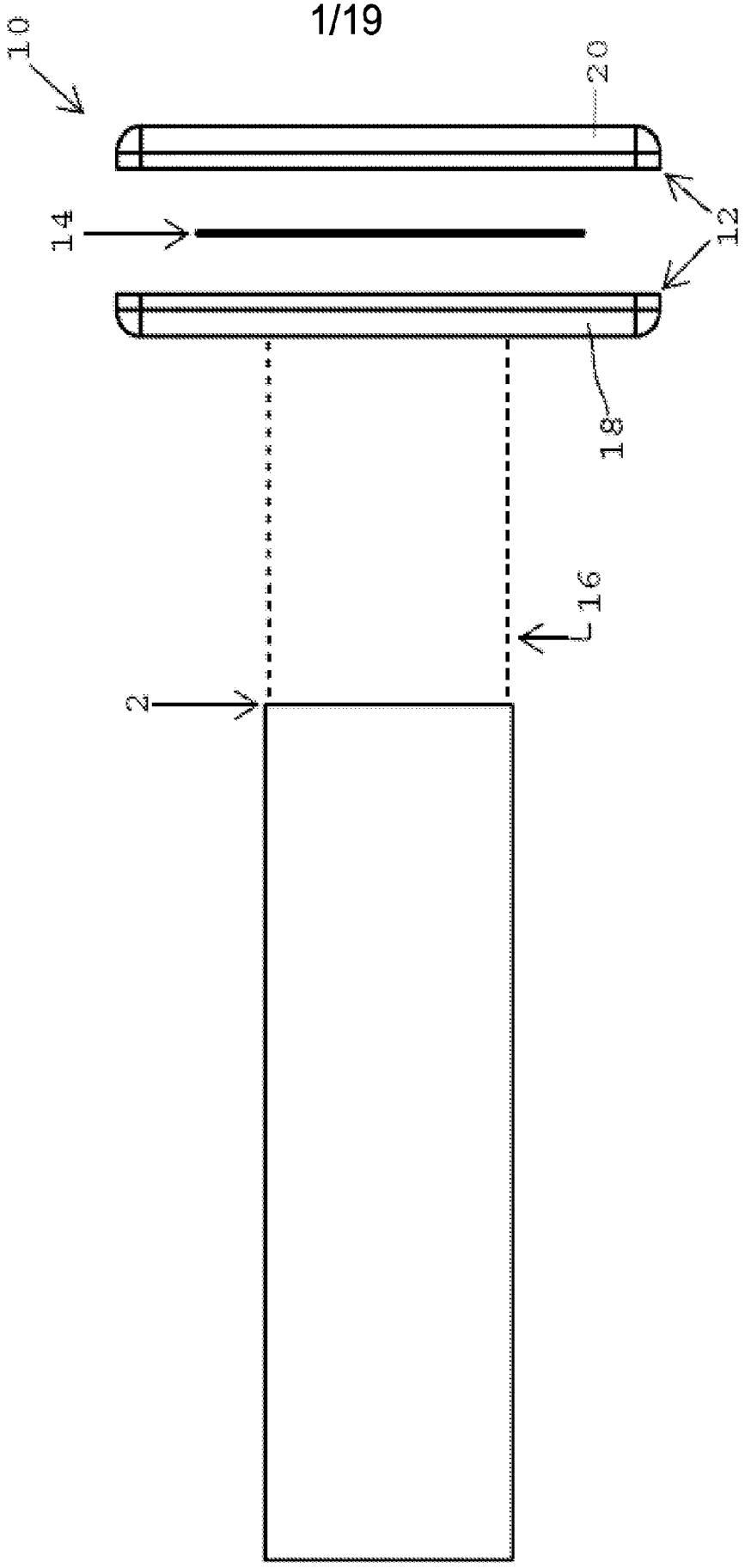

FIG. 1

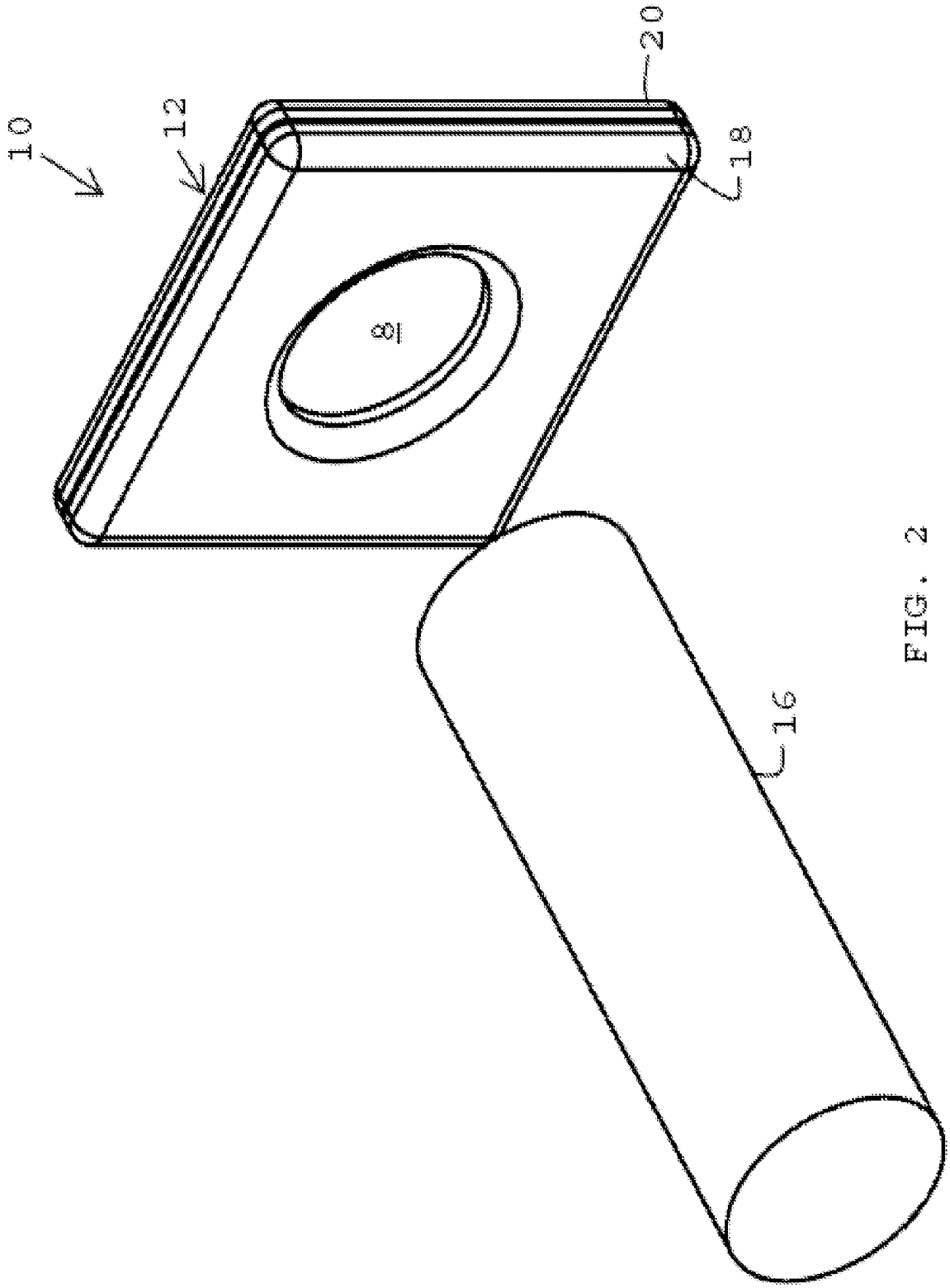

FIG. 2

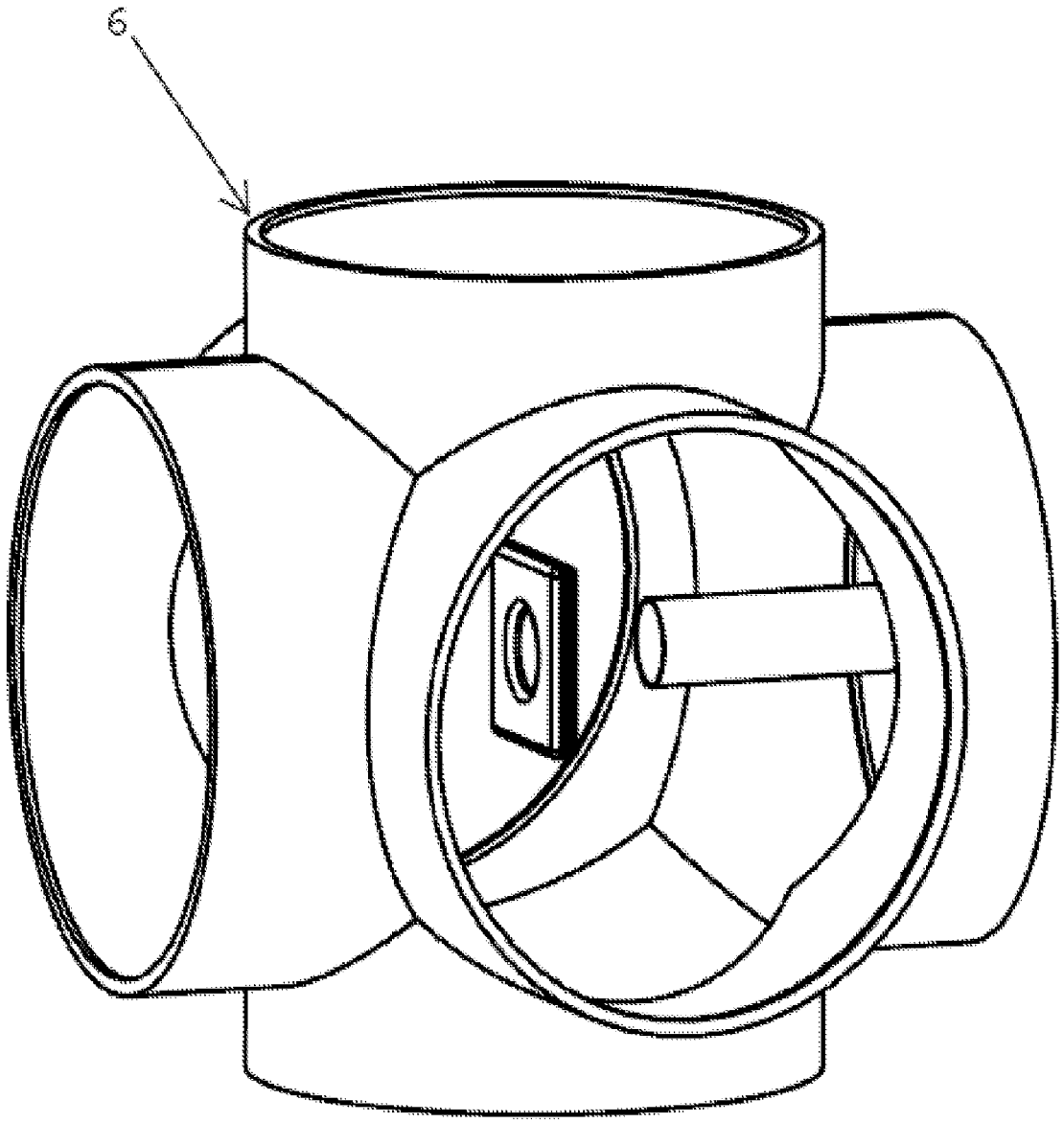

Fig. 3

FIG. 4

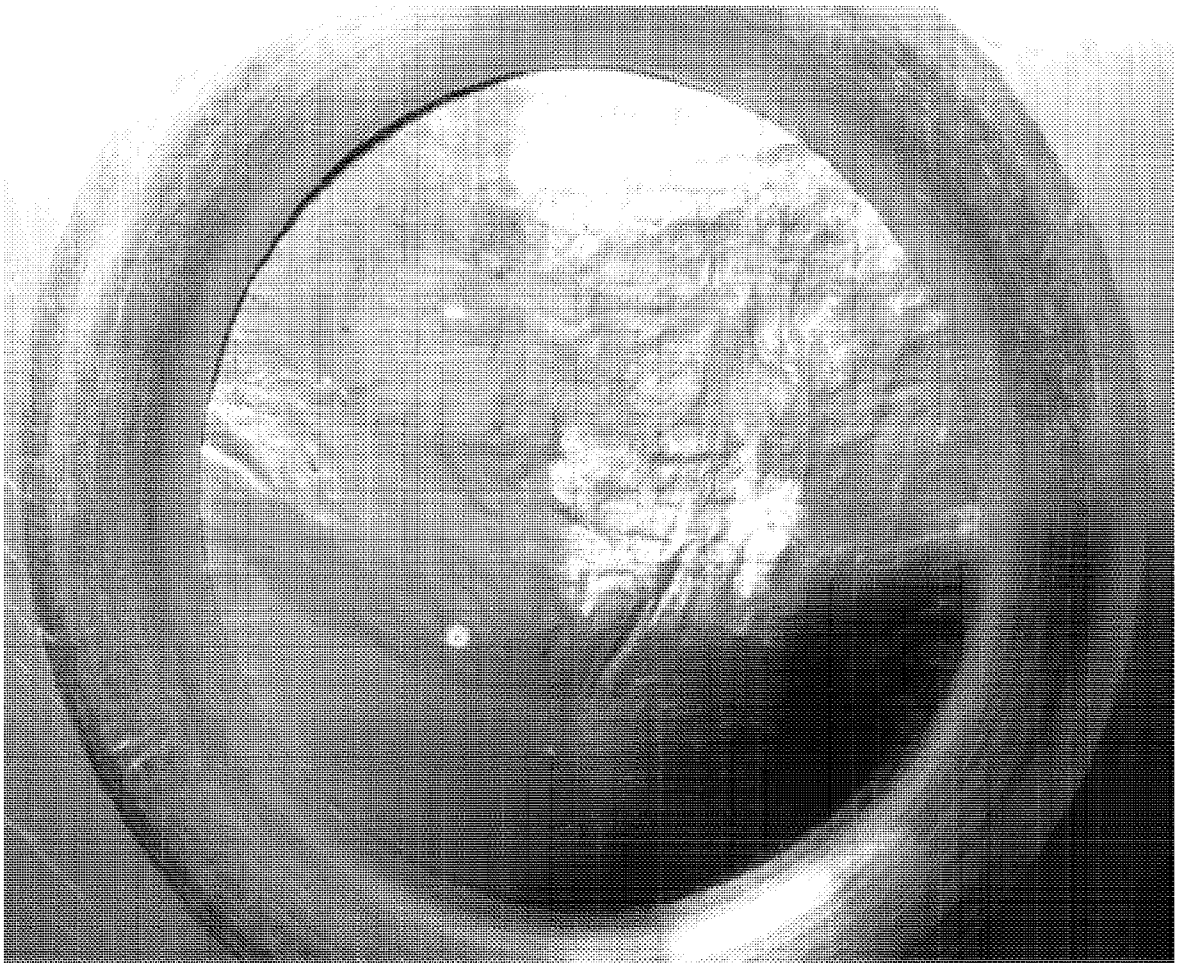

FIG. 5

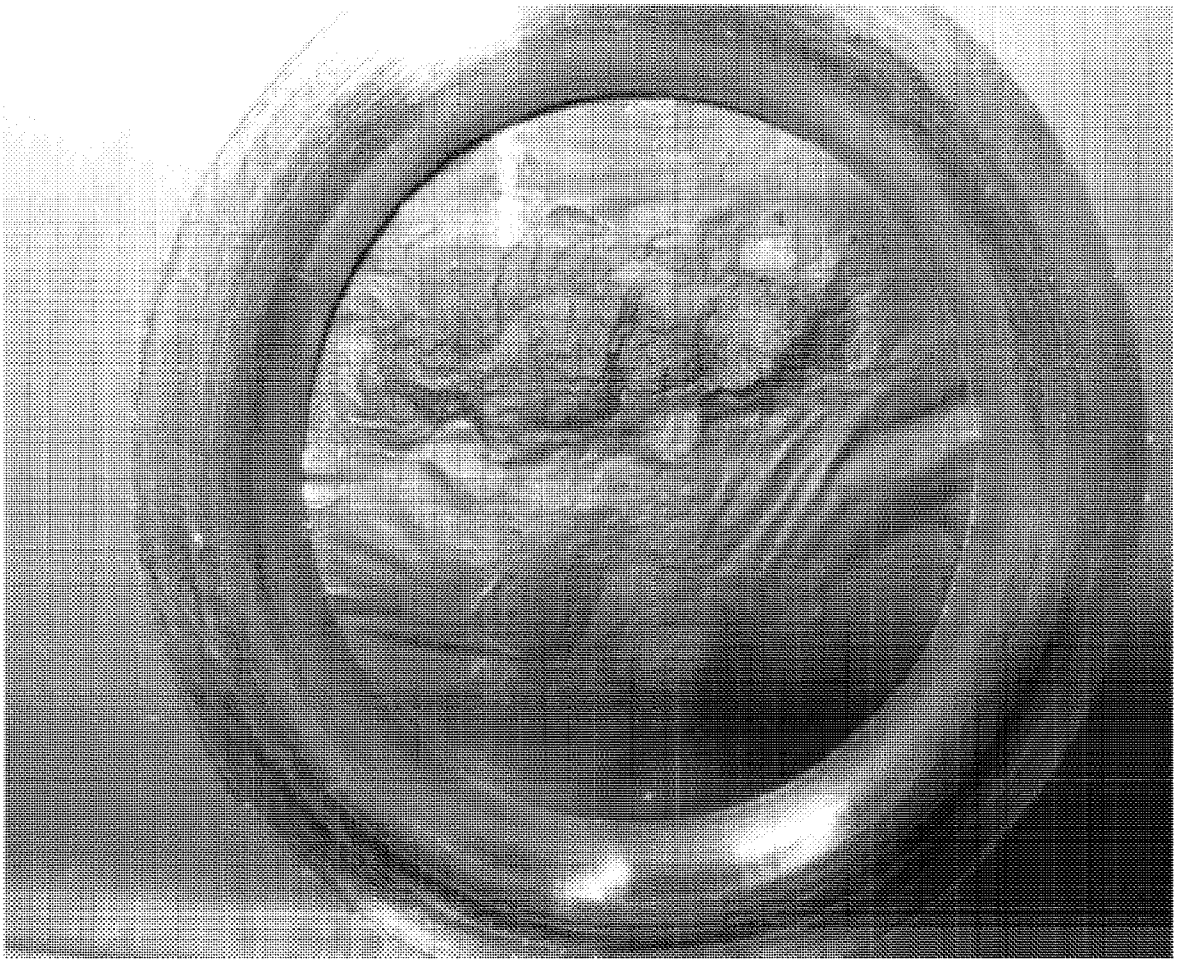

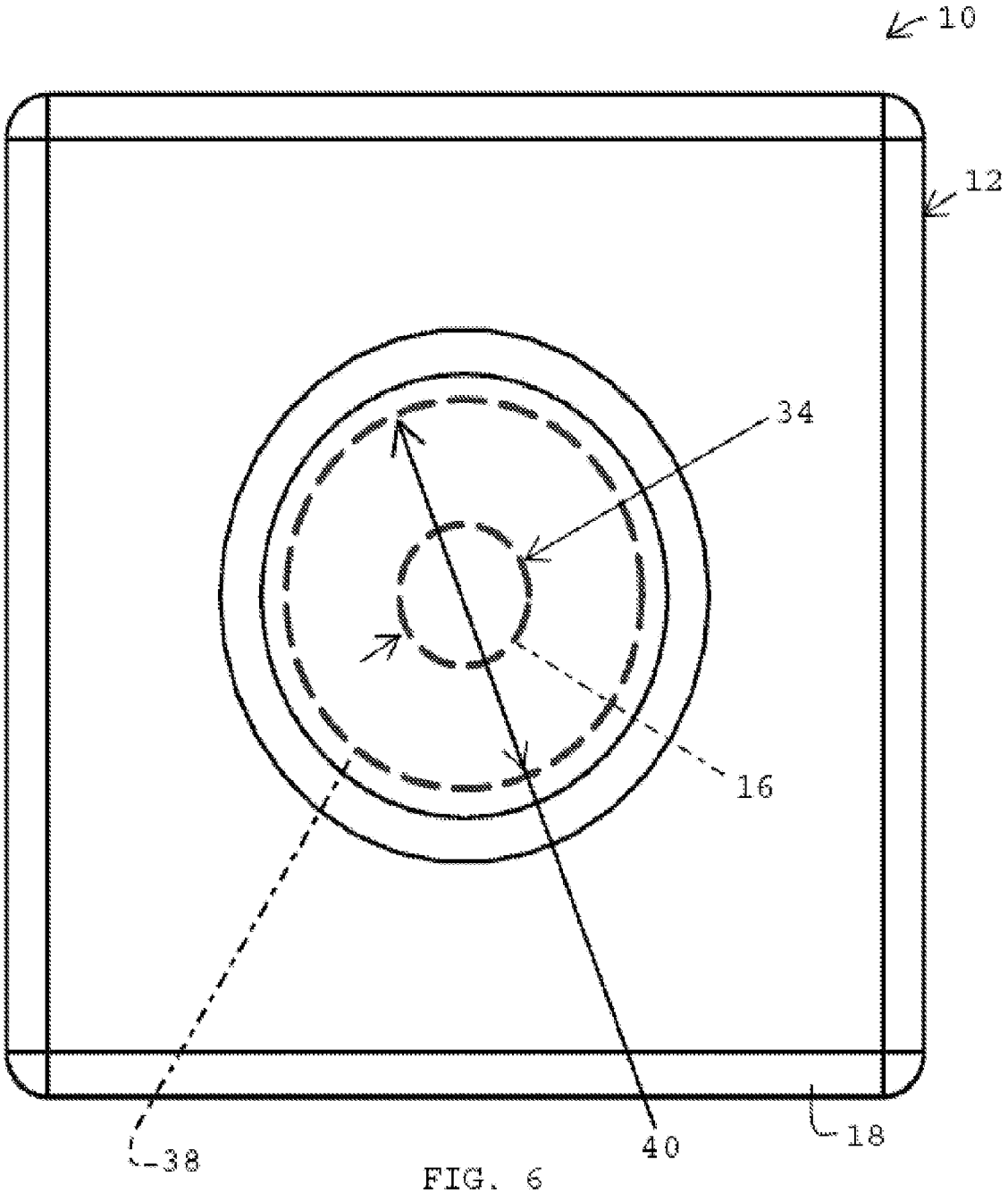

FIG. 6

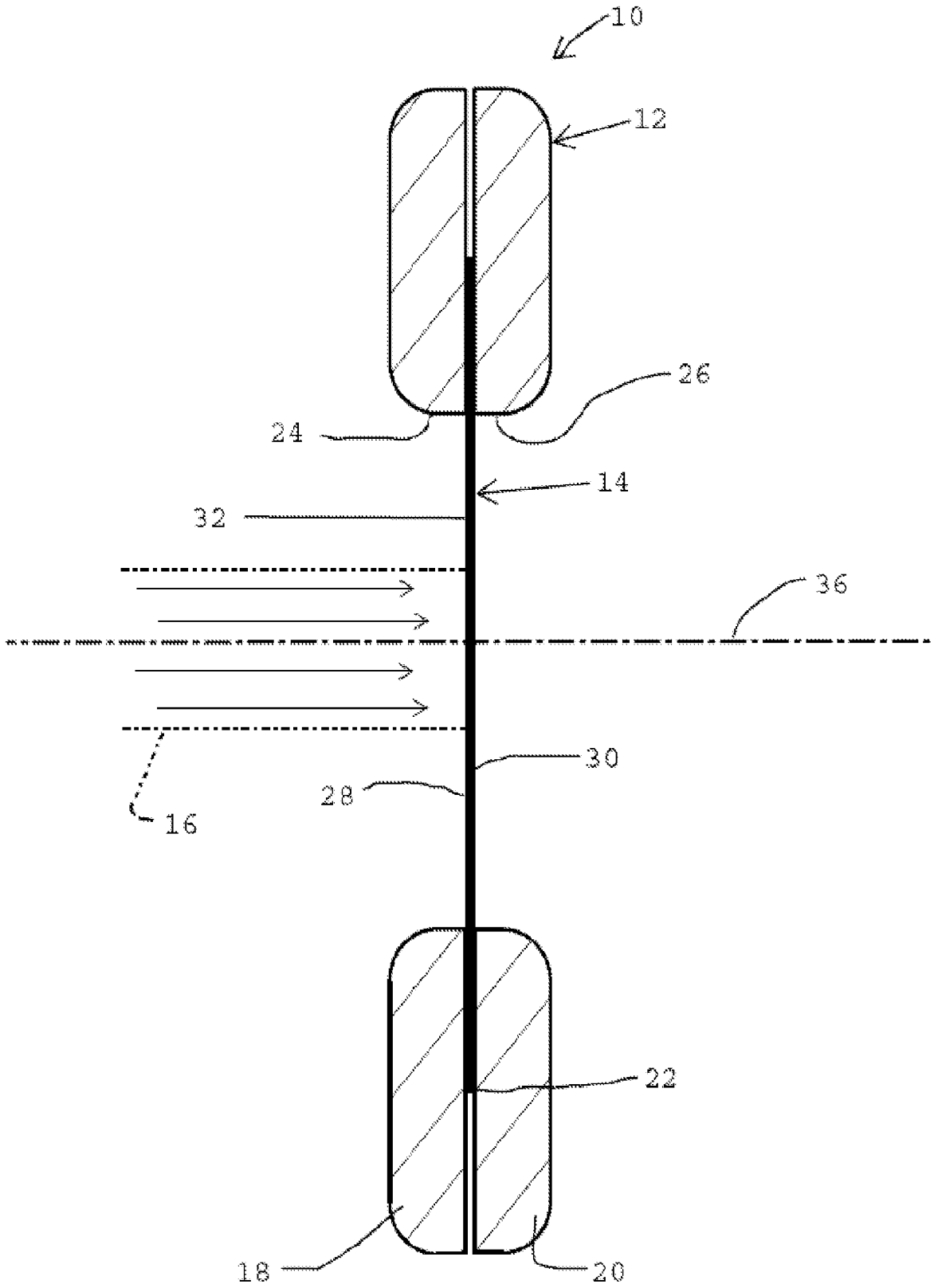

Fig. 7

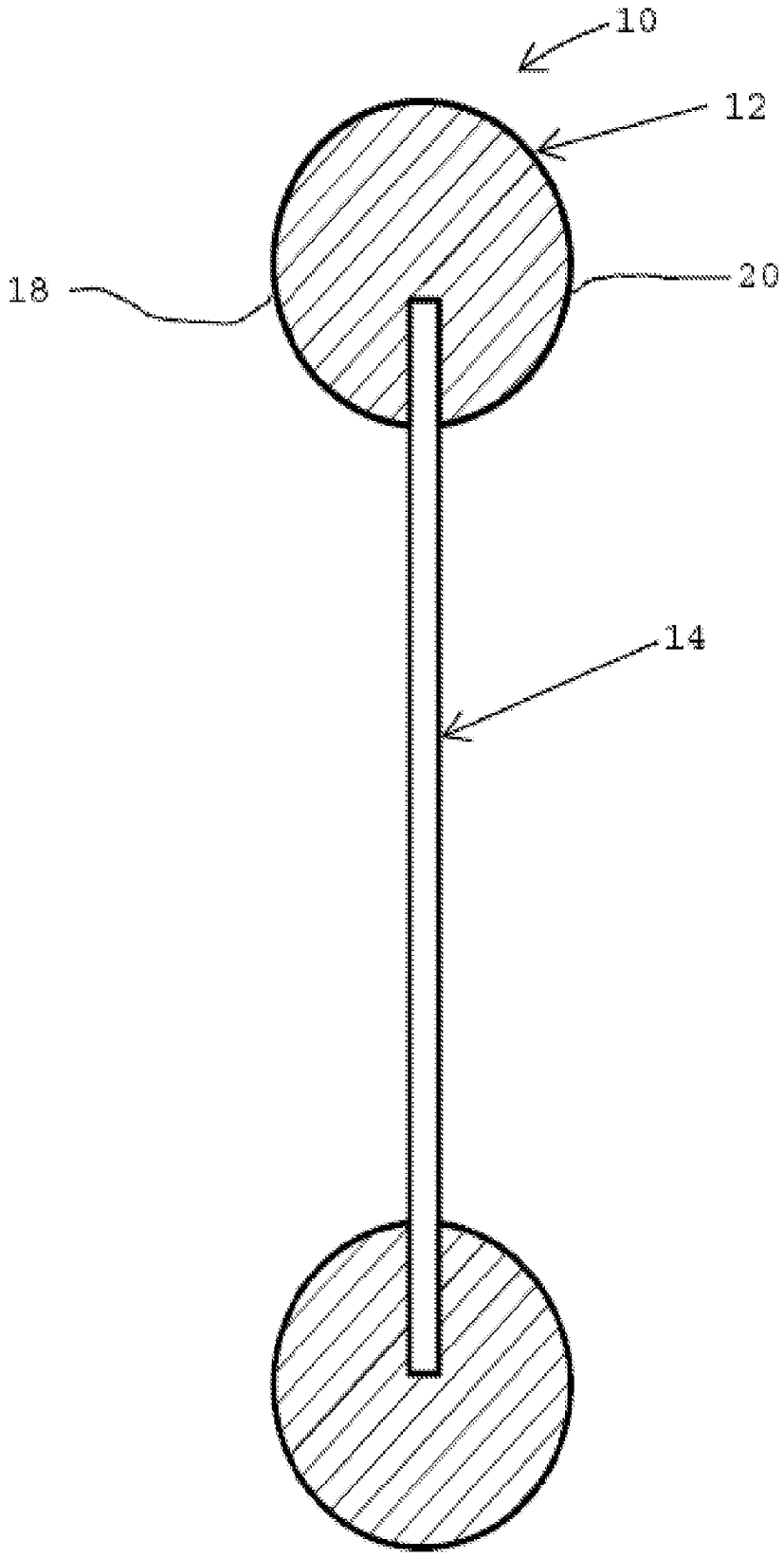

FIG. 8

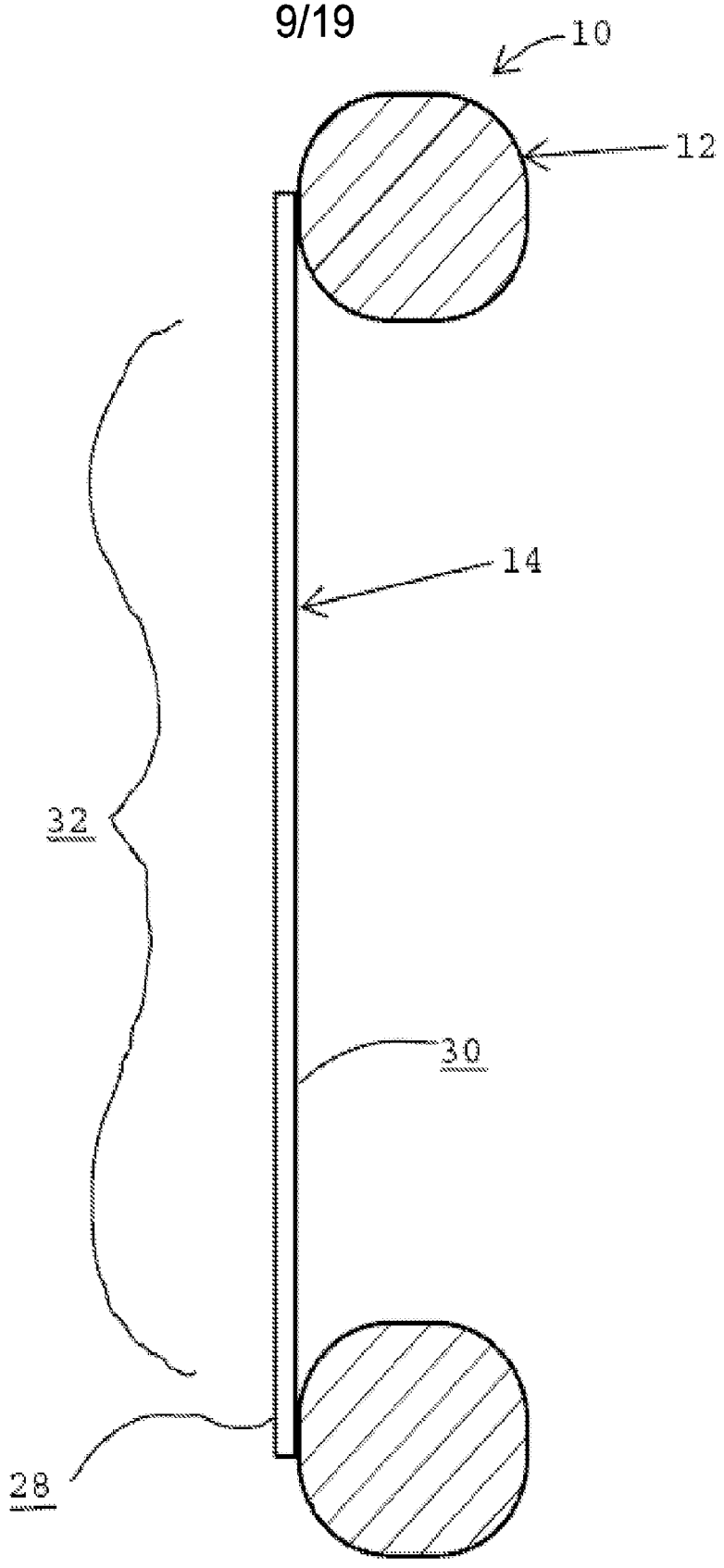

Fig. 9

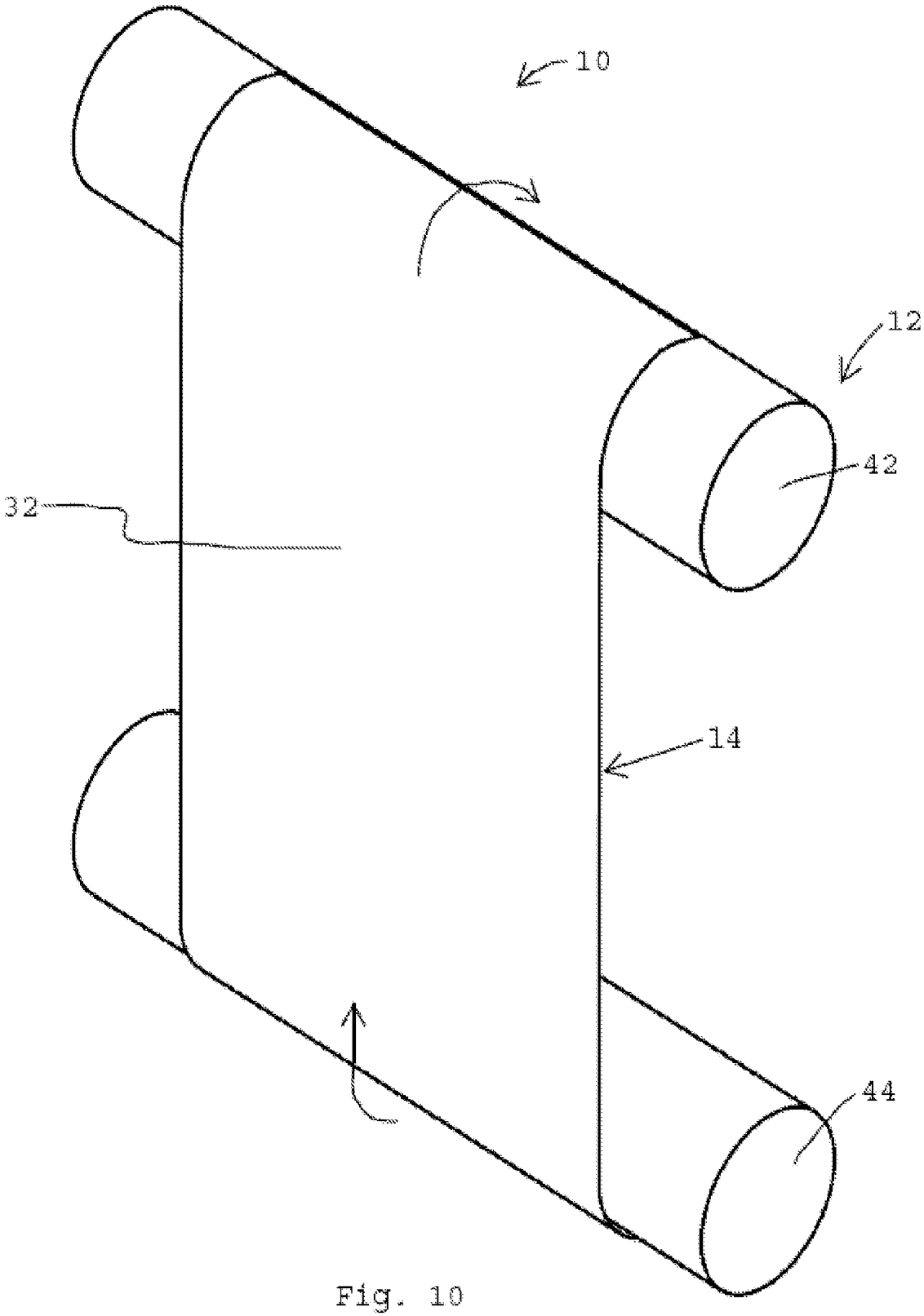

Fig. 10

Fig. 11

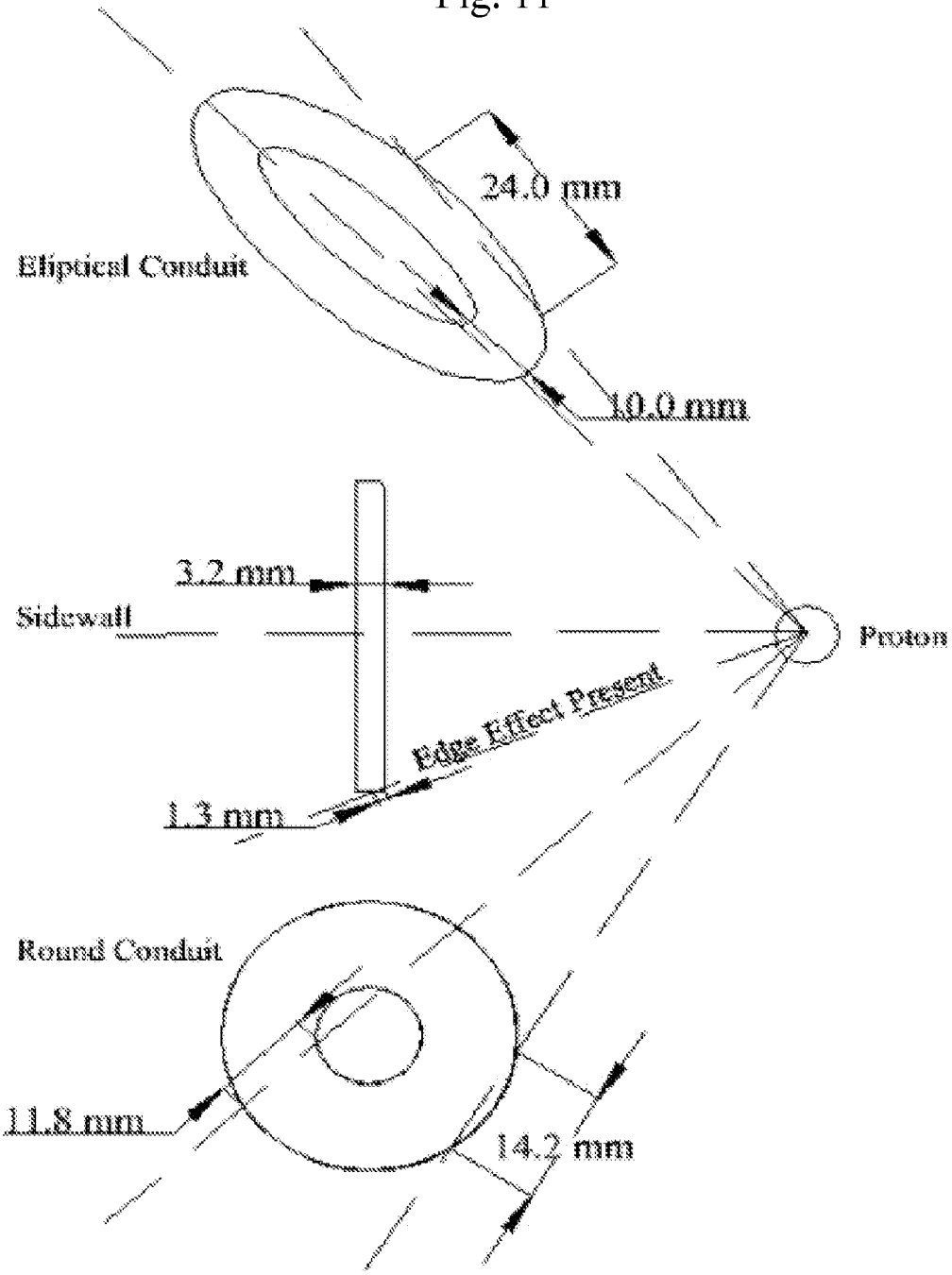
24.0 mm
Eliptical Conduit
10.0 mm
3.2 mm
Sidewall
Proton
Edge Effect Present
1.3 mm
Round Conduit
11.8 mm
14.2 mm

Fig. 12

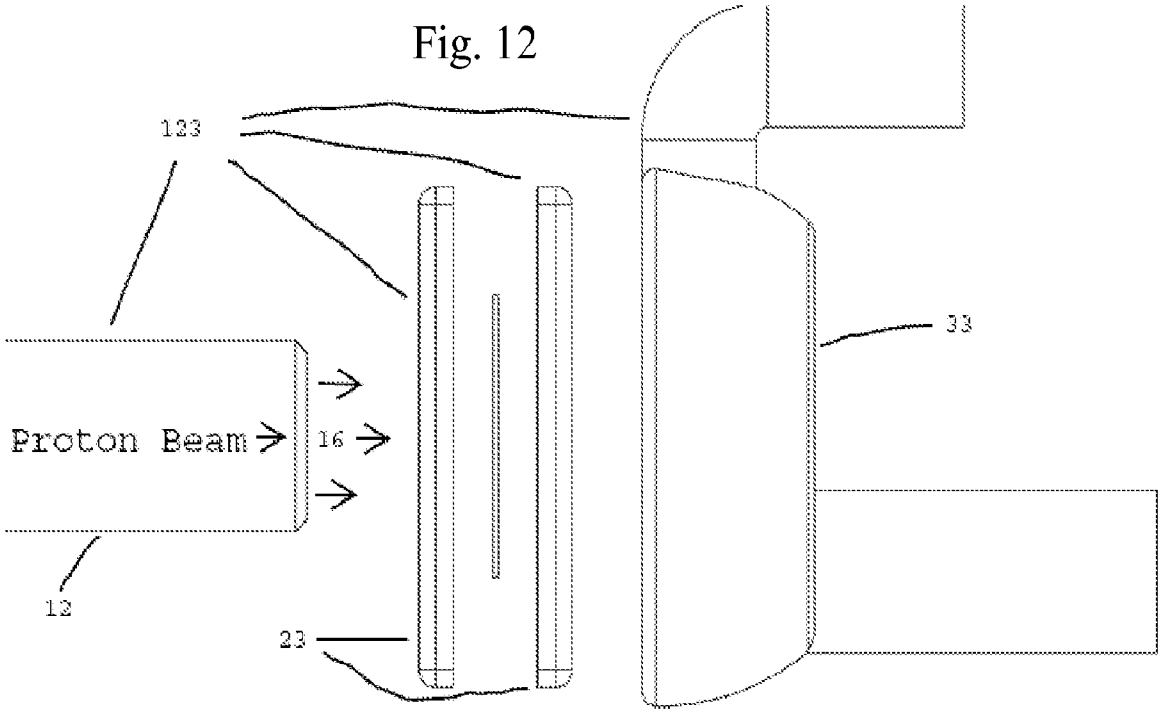

Fig. 13

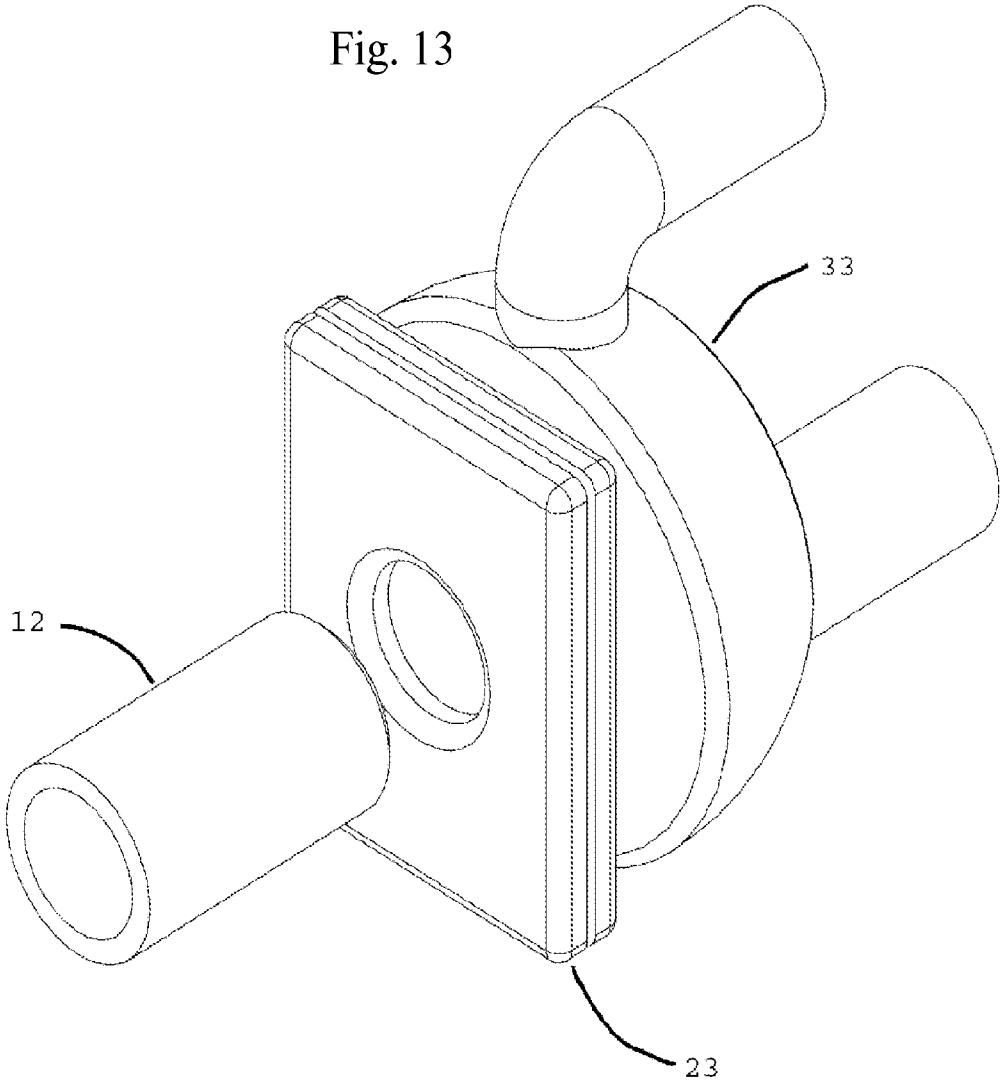

Fig. 14

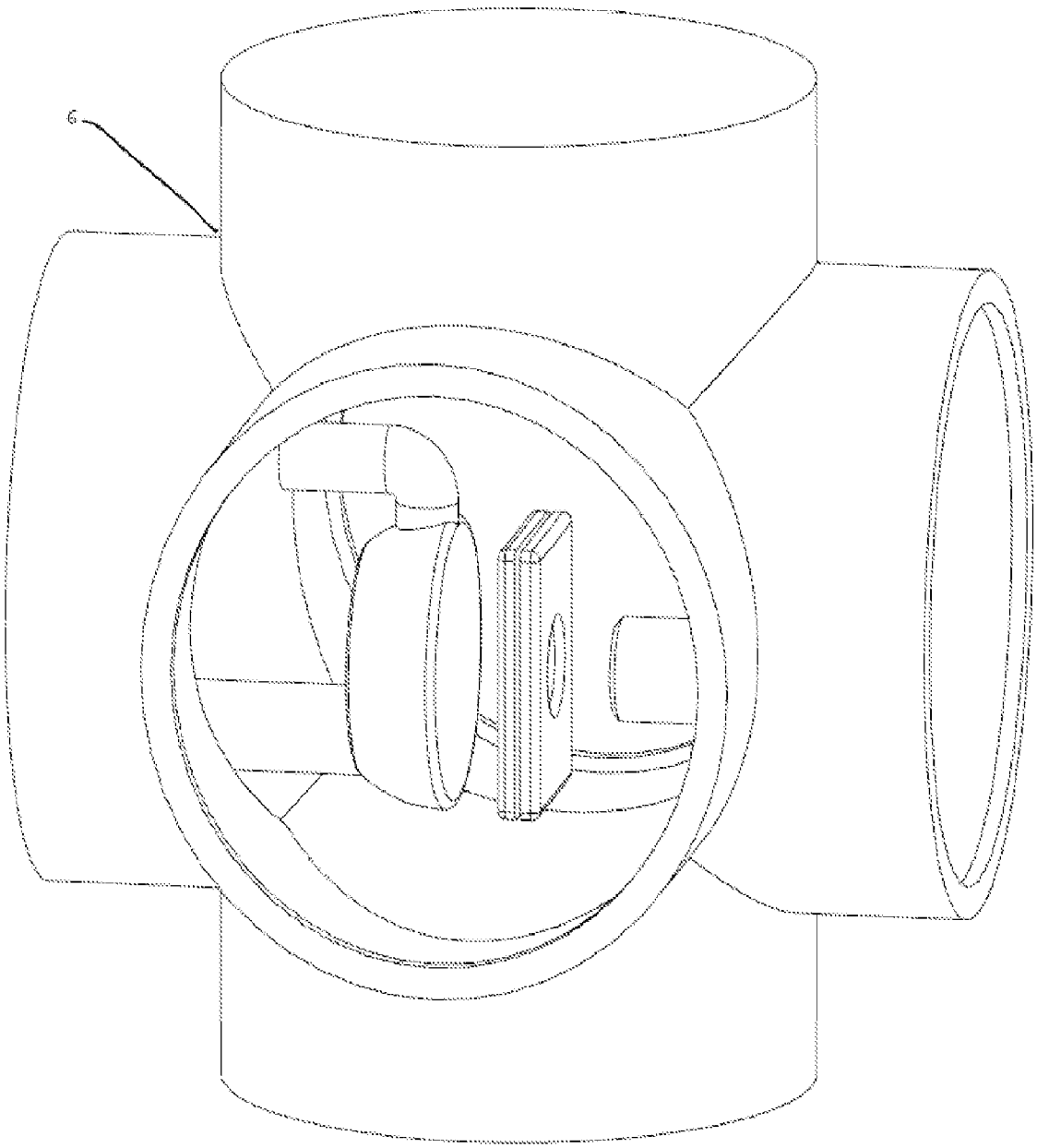

Fig. 15

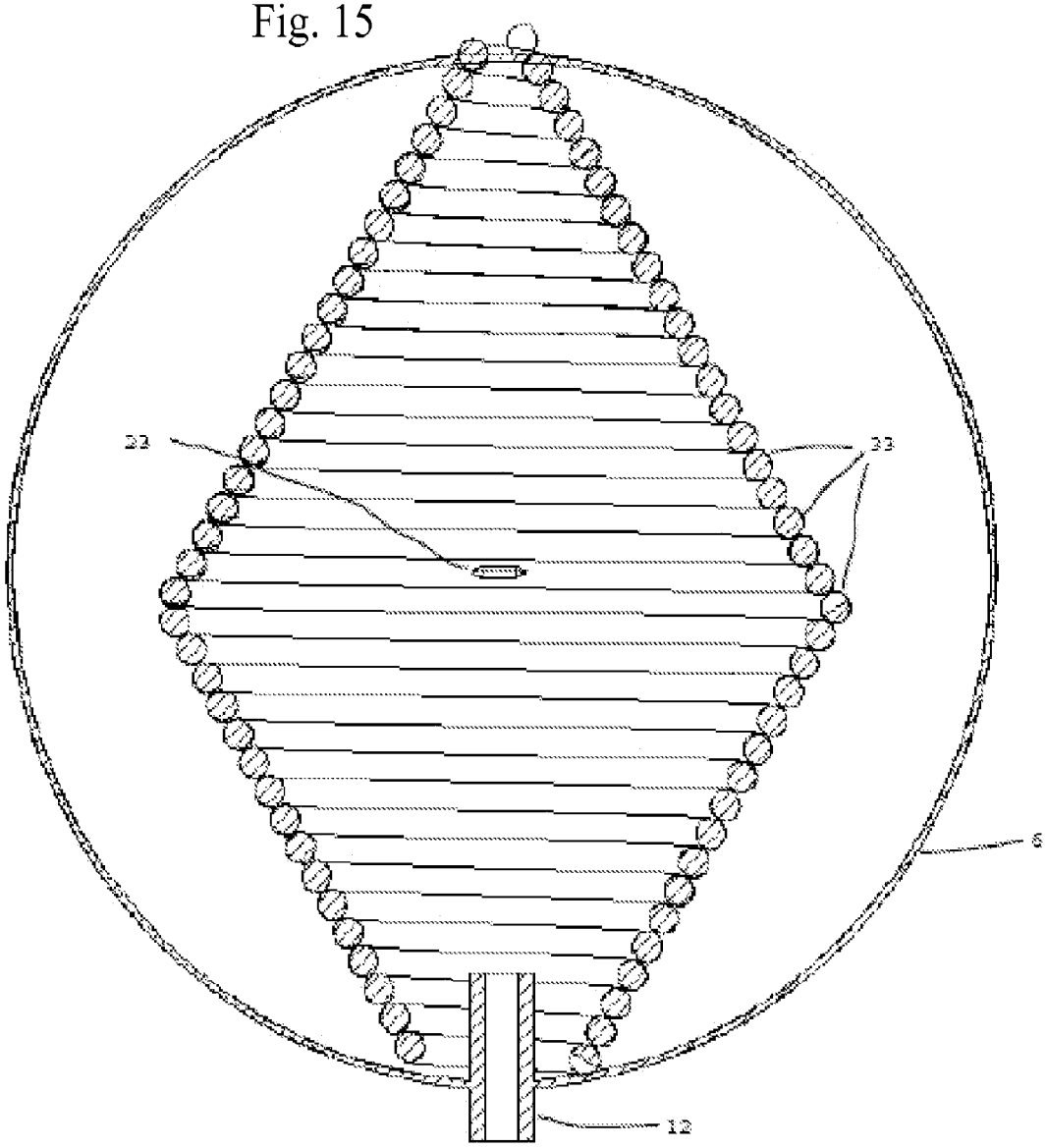

Fig. 16

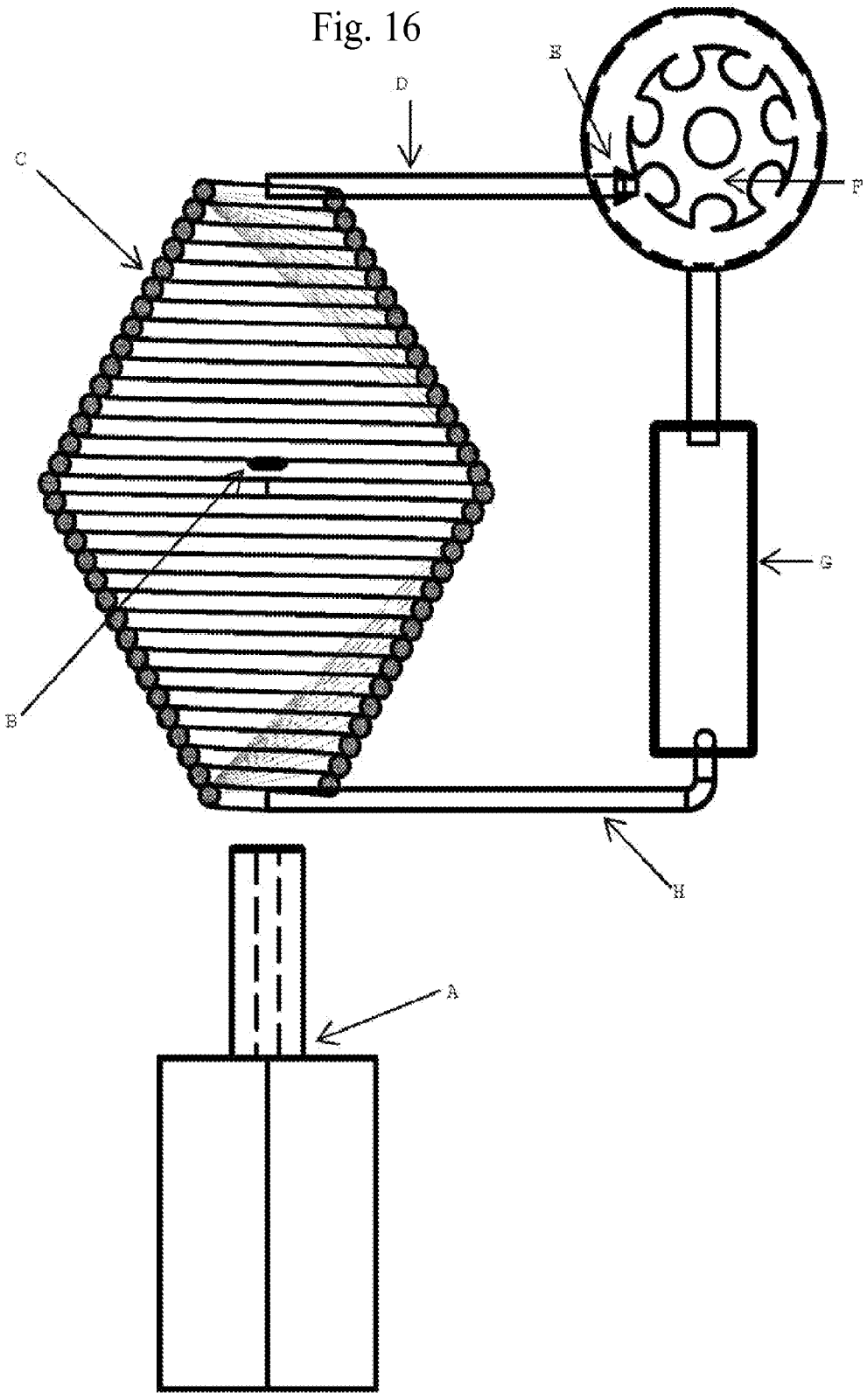

Fig. 17

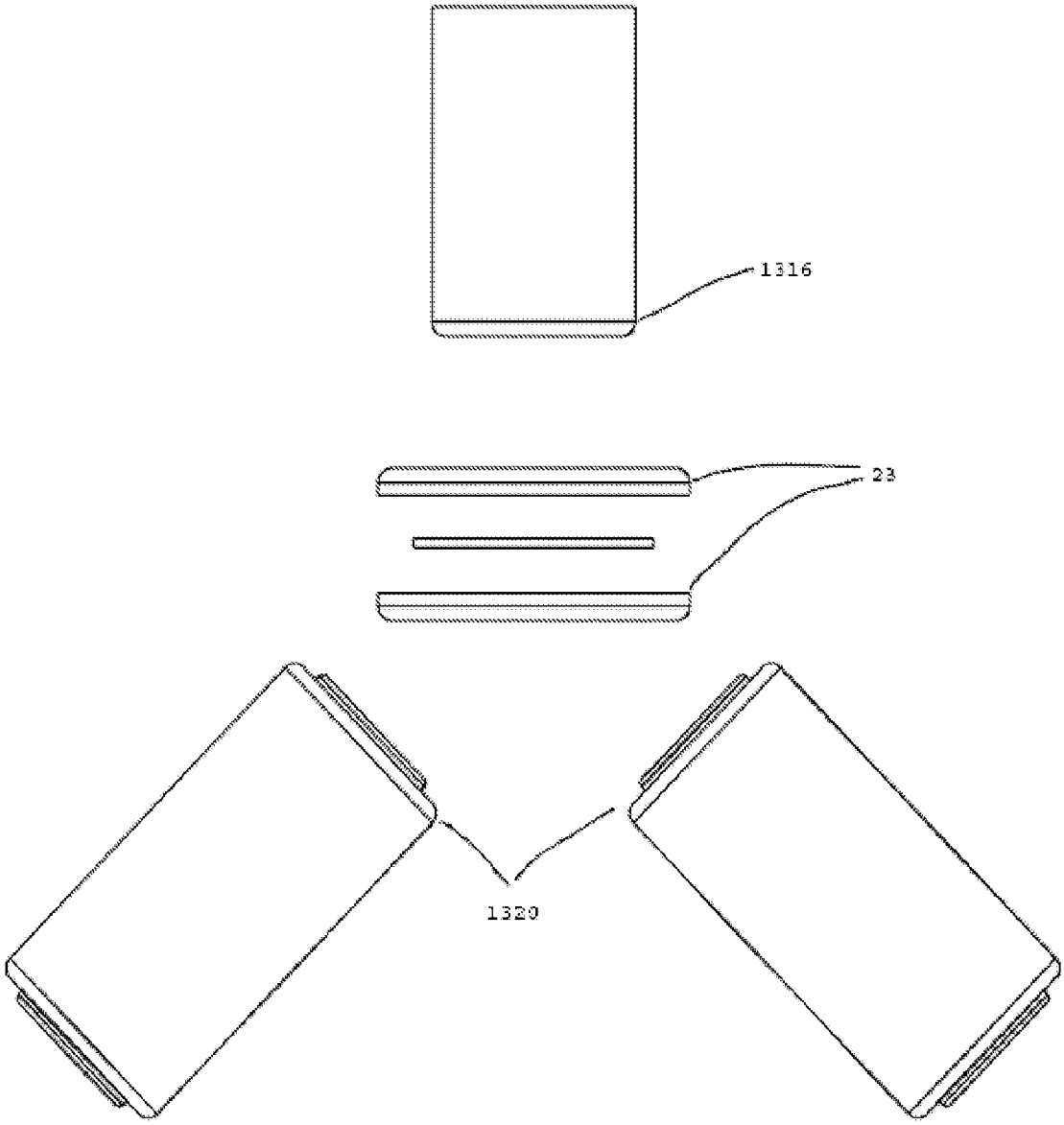

Fig. 18

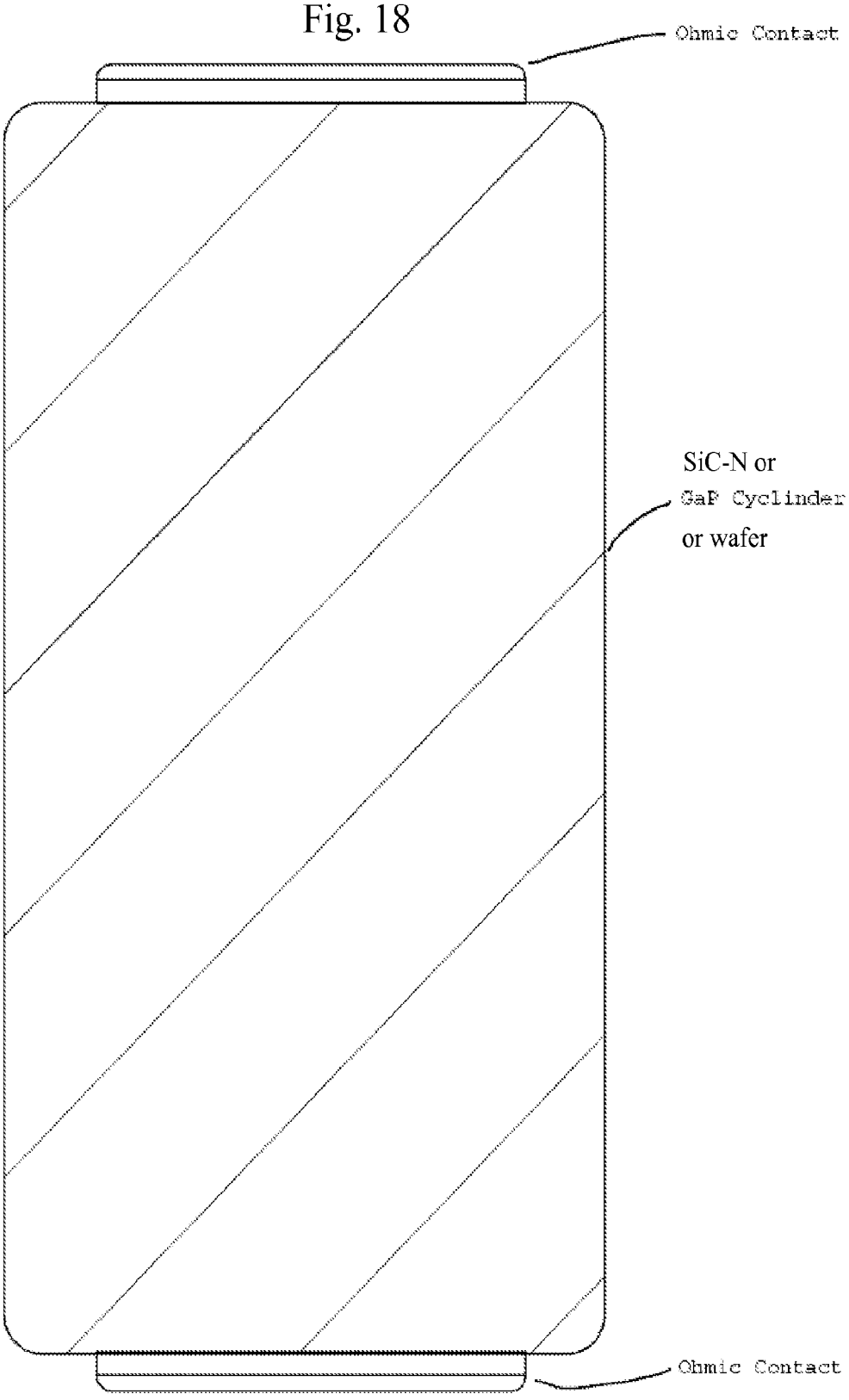

Fig. 19